Titre: Title:	Chipeless Substrate Integrated Waveguide Tag for a Millimeter Wave Identification
Auteur: Author:	Jiming Li
Date:	2017
Type:	Mémoire ou thèse / Dissertation or Thesis
Référence: Citation:	Li, J. (2017). Chipeless Substrate Integrated Waveguide Tag for a Millimeter Wave Identification [Master's thesis, École Polytechnique de Montréal]. PolyPublie. https://publications.polymtl.ca/2728/

URL de PolyPublie: PolyPublie URL:	https://publications.polymtl.ca/2728/
Directeurs de recherche: Advisors:	Ke Wu
Programme: Program:	génie électrique

UNIVERSITÉ DE MONTRÉAL

CHIPLESS SUBSTRATE INTEGRATED WAVEGUIDE TAG FOR MILLIMETER WAVE IDENTIFICATION

JIMING LI

DÉPARTEMENT DE GÉNIE ÉLECTRIQUE
ÉCOLE POLYTECHNIQUE DE MONTRÉAL

MÉMOIRE PRÉSENTÉ EN VUE DE L'OBTENTION

DU DIPLÔME DE MAÎTRISE ÈS SCIENCES APPLIQUÉES

(GÉNIE ÉLECTRIQUE)

JANVIER 2017

UNIVERSITÉ DE MONTRÉAL

ÉCOLE POLYTECHNIQUE DE MONTRÉAL

Ce mémoire intitulé :

CHIPLESS SUBSTRATE INTEGRATED WAVEGUIDE TAG FOR MILLIMETER WAVE IDENTIFICATION

présenté par : LI Jiming

en vue de l'obtention du diplôme de : Maîtrise ès sciences appliquées

a été dûment accepté par le jury d'examen constitué de :

M. CARDINAL Christian, Ph. D, président

M. WU Ke, Ph. D, membre et directeur de recherche

M. TATU Serioja Ovidiu, Ph. D, membre

DEDICATION

To my family

ACKNOWLEDGEMENTS

First of all, I would like to express my sincere gratitude to my supervisor Professor. Ke Wu, who offered me the opportunity to pursue the master's degree at École Polytechnique de Montréal. His guidance, novel ideas and the patience helped me a lot in the past two years, which is indispensable for me to write this thesis. His pursuit and persistence to highly original research impressed me and will help me throughout my life.

I would like to express my gratitude to Dr. Tarek Djerafi, for his continuous help throughout all the details during the master's studies, the discussion between us let me realize the beauty of science and drive me to explore the new space in my field.

I appreciate all the personnel at Poly-Grames Research Center, in particular Mr. Jules Gauthier, Mr. Traian Antonescu, Mr. Steve Dubé, for their outstanding job in circuit fabrication and the measurement, my appreciation is extended to Mr. Jean-Sébastien Décarie for his software support.

I would like to thank all my colleagues for the helpful discussion about my research work. In particular, Fengchao Ren, Lianfeng Zou, Kuangda Wang, Fang Zhu, Yangping Zhao, Wencui Zhu, Ruizhi Liu and Dinghong Jia. It's my honor to work with these wonderful guys.

I would like to thank all the jury members for their time and efforts in reviewing the thesis and providing the insightful comments and constructive suggestions.

Last but not least, I would like to express my gratitude to my parents, for their continuous love, support and encouragement.

RÉSUMÉ

Présentement, l'identification à ondes millimétriques (MMID) est une technologie émergente qui pourrait être présentée comme une évolution de l'identification par radiofréquence (RFID) qui fonctionne à des bandes de fréquence relativement basse aux bandes de fréquence à ondes millimétrique. Ces bandes de fréquences offrent les avantages d'avoir des antennes de plus petite taille, un débit de données plus élevé et des modules de lecteur plus compacts. Également, des antennes à faisceau étroit peuvent être mises en œuvre afin d'assurer la détection de l'emplacement. Le concept MMID peut être intégré avec les applications futures de la technologie à ondes millimétriques dans la communication sans fil tels que 5G.

Le guide d'ondes intégré au substrat (SIW) avec son blindage naturel présente des performances exceptionnelles dans la conception de circuits en bande d'ondes millimétriques, le SIW peut être intégré facilement avec d'autres circuits planaires (circuits passifs ou actifs). Des tags sans puce MMID basé sur la technologie SIW sont présentés dans ce mémoire.

Tout d'abord, un système MMID basé sur une modulation dans le domaine temporel est étudié. Un modèle théorique généralisé est construit prenant en compte le phénomène de multireflection existant dans un tag basé sur la technique de réflectométrie à dimension temporelle (TDR). Le bilan de liaison du système TDR MMID est étudié. Un procédé d'égalisation qui dépend de la largeur de l'impulsion, les caractéristiques de la ligne de transmission, l'intervalle temporel entre deux bits, la sensibilité du lecteur et de la fréquence de fonctionnement du système MMID est proposé dans le but de définir le nombre maximal de bits possible par rapport à la distance. Cette méthode définie aussi la valeur exact du coefficient de réflexion de chaque discontinuité du code binaire.

Deuxièmement, la propriété de la structure déployée SIW est étudiée. L'étiquette SIW proposée, composée de 4 iris symétriques dans le plan H avec antenne à fente intégrée, est étudiée théoriquement et expérimentalement. Une configuration de mesure est construite pour lire la balise fabriquée, et les résultats de mesure sont en bon accord avec les homologues théoriques. On étudie le guide d'ondes intégré au support demi-mode (HMSIW) qui peut réduire la largeur du guide d'ondes de moitié. L'étiquette HMSIW conçue se compose de 4 iris simple dans le plan H avec l'antenne à fente intégrée HMSIW. En outre, on étudie le guide d'onde intégré à substrat en ondes lentes (SW-SIW) afin de réduire la vitesse du groupe de SIW. La balise SW-SIW conçue se compose d'informations de 4 bits en changeant la hauteur des visités aveugles. Un nouveau guide

d'ondes intégré à demi-mode en ondes lentes (SW-HWSIW) est proposé afin de minimiser encore la taille de la balise MMID. La balise SW-HMSIW conçue montre également une bonne performance sur la fréquence de fonctionnement du système MMID. Enfin, la comparaison de ces quatre types d'étiquettes a été effectuée pour présenter la différence.

Troisièmement, un système MMID basé sur la modulation de phase est étudié. Un déphaseur SIW est proposé en ajoutant des stubs dans le plan H. Le tag MMID avec la référence et le déphasage de phase de 45 °, 90 ° et 135 ° sont mesurés. Les résultats expérimentaux correspondent aux résultats des simulations démontrent la validité de la technique proposée.

Ceci est le premier travail de recherche sur des tag MMID basée sur la modulation dans le domaine temporel et la modulation de phase, nous nous attendons à ce que travail sera combiné avec d'autres travaux sur MMID tag basé sur d'autres types de modulation afin de maximiser le nombre des bits codables dans la conception de MMID tag.

ABSTRACT

Presently, millimeter-wave identification (MMID) becomes an emerging technology as an alternative development of the conventional radiofrequency identification (RFID), which extends operating frequency from low-frequency band to millimeter-wave range. Over these millimeter-wave frequency bands, the advantages of smaller antenna size, higher data rate and more compact reader module could be realized and the function of location sensing could be implemented through narrow-beam antennas. Furthermore, the MMID concept could provide a compatible design platform in connection with the future applications of millimeter-wave technology in wireless communication such as 5G.

Substrate integrated waveguide (SIW) with its self-shielding nature presents an outstanding performance in circuit design over the millimeter-wave band, SIW can be integrated with planar circuits (passive or active). Chipless MMID tag based on SIW technology is presented in this dissertation.

Firstly, MMID system based on time-domain modulation is studied, and a generalized theoretical modeling is developed, which accounts for the existing multireflection issue during the tag design. An equalization method is examined based on the link budget of the TDR MMID system, which could be used for finding the maximum encodable bits versus the distance.

Secondly, the property of the deployed SIW structure is investigated. The proposed SIW tag, consisting of 4 symmetrical iris in H-plane with integrated slot-antenna, is studied theoretically and experimentally. A measurement setup is constructed to read the fabricated tag, and measurement results are in good agreement with theoretical counterparts. Half mode substrate integrated waveguide (HMSIW) that can reduce the waveguide width by half is investigated. The designed HMSIW tag consists of 4 single iris in H-plane with the integrated HMSIW slot-antenna. In addition, slow-wave substrate integrated waveguide (SW-SIW) is studied in order to reduce the group velocity of SIW. The designed SW-SIW tag consists of 4 bits information by changing the height of the blind vias. A novel slow-wave half mode substrate integrated waveguide (SW-HWSIW) is proposed in order to further minimize the size of the MMID tag. The designed SW-HMSIW tag also shows a good performance over the operating frequency of the MMID system. Finally, the comparison of these four types of tag is conducted to present the difference.

Thirdly, the MMID system based on phase modulation is studied. The SIW shifter is realized by adding the stub in H-plane. The MMID tags with the phase shift of 45°, 90° and 135° are measured. A good agreement found between experimental results and simulation results validates the proposed technique.

To the author’s knowledge, this is the first work about the MMID tag based on time-domain modulation and phase-domain modulation, we expect this work will be combined with the future work of MMID tag based on other modulation types, so as to maximize the encodable bits in the design of MMID tag. RÉSUMÉ

TABLE OF CONTENTS

LIST OF TABLES

LIST OF FIGURES

LIST OF SYMBOLS AND ABBREVIATIONS

CST	CST Microwave Studio
EPC	Electronic Product Code
HF	High Frequency
HFSS	High Frequency Structure Simulator
HMSIW	Half Mode Substrate Integrated Waveguide
IC	Integrated Circuit
KCL	Kichhoff's Current Law
KVL	Kichhoff's Voltage Law
LF	Low Frequency
MDP	Minimum Detectable Power
MMID	Millimeter-wave Identification
OOK	On-Off Keying
PA	Power Amplifier
PM	Phase Modulation
PS	Phase Shifter
RFID	Radio Frequency Identification
SIW	Substrate Integrated Waveguide
SW-SIW	Slow-Wave Substrate Integrated Waveguide
SW-HMSIW	Slow-wave Half Mode Substrate Integrated Waveguide
TDR	Time Domain Reflectometry
TE	Transverse Electric
TM	Transverse Magnetic
UHF	Ultra High Frequency

INTRODUCTION

Radiofrequency Identification (RFID) is a wireless technology that enables automated remote identification of the physical objects [1].

The history of the RFID technology can be traced back to World War II, under the supervision of Scottish physicist Sir Robert Alexander Watson-Watt. The British developed the first active identity friend of foes (IFF) system, a transmitter was installed on each British plane, so the radar on the ground could distinguish whether the plane is friend or enemy by receiving the signal from the plane. By the early 1980s, the first commercial RFID was used by the United States in order to track the animal. In 1999, the Auto-ID center was established at the Massachusetts Institute of Technology (MIT) to formulate the protocols and standards for the RFID technology [2].

Thanks to the explosive growth of global economy and the increased interest from governments, as well as the rapid development in integrated circuits (ICs), RFID has experienced a significant expansion over the last few decades. Nowadays, due to its low cost and ease of use, RFID has been widely deployed in various fields, such as logistics & supply chain visibility, item level inventory tracking, race timing, access control, IT asset tracking, library system, etc. [3, 4]

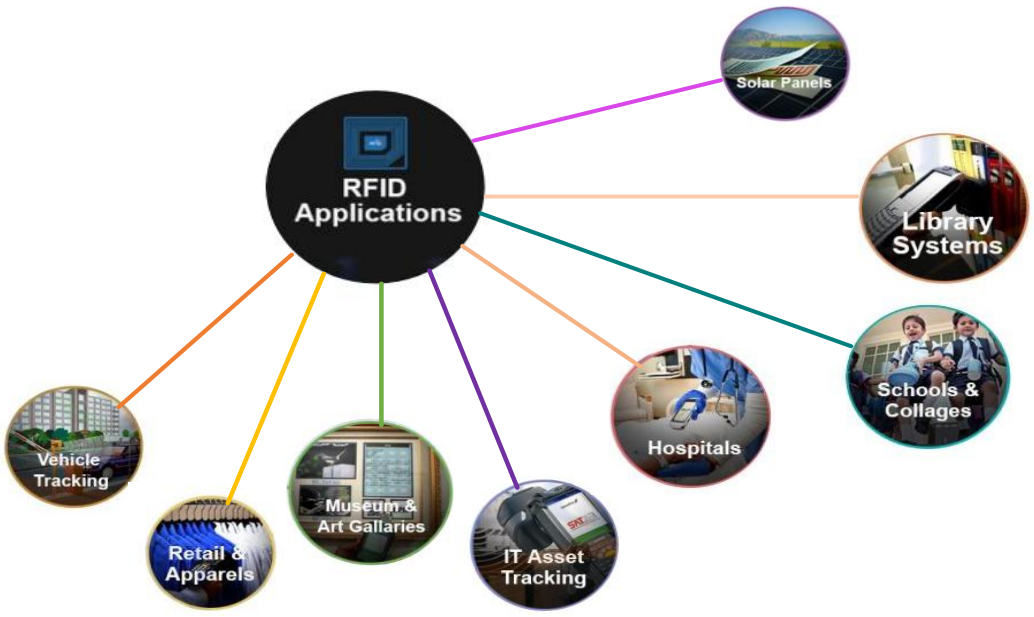

Figure I.1, RFID applications

In RFID system, radiofrequency signal is employed for communication between the two key components: the tag and the reader. The tag with the electronic product code (EPC) stored is attached to containers, books, animals and even humans, which can provide a unique identity for these physical objects. Antenna integrated with the tag can communicate with the reader by means of electromagnetic wave. The reader primarily consists of two components: the antenna and the reading circuits. By sending the interrogation signal, the data stored in the RFID tags can be extracted. The reader device could be handheld, mobile, or stationary[5].

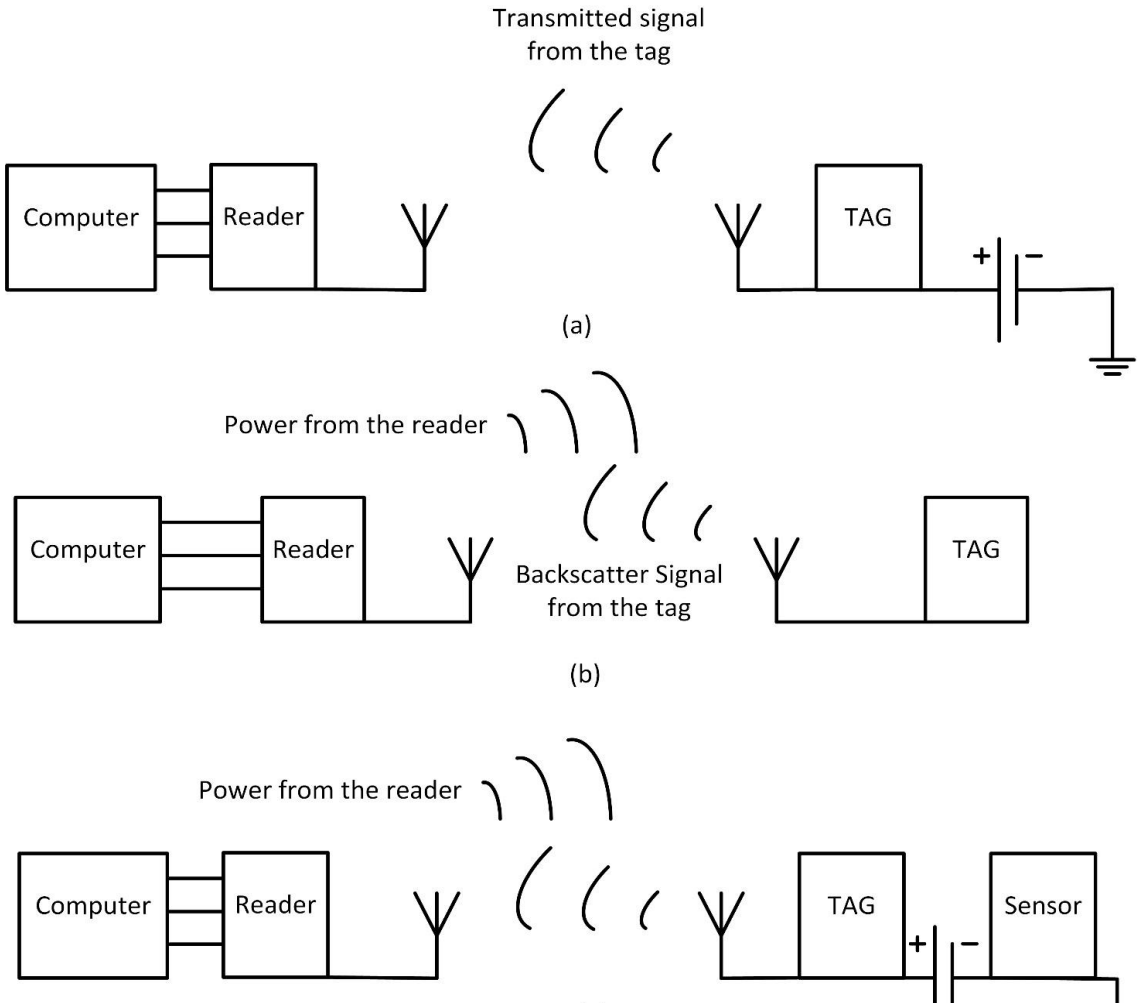

Figure I.1 (a) Active RFID system (b) Passive RFID system (c) Semi-passive RFID system

Generally, the communication technique of RFID system depends upon the property of the tag that can be typically classified into three types: active RFID system, passive RFID system and semi-passive RFID system[6].

As shown in Figure 1.2 (a), the active tag has its own power source - the internal battery that helps to deliver the energy for transmitting the data from the tag to the reader and the “on-board” battery can also be used for the power supply of components integrated into the tag. As a result, these tags have longer reading ranges (up to 100m) and greater memory compared with the passive RFID tag. However, the tag needs to be replaced when the on-board battery fails, which increases the cost.

As shown in Figure 1.2 (b), unlike the active tag, the passive tag does not have the on-board battery during the operation and it needs to operate with the power from the reader. Once the tag is in the reading zone, it will collect the energy from the RF waves by the integrated antenna. Following the logical signal processing in the tag, it will send back the signal carrying the bits information, which is called backscatter. At the expense of shorter reading range (up to 5m) and lower memory, passive RFID tags have more advantages on size, cost and lifetime.

As shown in Figure 1.2 (c), the semi-passive RFID tag also has on-board battery, but the battery is only used for the power supply of components (sensor, chips) rather than sending the signal during the operation. Similar to the passive RFID system, it operates with the power from the reader to “start” the tag and to send back the signal containing the bits information by using the backscatter technique. This kind of tag has both medium reading range (up to 30m) and medium lifetime compared with the active and passive RFID systems.

The operating frequency in RFID systems determines the application fields as shown in Table 1-1. Generally, the higher the operating frequency is, the greater the reading range becomes. For low frequency (LF) RFID systems, the 125 kHz or 134 kHz band are assigned in most of the countries. For high frequency (HF) RFID systems, countries have reached the agreement for the use of 13.56 MHz. However, for the ultra-high frequency (UHF) range, different countries have allocated different operating frequency bands. In European Union, the frequency range is from 865 to 868 MHz, in North America it is from 902 MHz to 928 MHz, while in Australia it is from 920 MHz to 926 MHz. China has approved the bandwidth from 840.25 MHz to 844.75 MHz and 920.25 MHz to 924.75 MHz for the RFID technology.

Table I-1 Operating frequency of RFID systems

RFID Type	Frequency Range	Read Distance	Applications
Low frequency (LF)	<0.3 MHz	0.1 m-0.3 m	• Animal tracking • Industrial application
High frequency (HF)	3-30 MHz	0.4 m-1 m	• Electronic ticketing • Contactless payment
Ultra-high frequency(UHF)	860-950 MHz	1 m-3 m	• Asset management • Container tracking
Microwave frequency	2.45-5.8 GHz	>3 m	• Auto toll roads
Millimeter-wave band	30-60 GHz	<1 m	• Location sensing • Future compatibility

Based on the type of modulation, chipless RFID tags could be categorized into three general types as shown in Figure 1.3[7, 8].

- Chipless RFID tag based on time-domain reflectometry (TDR) technique.
- Chipless RFID tag based on spectral signature.
- Chipless RFID tag based on amplitude/phase domain modulation.

For the chipless TDR-based RFID tags, the reader sends the interrogation signal with the time width of ΔT and listens to the echoes from the tag, the tag will generate a train of pulses by adding discontinuities in the transmission line to encode the bits information. The advantages of this kind of tag are low cost, narrow bandwidth, location sensing and greater reading range, etc. The disadvantages of these tags are related to a limited encodable number of bits, and the requirement of high-speed reader RF front-ends to generate the pulse signal.

For the chipless spectral signature-based tag, the reader sends the swept-frequency signal based on the operating frequency of the system and listens to the echo from the tag. The tag generates the encoded data in the spectrum by using resonant structures, the presence of the resonant part means binary code “1”, and the absence of the resonant part means the binary code “0”. The advantages of this kind of tag could be concluded as greater data storage, full printable and low cost, and the disadvantage of this kind of tag is that large bandwidth is required for encoding the information.

For the chipless amplitude/phase-based tag, the tag encodes the data by varying the amplitude and the phase of the backscattered signal. The advantage of this kind of tag is the narrow bandwidth requirement during the operation, and the disadvantage of this kind of tag is the requirement of high resolution of the phase for the reader part to read more bits information.

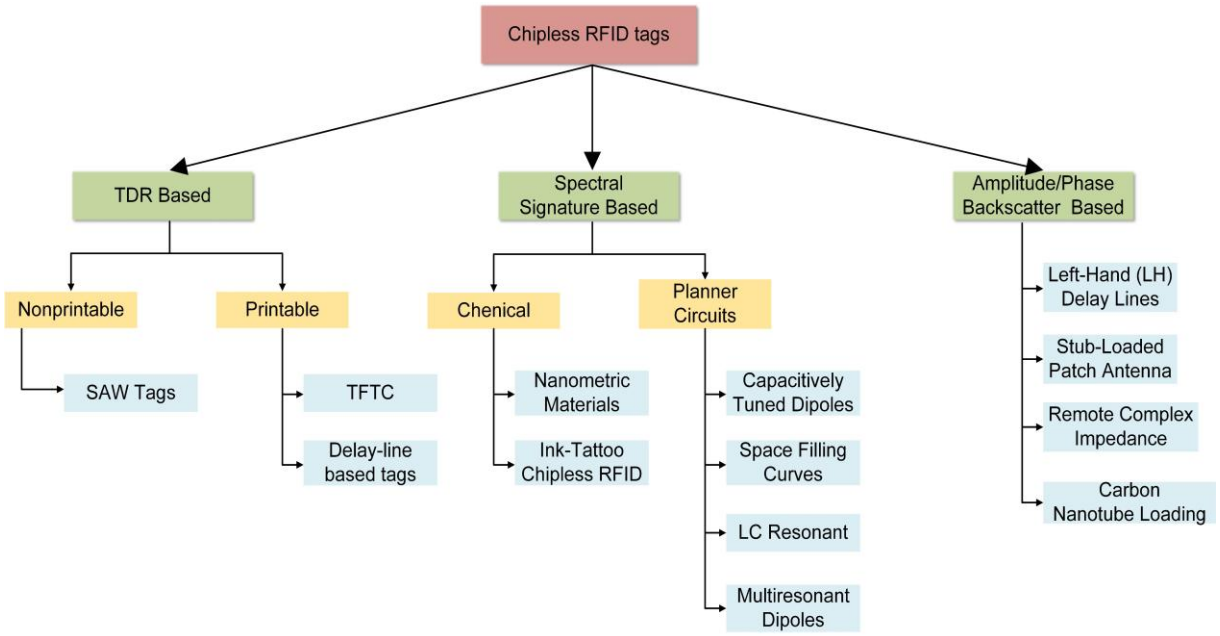

Figure I.2 Classification of RFID tags

Millimeter-wave identification (MMID) upgrades the operation frequency to millimeter-wave range. Compared with the conventional RFID system operating at low frequency, the MMID system has the following advantages:

- The wavelength of millimeter wave is much shorter, which reduces the size of the integrated antenna. Furthermore, the short wavelength makes it possible to design a small directive antenna array, which can achieve the function of location sensing.

- Over the millimeter-wave frequency band, higher data rate (higher than gigabit) communication can be implemented, making it possible for the mass memory transmission over a very short distance.
- Applications such as automotive radars have been used over millimeter-wave range, which is possible to be used as MMID readers to detect the MMID tag.
- Over the millimeter-wave bands, its effective wavelength is close to the size of a CMOS die, which offers the possibility to integrate the antenna, the MMID tag and the rectifier on the same chip [9].
- The MMID concept offers a compatibility with the future applications over millimeter-wave band, such as 5G platform, etc.

A considerable amount of research works on the chipless RFID tag design have been done during the last decade. In [10], transmission delay line was used to build the tag with four bits information at 915 MHz, SAW tag was proposed due to its unique feature of piezoelectric materials which enables much slower surface acoustic waves [11]. In [12], a fully printable planar chipless MMID tag was proposed at 30 GHz, and the tag encodes the data into a spectral signature by using multiresonator. This MMID tag comprises of a multiresonating circuit with 6 spiral resonator and two cross-polarized UWB monopole antennas, but a large bandwidth is occupied during the operation (24 GHz to 36 GHz) and no experimental results were reported in the article. In [13], a 6-bits chipless MMID tag was proposed at 25 GHz, and this MMID tag comprises of 2 orthogonally polarized slot loaded circular patch antennas, which are connected by a right angle transmission line. The resonant frequency is determined by the slot on the patch, hence the number of the identification data bit. In [14], a novel compact chipless MMID tag was presented, and this MMID tag consists of a slot etched on the top of the circular Substrate Integrated Waveguide (SIW) cavity, multi-numbered bits are achieved by adding an array of cavities with frequency and polarization diversity. The challenge is in the reader part, which must be accurate enough to distinguish those very close frequencies and thus the cavities need to achieve a very narrow resonance in order to maximum the encodable number of bits at the fixed bandwidth.

However, previous works on TDR RFID tags were focused on the low-frequency and the works on chipless MMID tags were based on the spectral signature modulation. MMID tags based on TDR technique and phase-domain modulation have not been studied due to the high loss. In this

work, the SIW will be studied to explore the world of MMID, and the thesis is organized in the following way:

In chapter 1, the operating principle of the TDR MMID system is introduced. The theory of lossy transmission line is studied, and the way of encoding bits information in the tag is illustrated. The interval between the bits of information is set considering the distortion issue. A generalized theoretical model is built considering the multireflection issue during the TDR RFID tag design. The link budget is investigated to define the Minimum Detectable Power (MDP) of the system. An equalization method is proposed based on the theoretical modelling as well as the link budget of the system in order to maximize the encodable bits of the tag.

In chapter 2, the studies of the SIW are discussed and reviewed. The interrogation signal distortion caused by the dispersion issue is studied, the meander-line SIW MMID tag is designed and simulated, and the measurement setup is constructed in order to read the proposed tag. HMSIW that can reduce the SIW width by half is investigated. The meander-line HMSIW MMID tag is designed, simulated and measured. Slow-wave substrate integrated waveguide (SW-SIW) is investigated to reduce the group velocity and the slow-wave effect is achieved by the blind vias array which separates the electric field and the magnetic field, and the meander-line SW-SIW MMID tag is designed and simulated. A novel slow-wave half mode substrate integrated waveguide (SW-HMSIW) is proposed to minimize the size of the MMID tag, and the meander-line SW-HMSIW tag is designed and simulated. Finally, the comparison of these four types of tags is conducted to show the difference.

In chapter 3, the operating principle of the MMID system based on the phase modulation is introduced. The SIW phase shifter is proposed by adding the stubs in H-plane which could cover the phase shift range from 0° to 180°. The resolution of 45° is selected to build the tag, two cross-polarized slot antennas are integrated to the two ports of SIW phase shifter in order to avoid the interaction between them. Reader concept based on the VNA together with the two horn antennas is proposed to demonstrate the proposed technique.

The contribution of this work is summarized in the last part. Firstly, the generalized theoretical modelling is adopted for the multireflection issue during the TDR tag design. Secondly, the proposed equalization method is used to maximize the encodable bits of the tag. Thirdly, the MMID tags based on both time domain modulation and phase modulation are studied and measured, showing the feasibility of the MMID system.

CHAPTER 1 EQUALIZATION METHOD FOR CHIPLESS TDR RFID TAG

1.1 Introduction

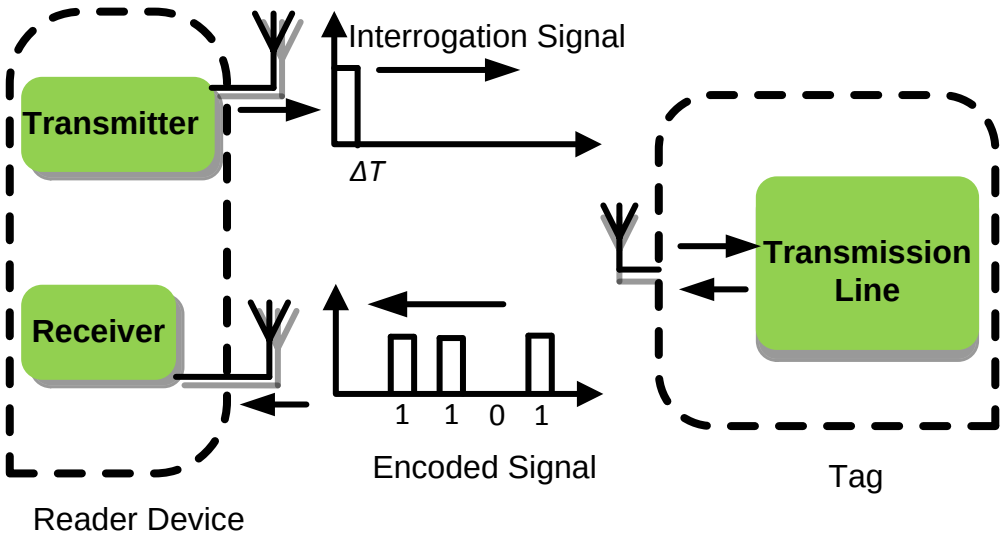

Figure 1.1 Operating principle of TDR RFID system

Figure 1.1 shows the operating principle of the chipless RFID system based on time-domain reflectometry (TDR) technique. This system consists of two main components: reader device and transmission line based RFID tag. The transmission line could be microstrip line, coaxial line or other kinds of transmission line. The tag attached on the object can generate a unique ID code. During the operation, the reader sends the interrogation signal (usually a short-pulse signal with fixed time width ΔT), then the signal will be received by the tag antenna. With a calculated transmission length, the received signal will transmit through a fixed delay. By adding discontinuities during the transmission, it will cause the reflected waves at the fixed time position, which are used for coding the unique binary code, then the encoded signal will be transmitted back through the antenna. Finally, the reader will receive the signal back and extract the ID code, which is also called “On-Off keying (OOK) modulation”.

1.2 Transmission line equations

1.2.1 Lossy transmission lines

A uniform lossy transmission line can be represented by a "distributed circuit", which is divided into an infinite number of cells with infinitesimal length dz. Every infinitesimal cell consists of conductor resistance (*R*), series inductance (*L*), leakage capacitance (*C*) and leakage conductance (*G*) as shown in Figure 1.2[15].

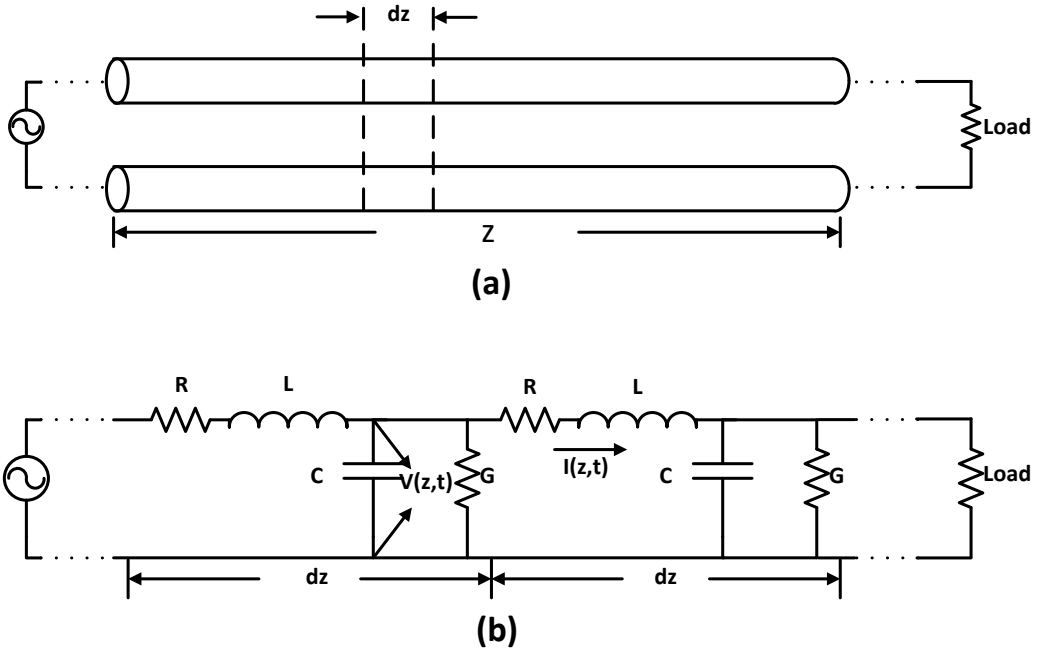

Figure 1.2 (a) A uniform transmission line (b) Distributed circuit representation of transmission lines

Parameter *L* represents the series inductance per cell of the transmission line, *R* represents the series resistance per cell of the transmission line, *C* represents the shunt capacitance per cell of the transmission line, and *G* represents the shunt conductance per cell of the transmission line.

The voltage and the current at *z* and *z*+Δ*z* can be expressed as:

KVL

$$\mathrm{v(z,t)} - \mathrm{R\Delta z i(z,t)} - \mathrm{L\Delta z}\frac{\partial \mathrm{i(z,t)}}{\partial \mathrm{t}} = \mathrm{v(z+\Delta z,t)} \tag{1.1}$$

KCL

$$i(z,t) - G\Delta z v(z+\Delta z,t) - C\Delta z \tag{1.2}$$

Assuming the length $\Delta z \rightarrow 0$, the KVL and KCL equations can be expressed as:

$$\frac{\partial v(z,t)}{\partial z} = -Ri(z,t) - L\frac{\partial i(z,t)}{\partial t} \tag{1.3}$$

$$\frac{\partial i(z,t)}{\partial z} = -Gi(z,t) - C\frac{\partial v(z,t)}{\partial t} \tag{1.4}$$

Equations (1.3) and (1.4) are the time-domain transmission line equations, where the voltage and the current on the line are formulated in terms of the position and the time.

For instantaneous voltage and current, it can be expressed as a function of phasor such that:

$$v(z,t) = Re\{V(z)e^{jwt}\} \tag{1.5}$$

$$i(z,t) = Re\{I(z)e^{jwt}\} \tag{1.6}$$

The derivatives of voltage and the current can be represented in terms of the phasor in equations (1.7) and (1.8), which are also regarded as "frequency-domain transmission line equations".

$$\frac{dV(z)}{dz} = -(R + jwL)I(z) \tag{1.7}$$

$$\frac{dI(z)}{dz} = -(G + jwC)V(z) \tag{1.8}$$

Taking the derivatives of the above equations with respect to *z*.

$$\frac{d^2V(z)}{dz^2} = -(R + jwL)\frac{dI(z)}{dz} \tag{1.9}$$

$$\frac{d^2I(z)}{dz^2} = -(G + jwC)\frac{dV(z)}{dz} \tag{1.10}$$

Then combine the equations (1.7), (1.8) with the equations (1.9), (1.10), the following equations can be found as:

$$\frac{\mathrm{d}^2\mathrm{V}(\mathrm{z})}{\mathrm{dz}^2} = (\mathrm{R} + \mathrm{jwL})(\mathrm{G} + \mathrm{jwc})\mathrm{V}(\mathrm{z}) = \gamma^2\mathrm{V}(\mathrm{z}) \tag{1.11}$$

$$\frac{\mathrm{d}^2\mathrm{I}(\mathrm{z})}{\mathrm{dz}^2} = (\mathrm{R} + \mathrm{jwL})(\mathrm{G} + \mathrm{jwc})\mathrm{I}(\mathrm{z}) = \gamma^2\mathrm{I}(\mathrm{z}) \tag{1.12}$$

where γ is the complex propagation constant of the transmission given by:

$$\gamma = \sqrt{(R + jwl)(G + jwc)} = \alpha + j\beta \tag{1.13}$$

The real part α of the propagation constant γ means the attenuation of the signal in the transmission line with the unit of nepers per meter. The imaginary part β means the phase constant of the signal in the transmission line with the unit of radians per meter.

Finally, the general solutions for the voltage and current wave equations could be represented as functions of propagation constant γ and the position *z*.

$$V(z) = V^+e^{-\gamma z} + V^-e^{\gamma z} \tag{1.14}$$

$$I(z) = I^+e^{-\gamma z} + I^-e^{\gamma z} \tag{1.15}$$

where the $V^+e^{-\gamma z}$ and $I^+e^{-\gamma z}$ describe the wave transmitted in $+z$ direction and the $V^-e^{\gamma z}$ and $I^-e^{\gamma z}$ describe the wave transmitted in$-z$ direction.

The characteristic impedance $\mathrm{Z}_0$is given by

$$Z_0 = \frac{R + jwl}{\gamma} = \sqrt{\frac{R + jwl}{G + jwc}} \tag{1.16}$$

The wavelength of the waves during the transmission could be found as:

$$\lambda = \frac{2\pi}{\beta} \tag{1.17}$$

A key point of designing a TDR based RFID tag is to calculate the speed of electromagnetic wave. The phase velocity accounts for the speed at which a point of fixed phase propagates. For the waveguide with a chosen medium, the phase velocity could be given by:

$$V_p = \frac{w}{\beta} = \frac{w}{\sqrt{k^2 - k_c^2}} \tag{1.18}$$

where:

$$k = \frac{w}{c}\sqrt{\varepsilon_r} \tag{1.19}$$

$$k_c = \sqrt{\left(\frac{m\pi}{a}\right)^2 - \left(\frac{n\pi}{b}\right)^2} \tag{1.20}$$

Parameters a and b mean the width and the height of the rectangular waveguide, m and n represent modes TE_{mn} that propagate in the waveguide, ε_r is the relative permittivity of the waveguide.

The group velocity describes the speed at which the electromagnetic wave travels. For the waveguide with a chosen medium, the group velocity is expressed as:

$$V_g = \frac{c^2}{\varepsilon_r V_p} = \frac{c^2 \beta}{\varepsilon_r w} \tag{1.21}$$

Through equations (1.18) and (1.21), it could be found that phase velocity is faster than the group velocity in the waveguide.

Obviously, for the design of tag, we need to use the delay time along transmission line, which means that the exact travelling time needs to be set and the length of the transmission line needs to be calculated, so the group velocity is adopted.

1.2.2 Transmission line discontinuity

For the incident signal, when it encounters a discontinuity in the transmission line, part of its power will be reflected back and other part of the power will continue to travel along the electrical transmission line as shown in Figure 1.3[16].

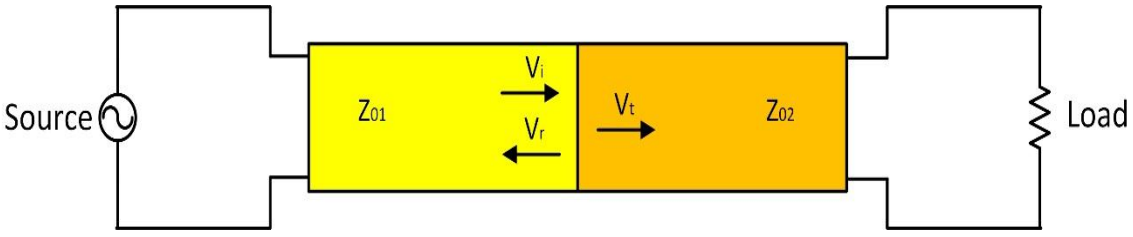

Figure 1.3 Transmission line discontinuity

Parameter Z_{01} represents the characteristic impedance of the left transmission line, Z_{02} represents the characteristic impedance of the right transmission line, V_i represents the voltage of the incident

signal at the boundary, V_t represents the voltage of the transmitted signal at the boundary and V_r represents the voltage of the reflected signal at the boundary.

The reflection coefficient Γ is given by:

$$\Gamma = \frac{V^-}{V^+} = \frac{Z_{02} - Z_{01}}{Z_{02} + Z_{01}} \tag{1.22}$$

The voltage and power of the reflected power are expressed as:

$$V_r = \Gamma \times V_i \tag{1.23}$$

$$P_r = V_r^2 / Z_{01} = \Gamma^2 P_i \tag{1.24}$$

The voltage and power of the transmitted power are expressed as:

$$V_t = (1 - \Gamma) V_i \tag{1.25}$$

$$P_t = 1 - P_r = (1 - \Gamma^2) P_i \tag{1.26}$$

The method of adding the discontinuity in the transmission line is employed to encode the bits of information in the TDR RFID tag design.

1.2.3 Multireflection issue

For the design of a TDR RFID tag with more than one bit of information, more than one discontinuity should be placed along the transmission line with the same interval for encoding the binary code, which will bring up the multireflection issue. For example, the multireflection issue of tag with four discontinuities is shown in Figure 1.4, *Vi* represents the amplitude of the incident wave, $\Gamma_1,\ \Gamma_2,\ \Gamma_3,\ \Gamma_4$ represent respectively the reflection coefficients of the first, second, third and fourth discontinuities, V_1, V_2, V_3, V_4 represent respectively the amplitude of the first, second, third and the fourth reflected waves, *R* represents the interval between two discontinuities, and *Z* represents the distance from the excitation to the first discontinuity.

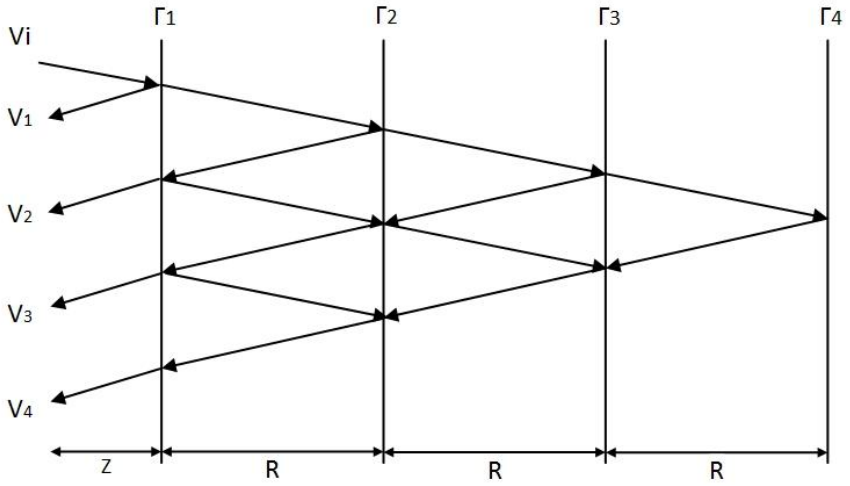

Figure 1.4 Multireflection issue (4 discontinuities)

By utilizing the equations (1.14), (1.25) and (1.26), the amplitude of V_1, V_2, V_3, V_4 could be expressed in terms of propagation constant γ, position z, reflection coefficients $\Gamma_1,\ \Gamma_2,\ \Gamma_3,\ \Gamma_4$ and interval between the two discontinuities R as follows:

$$V_1 = \Gamma_1 e^{-\gamma z} \tag{1.27}$$

$$V_2 = (1-\Gamma_1^2)\Gamma_2 e^{-\gamma(z+2R)} \tag{1.28}$$

$$V_3 = (1-\Gamma_1^2)\Gamma_2^2\Gamma_1 e^{-\gamma(z+4R)} + (1-\Gamma_1^2)(1-\Gamma_2^2)\Gamma_3 e^{-\gamma(z+4R)} \tag{1.29}$$

$$V_4 = (1-\Gamma_1^2)(\Gamma_1\Gamma_2)^2\Gamma_2 e^{-\gamma(z+6R)} + (1-\Gamma_1^2)(1-\Gamma_2^2)\Gamma_2\Gamma_3^2 e^{-\gamma(z+6R)} + (1-\Gamma_1^2)(1-\Gamma_2^2)(1-\Gamma_3^2)\Gamma_4 e^{-\gamma(z+6R)} \tag{1.30}$$

1.2.4 Design equations for TDR RFID tag

In the RFID system based on TDR technique, the tag could be regarded as one-port component. The integrated antenna is not only used for receiving the interrogation signal but also for reflecting back the encoded signal. Assuming t_t represents the total transmission time from the integrated antenna to the terminal of the tag, t_r represents the transmission time between two discontinuities, n is the number of the bits of information, t_s represents the time width of the interrogation signal, t_0 means the time from the antenna to the first discontinuity, t_f means the transmission time in the free space, t_a represents the duration of system operation, the relationship among them should be arranged as Figure 1.5 shows.

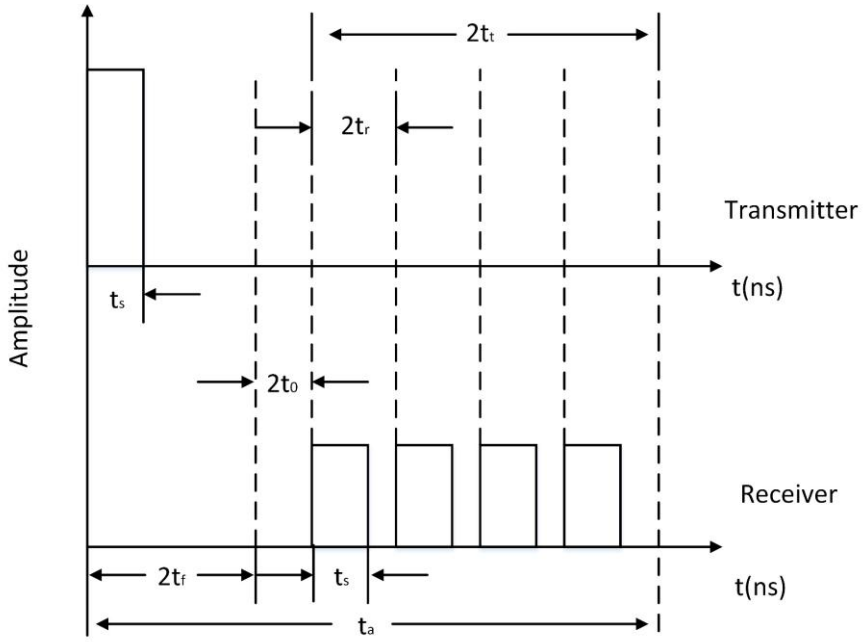

Figure 1.5 Rules of TDR RFID tag design

where:

$$t_a = 2\left(t_f + t_0 + 3t_r\right) \tag{1.31}$$

$$L = 3R + Z = t_t V_g = (3t_r + t_0)V_g \tag{1.32}$$

$$2t_r > t_s \tag{1.33}$$

Equation (1.31) means that because the reader sends the interrogation signal and listens to the echoes from the tag, parameters t_f, t_0 and t_r will be doubled. Equation (1.32) represents the calculation of total transmission length L of the tag. Equation (1.33) is arranged in order to distinguish the two neighbouring bits of information.

1.2.4.1 Interrogation signal

Generally, the time width of the interrogation signal t_s will affect the size of the tag and the bandwidth of it will determine the bandwidth of the tag antenna. Nowadays, the commercial reader device could generate a 2 ns time width pulse signal, so this pulse signal with the carrier of 35 GHz is considered as the interrogation signal of the system. The waveform and the spectrum of it could be expressed in Figure 1.6 and Figure 1.7.

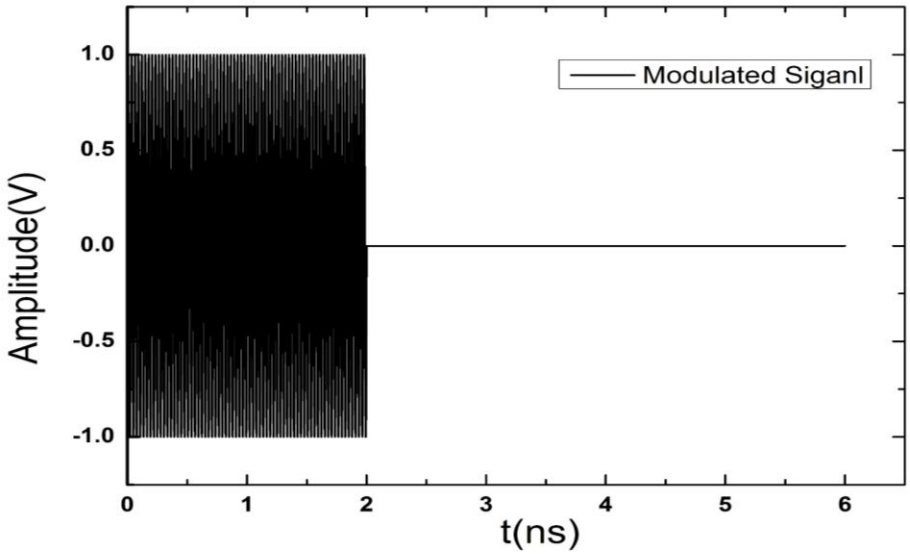

Figure 1.6 Interrogation signal

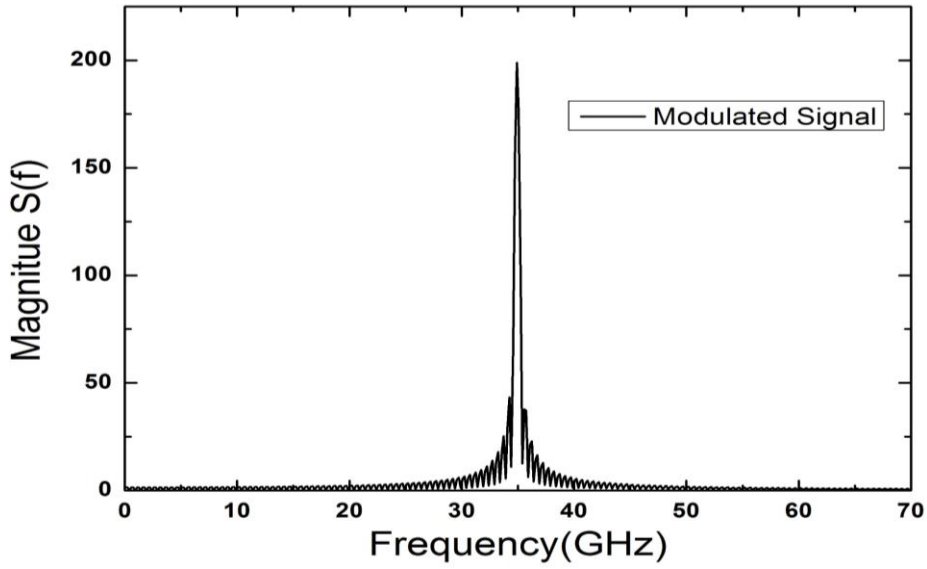

Figure 1.7 Spectrum of the interrogation signal

1.2.4.2 Interval between two neighbouring discontinuities

In the TDR MMID tag design, the doubled transmission time $2t_r$ should be larger than the time width of the interrogation signal t_s in order to distinguish the two neighbouring "1" information, and t_r should be as small as possible in order to reduce the tag size.

In RFID system, the interrogation signal will encounter some distortion upon received by the tag antenna. Over the millimeter-wave band, it is possible to design the antenna with 1 GHz bandwidth, and after the interrogation signal received by the antenna with 1 GHz bandwidth, assuming the antenna acts as a perfect bandpass filter, the waveform of the signal in frequency domain and in time domain could be evaluated as in Figure 1.8 and Figure 1.9.

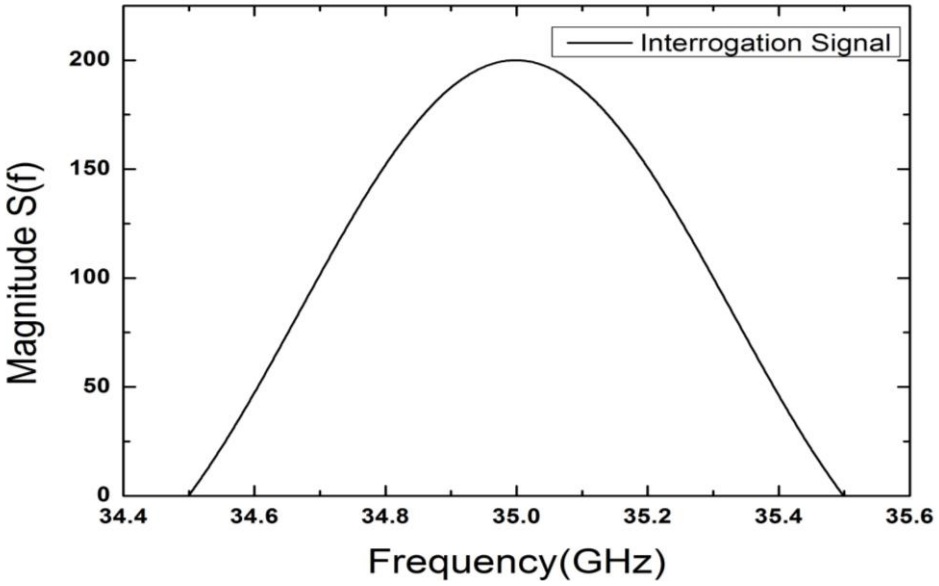

Figure 1.8 Spectrum of the interrogation signal after tag antenna

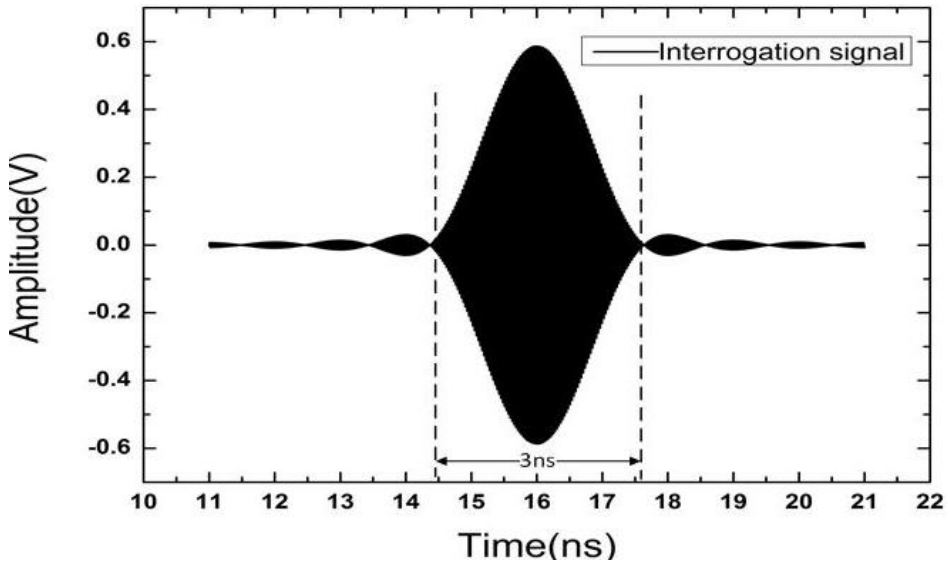

Figure 1.9 Interrogation signal received by tag antenna (time-domain)

Through Figure 1.8, it can be found that after received by the antenna with 1 GHz bandwidth, the high frequency and the low frequency are attenuated, central frequency of 35 GHz with 1 GHz bandwidth remains the same. Through Figure 1.9, the mutation from "0" to "1" of the interrogation signal is disappeared which is replaced by the smooth curve from "0" to "1", and the time width of the signal is expanded from 2 ns to 3 ns. In order to decode the two neighbouring "1" information, t_r should be at least 0.5 ns to read the binary code "11" as shown in Figure 1.10.

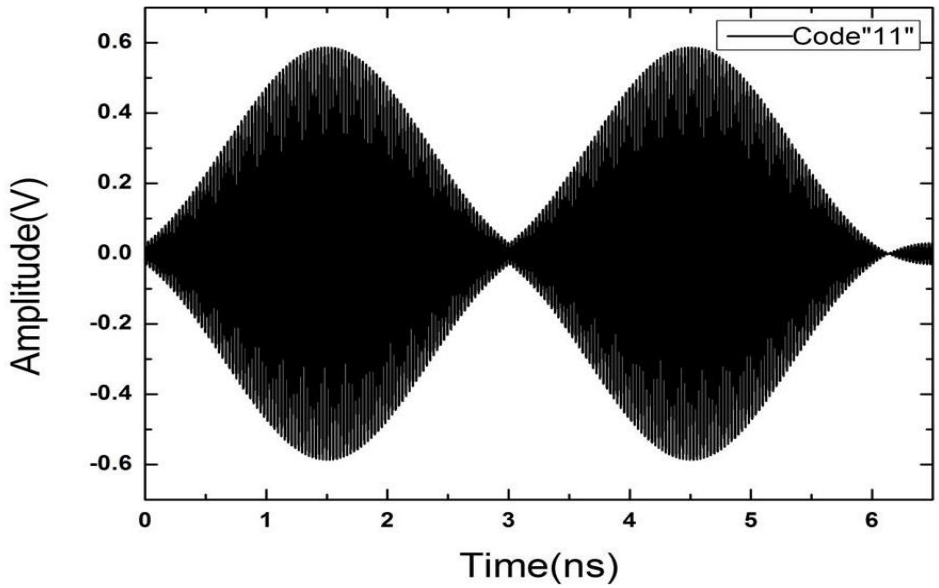

Figure 1.10 Binary code "11"

1.3 Equalization method

1.3.1 Theoretical modelling

In order to deal with the existing multireflection issue during the TDR MMID tag design, a theoretical modelling is developed by adopting the equations (1.27-1.30). In this modelling, the time width of the interrogation signal t_s=2 ns, the transmission time of the interval between two neighbouring discontinuities t_r =0.5 ns and the transmission time from the antenna to the first discontinuity t_0=0.1 ns. For the 4-bits TDR MMID tag design as an example in this work, the amplitude of the four reflected wave could be expressed as follows:

The first reflected wave:

$$V_1 = \Gamma_1 \times e^{-(\alpha+j\beta)\times 0.1 V_g \times 10^{-9}} \tag{1.34}$$

The second reflected wave:

$$V_2 = \left(1-\Gamma_1{}^2\right) \times \Gamma_2 \times e^{-(\alpha+j\beta)\times 3.1 \times V_g \times 10^{-9}} \tag{1.35}$$

The third reflected wave:

$$V_3 = \left(1-\Gamma_1{}^2\right)\Gamma_2^2\Gamma_1 e^{-(\alpha+j\beta)\times 6.1 \times V_g * 10^{-9}} + (1-\Gamma_1{}^2)(1-\Gamma_2^2)\Gamma_3 e^{-(\alpha+j\beta)\times 6.1 \times V_g \times 10^{-9}} \tag{1.36}$$

The fourth reflected wave:

$$\begin{aligned} V_4 = {} & (1-\Gamma_1^2)(1-\Gamma_2^2)(1-\Gamma_3^2)\Gamma_4 e^{-(\alpha+j\beta)\times 9.1 \times V_g \times 10^{-9}} \\ & + (1-\Gamma_1^2)(\Gamma_1^2\Gamma_2^2)\Gamma_2 e^{-(\alpha+j\beta)\times 9.1 \times Vg \times 10^{-9}} \\ & + (1-\Gamma_1^2)(1-\Gamma_2^2)\Gamma_2\Gamma_3^2 e^{-(\alpha+j\beta)\times 9.1 \times Vg \times 10^{-9}} \end{aligned} \tag{1.37}$$

where parameters α and β represent the attenuation constant and the phase constant of the transmission line, V_g represents the group velocity and Γ_1, Γ_2, Γ_3, Γ_4 represent the reflection coefficient of the four discontinuities.

In the case of Γ_1, Γ_2, Γ_3, Γ_4 equal to 0.25, the amplitude of the interrogation signal equals to 1 and α=1.6 neper/m, β= 1000 rad/m, V_g=1.5×10^8 m/s, the amplitude of the reflected wave can be calculated by the above modelling approach as described in Figure 1.11.

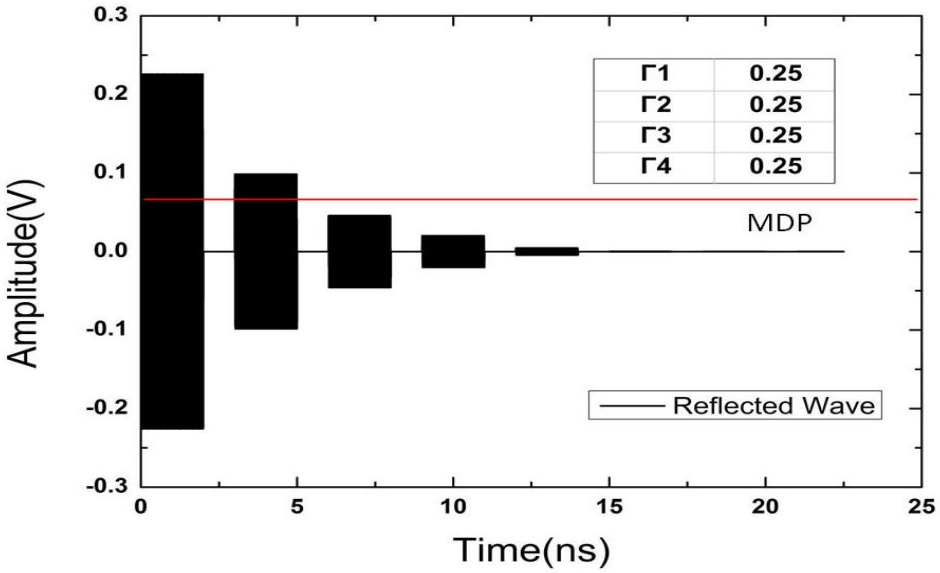

Figure 1.11 Non-optimized reflected wave

Through Figure 1.11, the amplitude of reflected wave will decrease with time, so the information encoded in the subsequent bits will be lost since they are below the minimum detectable power (MDP) of the system. It could be found that the amplitude of the first two bits are higher than MDP, it is possible to transfer part of power from the early bits to the subsequent bits to maximize the encodable bits of the tag.

1.3.2 Lsqcurvefit

Lsqcurvefit is one kind of optimization method in Matlab which is used to solve the nonlinear curve-fitting (data-fitting) problems in a least-squares sense, it could be expressed as [17, 18].

$$\min_x \|F(x, xdata) - ydata\|_2^2 = \min_x \sum_i (F(x, xdata_i) - ydata_i)^2 \tag{1.38}$$

where *x* is variable that defines the value of $F(x, xdata_i)$, which has the lower and upper bounds *lb* and *ub*, $F(x, xdata_i)$ is regarded as the input of the method, $ydata_i$ is considered as the goal of the optimization. All the parameters can be vectors or the matrices, for $F(x, xdata_i)$ and $ydata_i$, they need to have the same length during the operation.

1.3.3 Equalization method

The equalization method is proposed in this work based on the above-presented theoretical modelling and "lsqcurvefit" in order to maximize the encodable bits of the tag.

In this method, the parameters should be set as follows:

$$x = [\Gamma_1, \Gamma_2, \Gamma_3, \Gamma_4\ ] \tag{1.39}$$

$$xdata = [V_1, V_2, V_3, V_4] \tag{1.40}$$

$$lb = [0,0,0,0] \tag{1.41}$$

$$ub = [1,1,1,1] \tag{1.42}$$

$$ydata = [A(0), A(0), A(0), A(0)] \tag{1.43}$$

where *x* is set as four reflection coefficients of each discontinuity, *xdata* is set as the amplitudes of the reflected waves, *lb* and *ub* are set as the equation (1.41) and equation (1.42) show because the reflection coefficient has the range from 0 to 1, *ydata* could be set with respect to the binary code that needs to be encoded. For example, for the binary code "1111", *ydata* is set to be "[*A, A, A, A*]" and for the binary code "1101", *ydata* is set as "[*A, A, 0, A*]", where *A* represents the amplitude of the reflected wave.

The advantage of this method is that during operation, we can increase the value of *A* to increase the value of Γ_1, Γ_2, Γ_3, Γ_4, the sign of the end of this optimization method is Γ_4=1, which reaches the upper bound and after the optimization, the maximum value of *A* is found. The physical meaning of it is the last discontinuity is short-circuited and all the power received by the antenna will be used for encoding the bits of information, *A* represents the maximum amplitude of the reflected wave. Meanwhile, the exact value of each reflection coefficient Γ_1, Γ_2, Γ_3, Γ_4 could be extracted through the matrix *x*.

By applying this equalization method to the non-optimized amplitude of the reflected wave in Figure 1.11, the optimized results of the binary code "1111" and the binary code "1101" could be calculated as shown in Figure 1.12 and Figure 1.13.

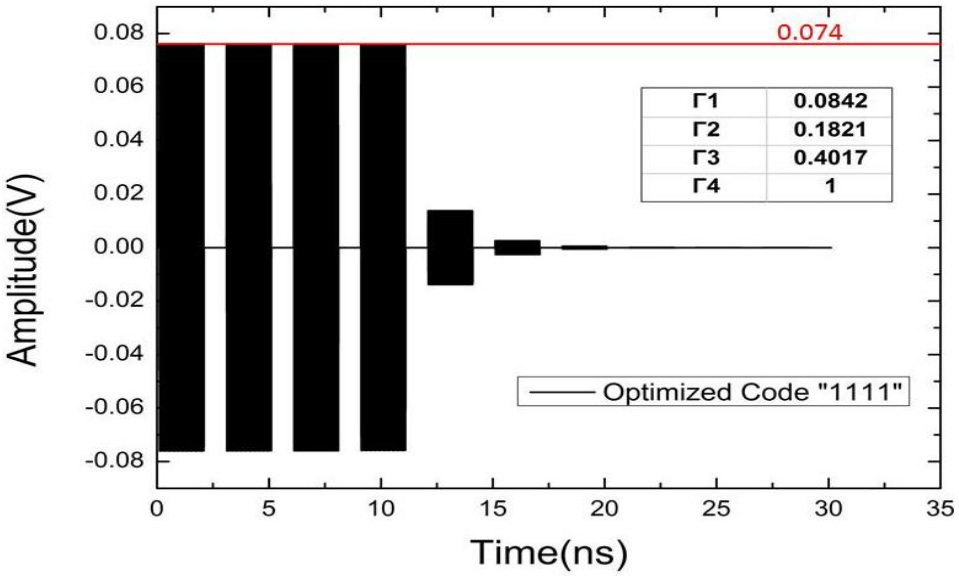

Figure 1.12 Optimized binary code “1111”

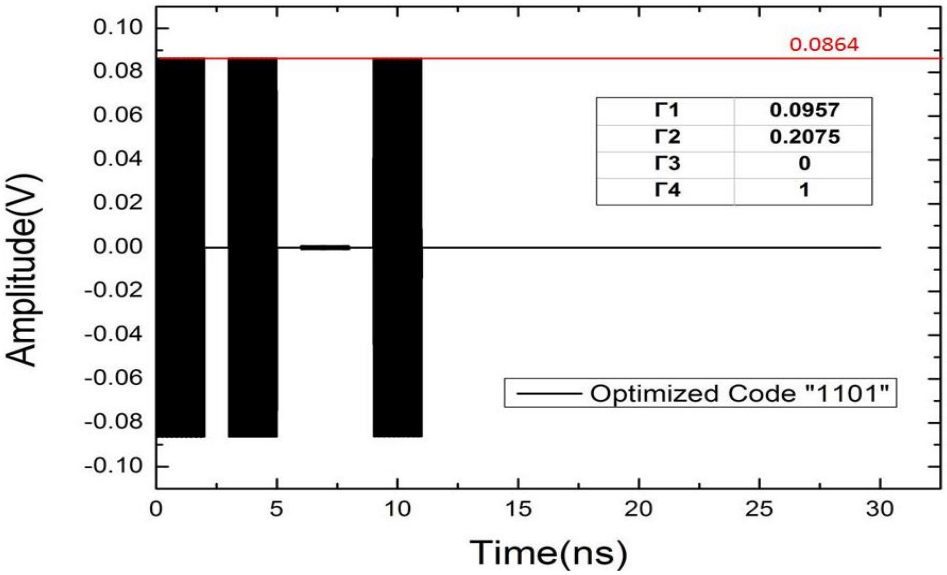

Figure 1.13 Optimized binary code “1101”

Through the above figures, we can find that “0.074” is the maximum amplitude for the binary code “1111” and “0.0864” is the maximum amplitude for the binary code “1101”. The reflection coefficient of each discontinuity for generating the results is also tabulated in the figures, and compared with the non-optimized results, two more bits of information could be detected.

1.4 Link budget of TDR MMID system

The link budget is used for calculating all the gains and the losses from the transmitter to the receiver, it describes the power of the RF signal at any point of the system. The link budget of a passive TDR MMID system is easy to get analyzed because the receiver (tag) has no on-board power supply, it only relies on the power from the reader for encoding the bits of information. The goal of the investigation is to find the power received by the tag and the power finally reflected back to the reader at the particular condition. Furthermore, it will help define MDP of the system [19-23].

Figure 1.14 shows the schematic of the link budget in a TDR MMID system, where Pt_{reader} represents the power transmitted from the reader, Pr_{tag} represents the power received by the tag, G_{reader} represents the gain of the reader antenna, G_{tag} represents the gain of the tag antenna, Pr_{reader} represents the power finally received by the reader, *R* represents the distance between the tag and the reader.

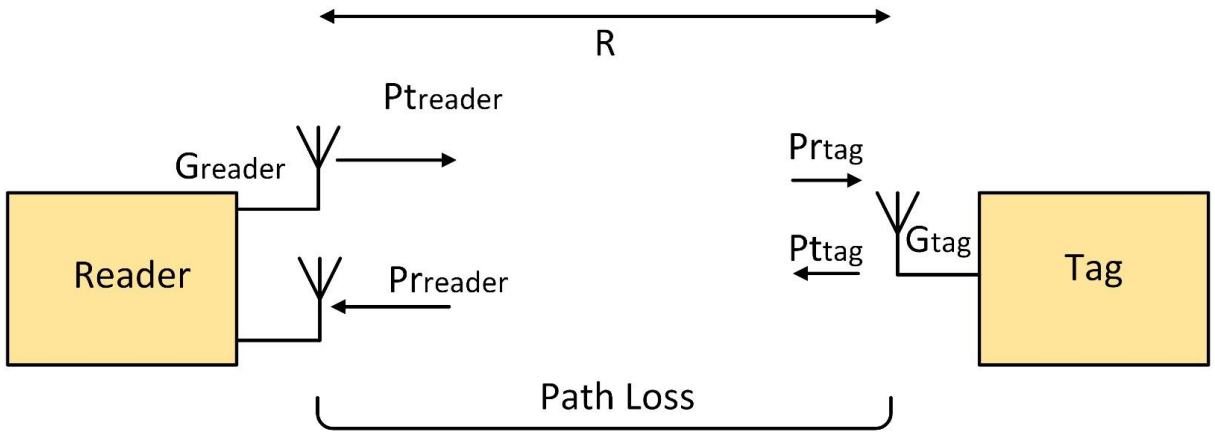

Figure 1.14 Link budget of TDR RFID system

Typically, the link budget of the MMID system could be evaluated by the famous Friis equation, which can describe the power transmission between two antennas in ideal case [24].

The power received by the tag can be expressed as follows:

$$Pr_{tag} = Pt_{reader} + G_{reader} + G_{tag} + 20Log\left(\lambda/_{4\pi R}\right) \tag{1.44}$$

The power finally received by the receiver can be expressed as follows:

$$Pr_{reader} = Pt_{tag} + G_{reader} + G_{tag} + 20Log\left(\lambda/_{4\pi R}\right) \quad (1.45)$$

The relationship between Pr_{tag} and Pr_{reader} can be expressed as follows:

$$Pt_{tag} = Pr_{tag} \times e^{-\alpha z} \times \Gamma_i^2 \qquad i = 1,2,3,4 \quad (1.46)$$

where α represents the attenuation constant of the transmission line, $20Log\left(\lambda/_{4\pi R}\right)$ represents the path loss in the MMID system, and Γ_i $(i = 1,2,3,4)$ represents the reflection coefficient of each discontinuity.

The characteristics of the TDR MMID system is tabulated in Table 1-1, the sensitivity of the reader is set to be -80 dBm, which is available in today's market, the gain of reader antenna is set to be 20 dBi, which is possible to be realized by the use of a horn antenna, the gain of the tag antenna is set to be 5 dBi, which is also possible to be designed at 35 GHz.

Table 1-1 Characteristics of TDR MMID system

$\boldsymbol{Pt_{reader}}$	$\boldsymbol{Pr_{reader}}$	$\boldsymbol{G_{reader}}$	$\boldsymbol{G_{tag}}$	**Frequency**
-80 dBm	10 dBm	20 dBi	5 dBi	35 GHz

By applying the equation (1.44), the power received by the tag based on the characteristics in Table 1-1 versus the distance could be calculated in Figure 1.15. As shown here, the power received by the tag will decrease with the distance.

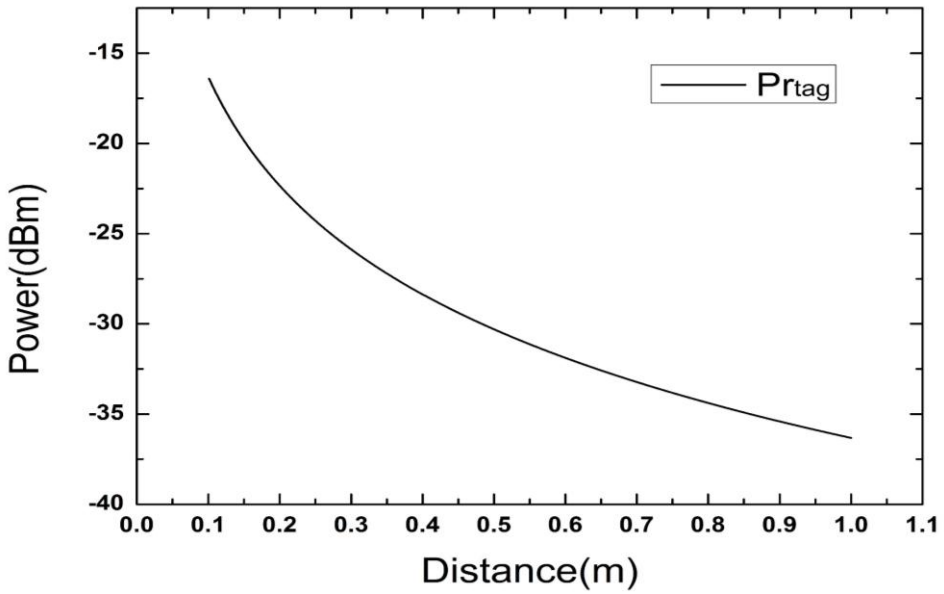

Figure 1.15 Power received by the tag

By applying the equation (1.45), the minimum power that needs to be reflected back from the tag to ensure the encoded bits of information detectable versus the distance could be calculated in Figure 1.16, it could be found that the value will increase with the distance.

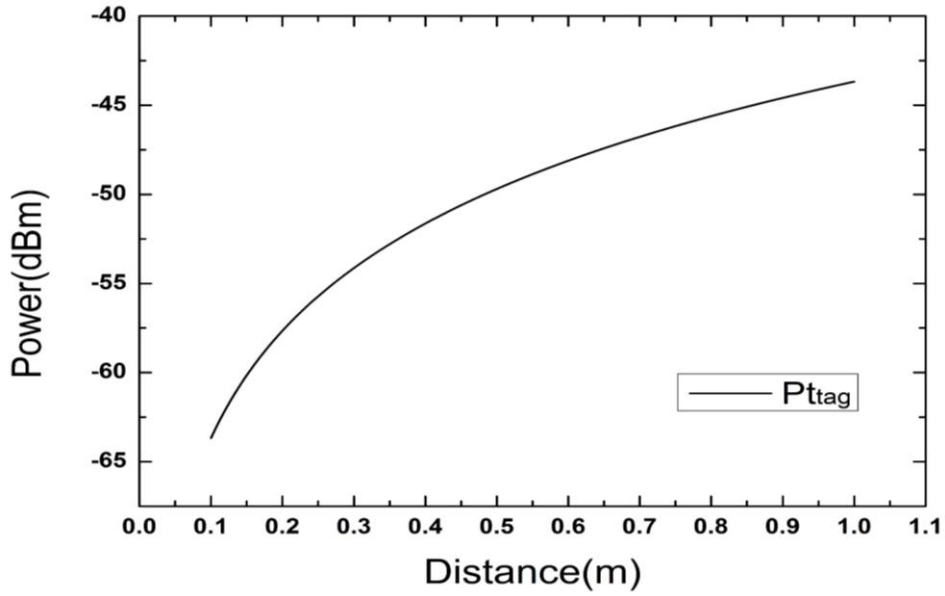

Figure 1.16 Minimum power to be reflected back

With the two values as discussed above, the ratio *K* between the minimum amplitude of the reflected signal *Vttag* and the amplitude of the signal received by the antenna *Vrtag* could be calculated by equation (1.47), and the relationship versus the distance is shown in Figure 1.17.

$$K = \sqrt{10^{Pt_{tag}/10}/10^{Pr_{tag}/10}} \tag{1.47}$$

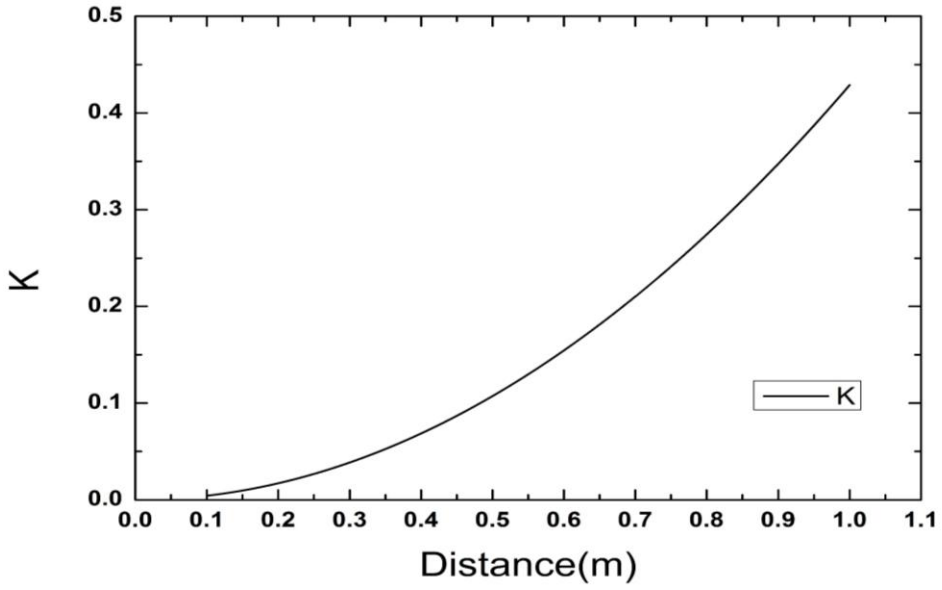

Figure 1.17 Ratio between *Vttag* and *Vrtag*

The MMID tag could be regarded as a black box as shown in Figure 1.18. In the previous equalization method, the *Vrtag* is normalized to 1, so the following design rule needs to be satisfied in order to ensure the encoded bits of information detectable.

Design rule:

$$A \geq K \tag{1.48}$$

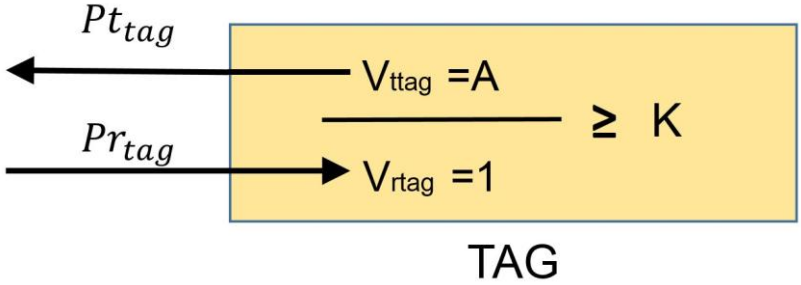

Figure 1.18 Design rules of TDR MMID tag

1.5 Maximum encodable bits

Based on the above analysis, a combination of the equalization method and the link budget of the TDR MMID system is proposed to maximize the encodable bits in the tag, which is processed by the following steps.

- Build the theoretical modelling of multireflection issue based on the capacity of the tag *N*.
- In the equalization method, by adjusting the value of *A* to make the reflection coefficient of the last discontinuity $\Gamma_N = 1$, then the maximum amplitude of the reflected signal *A* is obtained.
- Based on the characteristic of the MMID system, the power received by the tag and the minimum power that needs to be reflected back could be found, and the ratio *K* between *Vttag* and *Vrtag* versus the distance could be extracted.
- Set the condition that $A = K$, which means the maximum power of the bits of information equals to the Minimum Detectable Power (MDP) of the system. At a fixed distance, the maximum encodable bits could be found which equals to the length of the matrix *ydata*.

In order to verify the proposed method, the characteristic of the MMID system discussed above is considered as an example. Following the above-described execution and design procedure, the

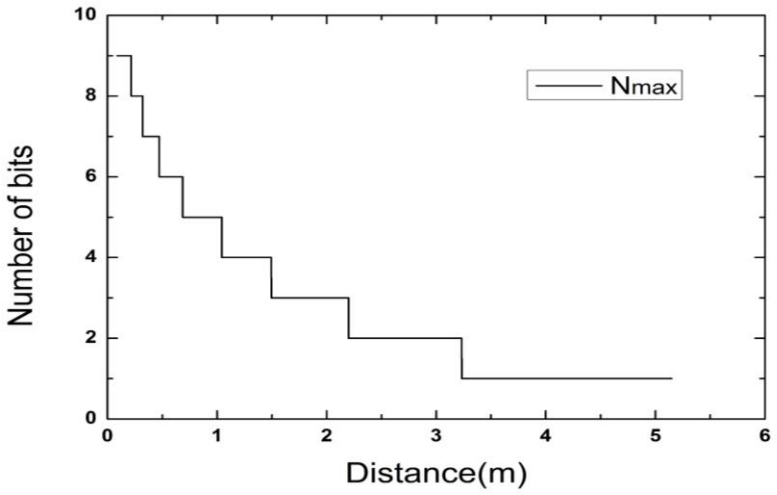

Figure 1.19 Maximum encodable bits

yielded result is shown in Figure 1.19.

As shown in Figure 1.19, the maximum encodable bits versus the distance will decrease with the range of the TDR MMID system, showing the feasibility of this proposed method. For example, at the fixed distance of 1 m, the maximum encodable bits for the tag is “4”, but for the fixed distance of 2 m, the maximum encodable bits is reduced to “3”.

CHAPTER 2 CHIPLESS MMID TAG BASED ON TDR MODULATION

2.1 Full-mode substrate integrated waveguide tag

2.1.1 Introduction

The substrate integrated waveguide (SIW) has received great interest in designing the components over millimeter-wave band in the past few decades [25] [26]. With this technique, passive components and active devices could be integrated in the same printed circuit board (PCB), which leads to the minimization of system size. Moreover, the SIW structure has a similar propagation constant as the classical rectangular waveguide, which offers the benefits of high-Q, high power capability and easy integration etc. Compared with the cost of traditional waveguide, SIW fabrication is cheaper which ensures the possibility of a mass-production of millimeter-wave integrated circuits.

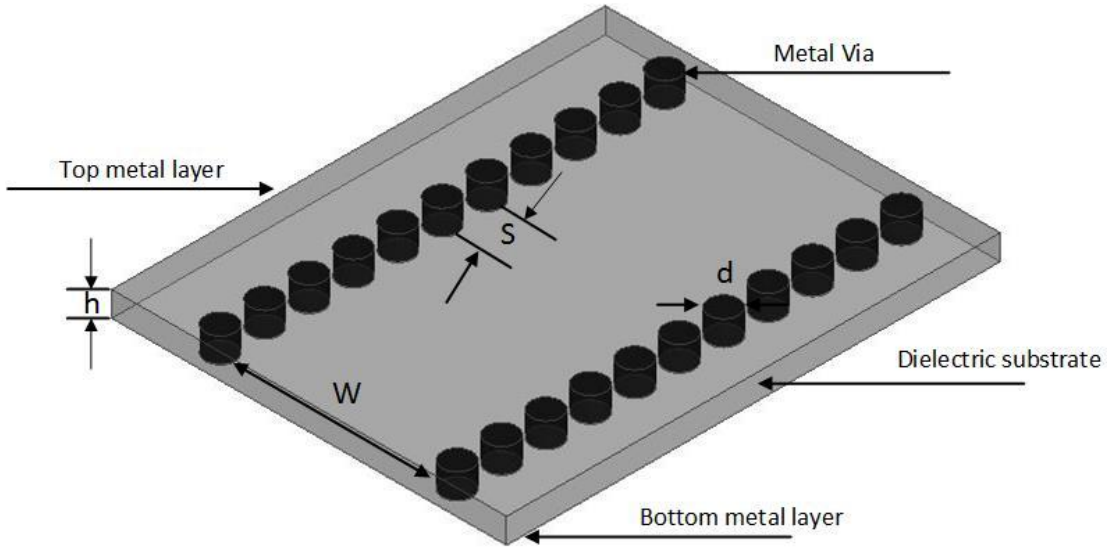

Figure 2.1 Geometry of SIW

Figure 2.1 shows the geometry of SIW, *h* represents the height of substrate, *w* represents the physical width of waveguide, *d* represents via diameter and *s* is the spacing between two adjacent vias. It is one kind of rectangular waveguide which is formed by the top metal layer and the bottom metal layer with the substrate sandwiched between them, the two bilateral sides are rows of periodic

metal vias which could be regarded as equivalent electrical walls, and the spacing between the two vias will affect the amount of leakage power during the transmission.

The transverse electric (TE) modes have no electric field in the direction of propagation and the transverse magnetic (TM) modes have no magnetic field in the direction of propagation. Due to the gaps between the metal vias, only TE_{mn} modes are supported in the SIW structures.

According to [27, 28], the effective width of SIW is calculated by the equation (2.1)

$$w_{eff} = w - 1.08\frac{d^2}{s} + 0.1\frac{d^2}{w} \tag{2.1}$$

The cut-off frequency of rectangular waveguide could be calculated by the equation (2.2)

$$f_c = \frac{c}{2\pi\sqrt{\varepsilon_r}}\sqrt{\left(\frac{m\pi}{a}\right)^2 + \left(\frac{n\pi}{b}\right)^2} \tag{2.2}$$

where ε_r represents the dielectric constant of the substrate, *m* and *n* represent the modes transmitted in the structure, *a* represents the width of the waveguide and *b* represents the height of the waveguide. In particular, the fundamental mode in SIW structure is the TE_{10} mode, by combining the equation (2.1) with equation (2.2), the cut-off frequency of SIW structure could be evaluated in equation (2.3).

$$f_c = \frac{c}{2w_{eff}\sqrt{\varepsilon_r}} \tag{2.3}$$

The bandwidth of the fundamental mode in SIW is from fc to nearly $2fc$. For the MMID tag based on the Rogers 6002 with the dielectric permittivity of 2.94, the minimum effective width is calculated to be 2.88 mm at 35 GHz. In order to avoid the propagation of potential higher modes, the SIW width is considered to be 4.2 mm.

2.1.2 Extraction of propagation constant of SIW

In order to characterize the modes supported in the SIW and to extract its propagation constant, the SIW model is simulated in the Ansoft High Frequency Structure Simulator (HFSS). The dielectric filled in the waveguide is Rogers 6002 with the thickness of 20mil, which has the dielectric permittivity of 2.94. The dimensions of the waveguides are tabulated in Table 2-1.

Table 2-1 Dimensions of SIW

d	***s***	***h***	***w***
0.6 mm	0.9 mm	20 mil	4.2 mm

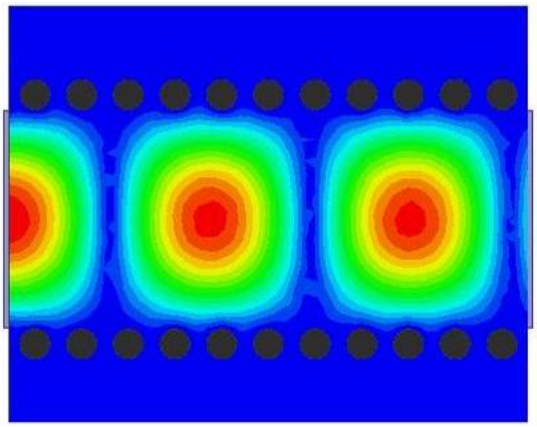

Figure 2.2 Magnitude of electric field in SIW

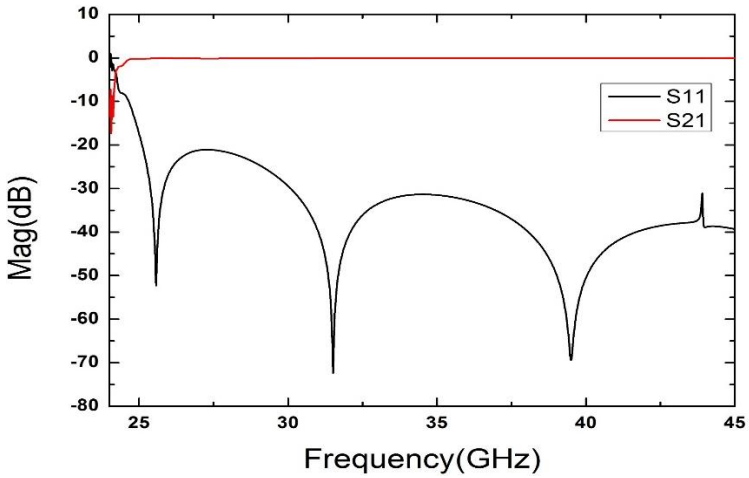

Figure2.3 S parameters of SIW transmission line

Figure 2.2 shows that the TE_{10} mode is supported in SIW at 35 GHz and through a full-wave simulation, forward gain or transmission coefficient S_{21} and return loss S_{11} could be calculated in Figure 2.3, where the cut-off frequency is found to be 25.5 GHz.

2.1.2.1 Attenuation constant α_{siw}

In [29], the loss in SIW could be concluded as the total contribution of: conductor loss α_c, dielectric loss α_d and radiation loss α_r. The conductor loss and the dielectric loss are similar to the traditional rectangular waveguide, but the radiation loss is a unique characteristic of SIW.

2.1.2.1.1 Conductor loss α_c

The conductor loss in SIW is caused by the finite conductivity in the top and bottom metal layer as well as the metal vias, by adopting the formula derived for the rectangular waveguide, the conductor loss α_c could be calculated with equation (2.4).

$$\alpha_c = \frac{\sqrt{\pi f \varepsilon_0 \varepsilon_r}}{h\sqrt{\sigma_c}} \frac{1 + \frac{2(f_0/f)h}{w_{eff}}}{\sqrt{1-(f_0/f)^2}} \tag{2.4}$$

where ε_o represents the dielectric permittivity of vacuum, ε_r represents the relative dielectric permittivity of substrate, h represents the thickness of SIW, σ_c represents the metal conductivity, and w_{eff} represents the equivalent width of SIW.

2.1.2.1.2 Dielectric loss α_d

The dielectric loss in SIW is caused by the dielectric filled in the rectangular waveguide, same as conductor loss, by adopting the formula derived for the rectangular waveguide, the dielectric loss could be calculated with equation (2.5).

$$\alpha_D = \frac{\pi f \sqrt{\varepsilon_r}}{c\sqrt{1-(f_0/f)^2}} tan\delta \tag{2.5}$$

where $tan\delta$ represents the loss tangent of the dielectric.

2.1.2.1.3 Radiation loss α_r

The radiation loss in SIW is caused by the gaps between the metal vias, the distance of the gaps will determine the power loss due to the radiation. For the reason that this is the unique characteristics in SIW structures, the traditional formula derived for the rectangular waveguide is not available for the calculation. The method based on the analytical decomposition of TE_{10} mode into two plane waves is proposed, where the radiation loss could be evaluated with equation (2.6).

$$\alpha_R = \frac{\frac{1}{w}\left(\frac{d}{w}\right)^{2.84}\left(\frac{s}{d}-1\right)^{6.28}}{4.85\sqrt{\left(\frac{2w}{\lambda}\right)^2-1}} \tag{2.6}$$

The comparison between the simulated results and the calculated results regarding the total loss in SIW has been given in Figure 2.4.

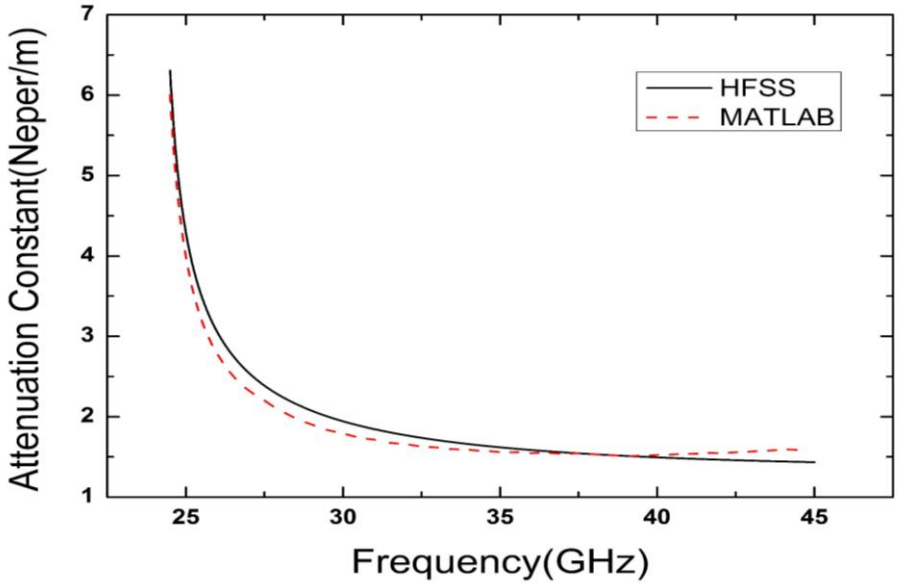

Figure 2.4 Attenuation constant of SIW

In Figure 2.4, the red curve represents the calculated results through Matlab, the black curve represents the simulated results by HFSS. It could be observed that the simulated results roughly correspond to the calculated results. Finally, the value of the attenuation constant α_{siw}=1.68 neper/m at 35 GHz (the operating frequency of the MMID system) is considered for the equalization method proposed in chapter 1.

2.1.2.2 Phase constant β_{siw}

The analysis of the phase constant β_{siw} of SIW is the key point for the MMID tag design because the value of β_{siw} will not only determine the group velocity of SIW but also arouse the dispersion issue.

The phase constant β_{siw} versus frequency is calculated in Figure 2.5. For the SIW tag design, the value of the phase constant β_{siw}=1008 rad/m at 35 GHz is considered for the equalization method proposed in chapter 1.

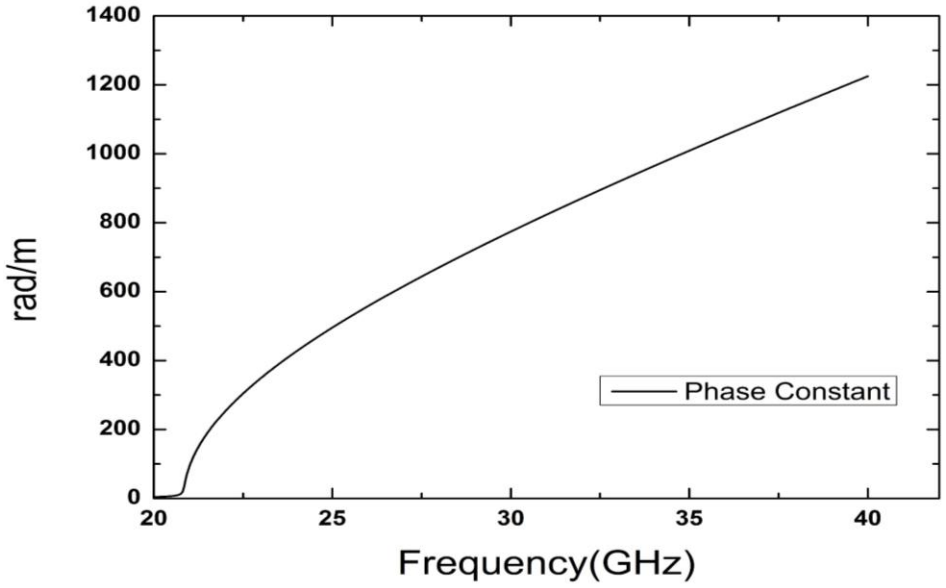

Figure 2.5 Phase constant of SIW

2.1.3 Distortion

2.1.3.1 Group velocity of SIW V_{gsiw}

When the interrogation signal transmits along the SIW, the distortion of the interrogation signal could be divided into two parts: dispersion and attenuation. The group delay τ_{gsiw} represents the time delay of amplitude envelopes versus frequency in SIW, which could be used to describe the dispersion issue as expressed in equation (2.7).

$$\tau_g = -\frac{d(\emptyset(e^{-(\alpha+j\beta)L}))}{d\omega} \tag{2.7}$$

where $\emptyset(e^{-(\alpha+j\beta)L})$ represents the total transmission radian of the interrogation signal and ω represents the angular velocity.

In order to characterize the distortion issue in SIW, the value of α_{siw} and β_{siw} over the frequency range from 34.5 GHz to 35.5 GHz is extracted through (2.7), we can adjust the value of the

transmission length L to make τ_{gsiw}= 3 ns at the centre frequency of 35 GHz, which meets the criteria set in chapter 1.

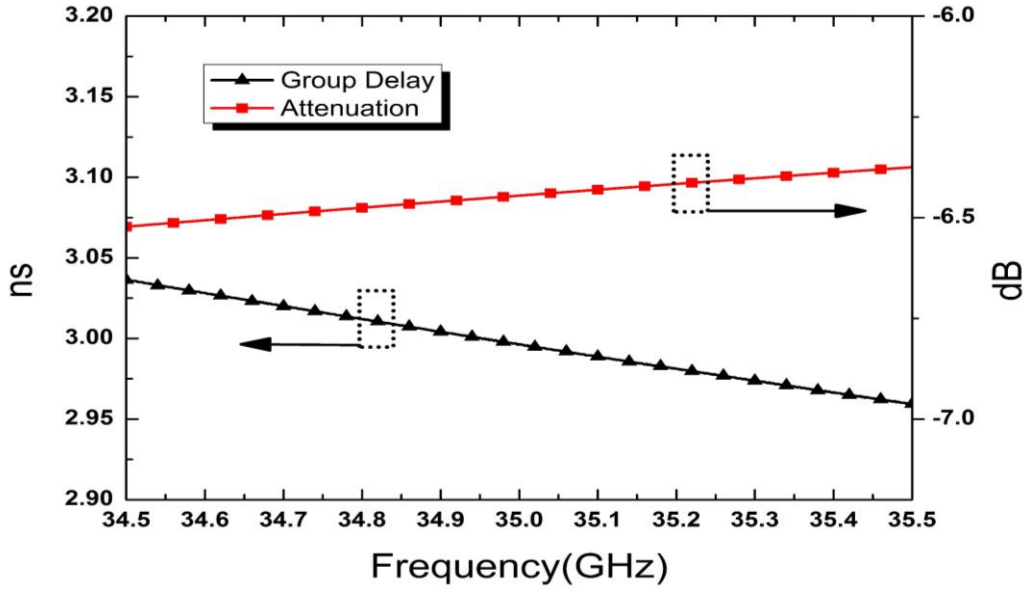

Figure 2.6 Group delay and attenuation (SIW)

As Figure 2.6 shows, the red curve represents the attenuation of the signal, which increases with frequency. The black curve represents the group delay of signal, which decreases with frequency. With the optimized L=42.3 cm, the group delay of 3 ns at 35 GHz is generated and it could be observed that the interrogation signal is expanded from 3 ns to 3.08 ns. This level of distortion is acceptable for the interval of 1 ns between two neighbouring pulses.

Then the group velocity of the signal in SIW V_{gsiw} can be calculated by the equation (2.8).

$$V_{gsiw} = \frac{L}{\tau_g} = 1.41 * 10^8\ m/s \tag{2.8}$$

2.1.3.2 Interrogation signal distortion

The spectrum of the interrogation signal after the transmission length of 42.3 cm could be calculated by (2.9), which is shown in Figure 2.7.

$$fo = fs * e^{-(\alpha + j\beta)L} \tag{2.9}$$

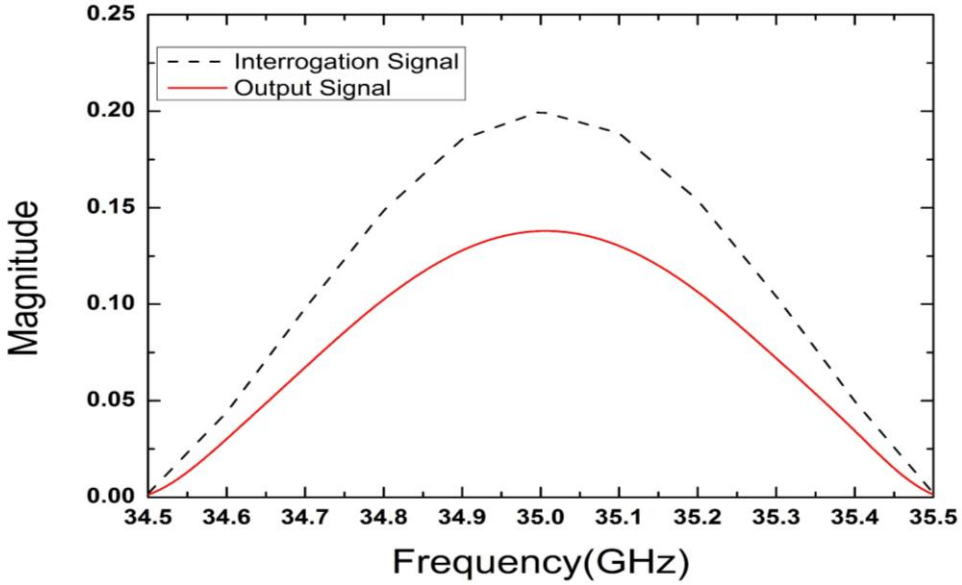

Figure 2.7 Spectrum of output signal (SIW)

Inverse Fourier transform is performed based on the spectrum of the output signal in order to find the output signal in time domain.

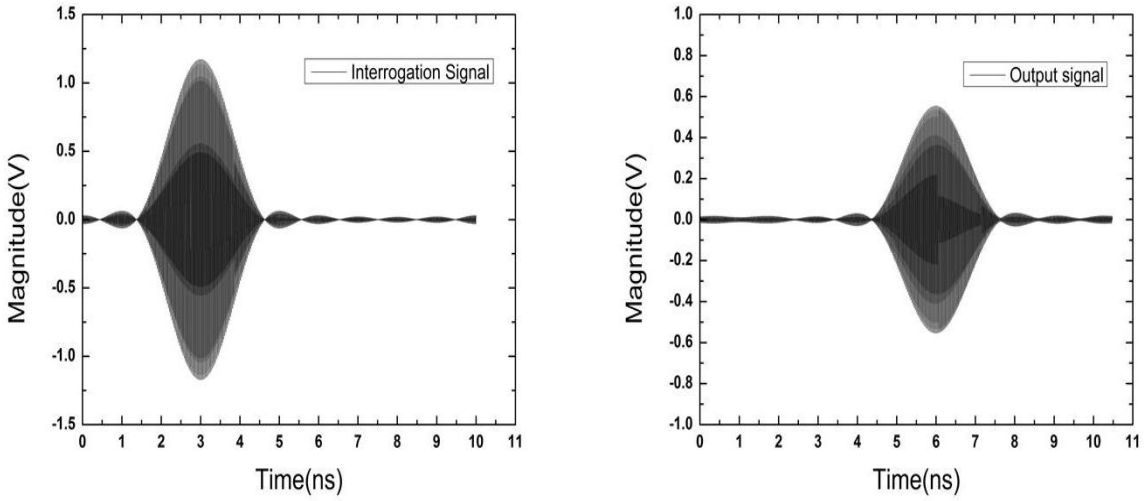

Figure 2.8 Interrogation signal and output signal (SIW)

Through Figure 2.8, it could be observed that the time delay of the amplitude envelope of 3 ns is achieved with the transmission length of 42.3 cm and the interrogation signal is expanded from 3 ns to 3.08 ns.

2.1.4 Meander-line based SIW tag

2.1.4.1 Discontinuities

With the extracted α_{siw}=1.68 neper/m, β_{siw}=1008 rad/m and V_{gsiw}=1.41*10^8 m/s, by applying the equalization method proposed in chapter 1, the reflection coefficient of every discontinuity could be calculated and given in Figure 2.9.

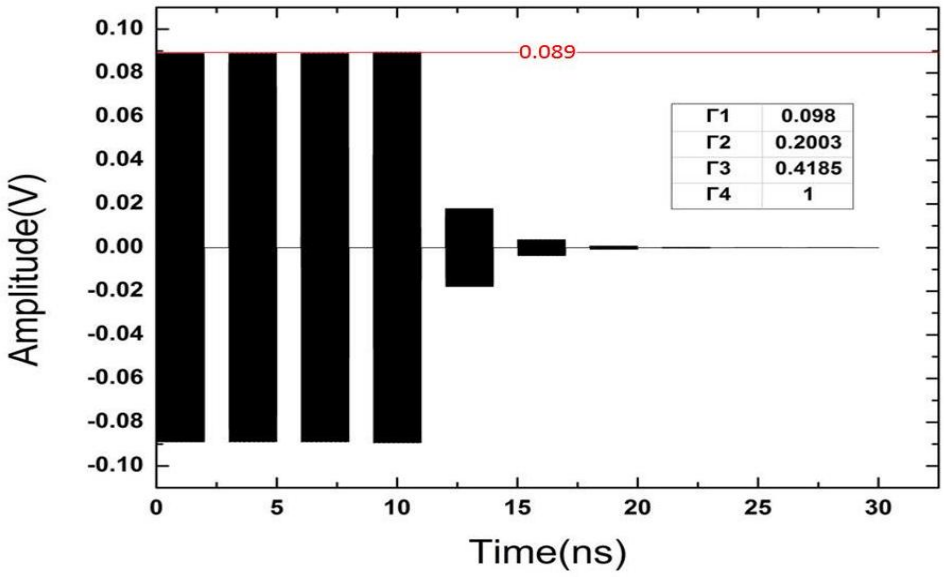

Figure 2.9 Reflected wave in SIW (Matlab)

There are three methods to create discontinuity through the transmission in SIW such as adding stubs, metal vias or symmetrical iris in H-plane as shown in Figure 2.10.

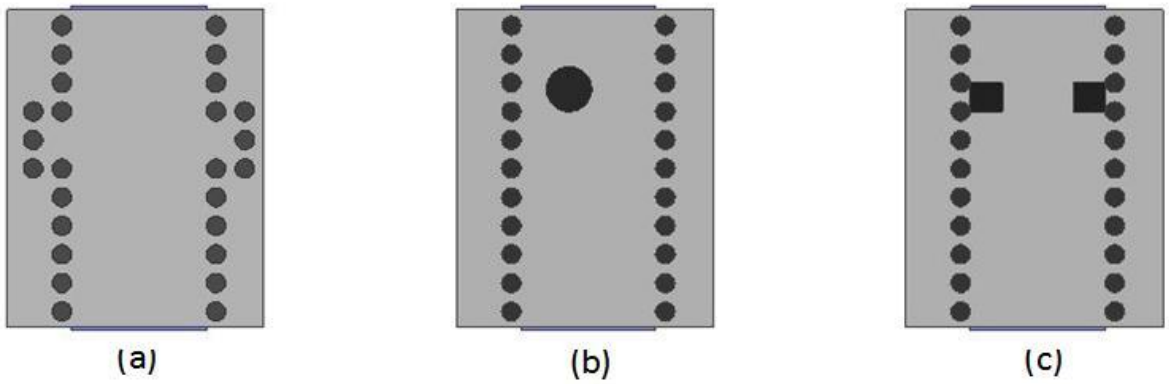

Figure 2.10 Discontinuity in SIW (a) H-stub (b) metal via (c) iris in H-plane

For the SIW tag design, the iris in H-plane is considered for encoding the bits of information. The equivalent circuit of this kind of discontinuity is shown in Figure 2.11 [30], its reflection coefficient can cover the range from 0 to 1 by adjusting width *w* as shown in Figure 2.12.

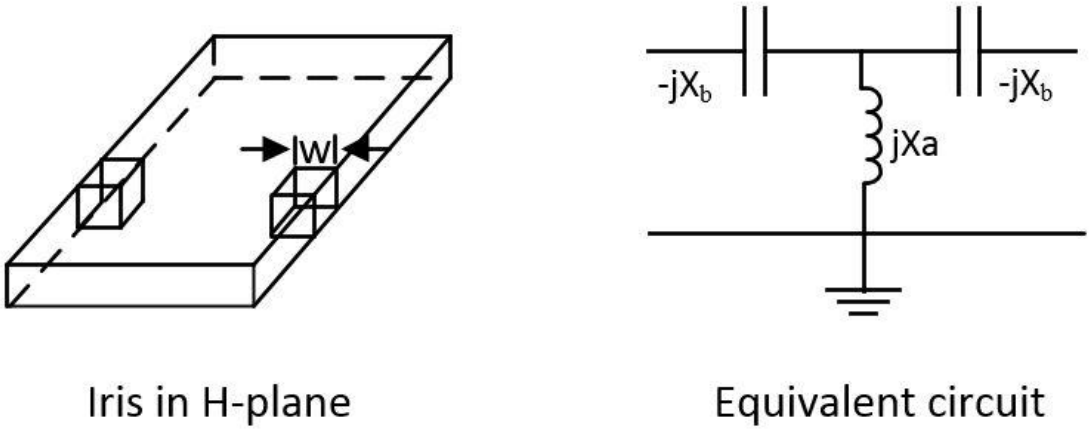

Figure 2.11 3 Discontinuity in SIW

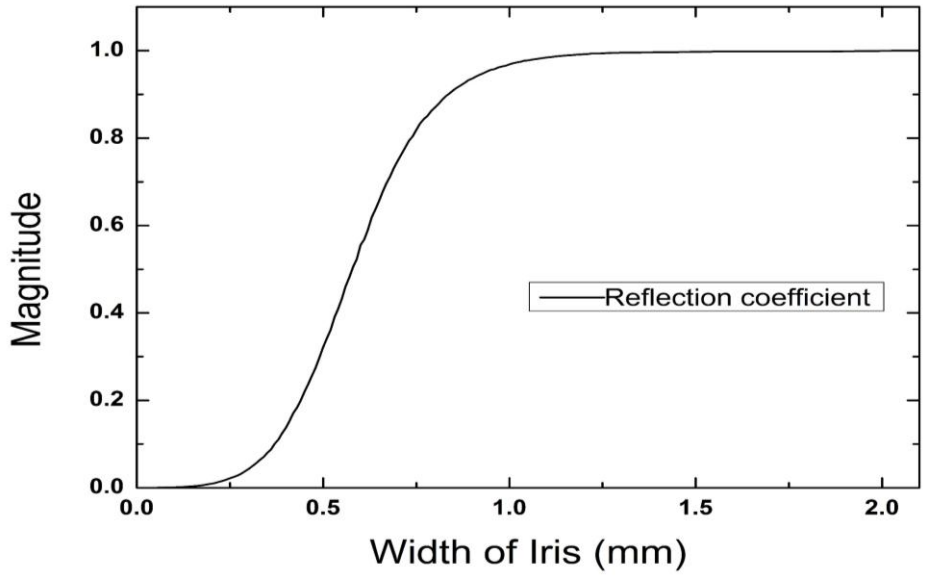

Figure 2.12 Reflection coefficient of symmetrical iris in H-plane

With the value of four calculated Γi as depicted in Figure 2.9, the dimensions of each iris can be extracted based on the curve in Figure 2.12, which are tabulated in Table 2-2.

Table 2-2 Dimensions of discontinuities (SIW)

	Γ_1	Γ_2	Γ_3	Γ_4
Magnitude	0.098	0.2003	0.4185	1
Width (mm)	0.365	0.443	0.545	2.1

2.1.4.2 Antenna of SIW tag

For the SIW tag design, the slot antenna is considered for its integration with the MMID tag. Generally, slots on the waveguide are assumed to have a narrow width (less than 0.1 of wavelength in the substrate) and the length of the slot is 0.5 of wavelength in the substrate [31-33].

Table 2-3 Dimensions of SIW slot antenna

	Thickness	**X_slot**	**Y_slot**	**P_slot**
Magnitude	20 mil	0.35 mm	2.1 mm	2.1 mm

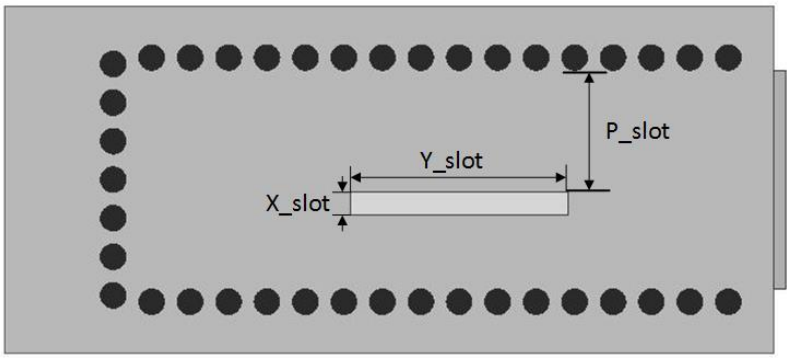

Figure 2.13 Topology of SIW slot antenna

Figure 2.13 shows the topology of an SIW slot antenna with the dimensions tabulated in Table 2-3, the model is simulated in HFSS with Rogers 6002 and the substrate thickness is 0.508 mm.

The antenna is proposed to operate at the center frequency of 35 GHz with the bandwidth of 1 GHz as discussed in chapter 1.

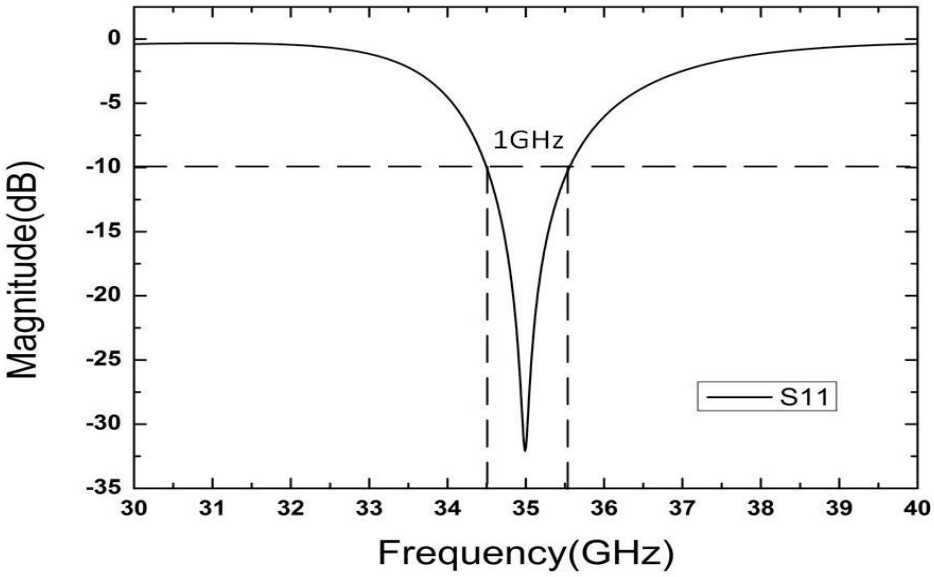

Figure 2.14 Return loss of SIW slot antenna

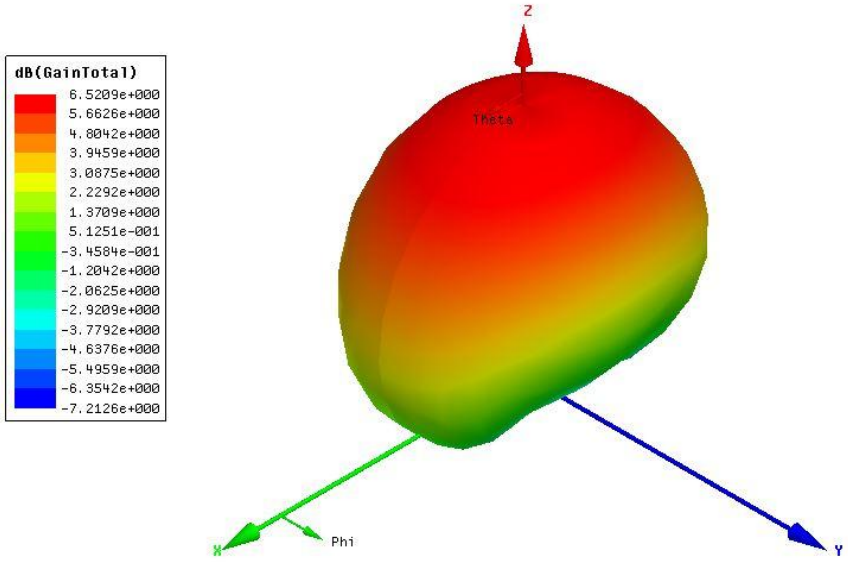

Figure 2.15 3D Radiation pattern of SIW slot antenna

Figure 2.14 shows the return loss of the SIW slot antenna, the antenna is operating at the centre frequency of 35 GHz, and the bandwidth is 1 GHz, which meets specification as mentioned above in chapter 1. Figure 2.15 shows the radiation pattern of this antenna with the gain of 6.52 dBi.

2.1.4.3 Simulation result

The 4-bits SIW tag is proposed to achieve the millimeter-wave identification as well as to verify the proposed equalization method.

The total transmission length of SIW tag L_{siw} is calculated in the following (2.10)

$$L_{siw} = \frac{(3 * (t_s + t_i) + t_0)v_{gsiw}}{2} = 70\ cm \tag{2.10}$$

The terminal of the tag is a short-circuit because by applying the proposed equalization method in chapter 1, all the power will be used for encoding the bits. But in the case of code "0000", an extra length of 5 cm between the last bit and the terminal of the tag is reserved for the reader to distinguish the terminal. So the total length of the SIW tag L_{siw} is 75 cm.

By connecting the SIW slot antenna, the topology of the SIW tag is shown in Figure 2.16.

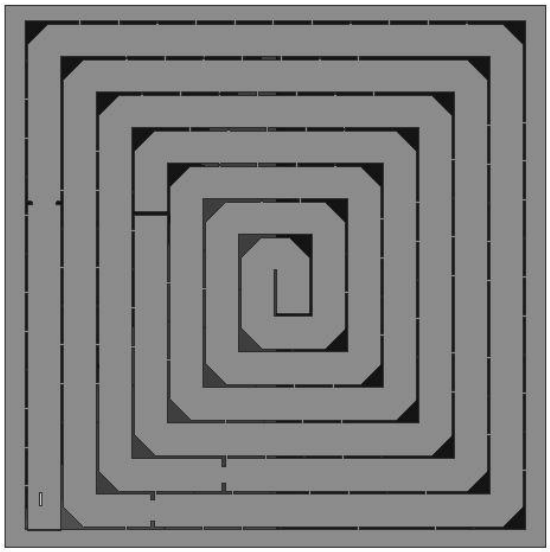

Figure 2.16 Topology of SIW tag

The size of the tag is 7 cm×7 cm with the total transmission length of 75 cm, the four symmetrical irises in H-plane during the transmission are employed for encoding the information. Time domain simulation of the tag is executed through the software CST MICROWAVE STUDIO (CST), the tag is excited at the bottom-left corner without the antenna. The simulation result is shown in Figure 2.17, the four peaks are easy to get identified which represent the unique binary

code “1111”, the magnitude of each is nearly equal which can prove that the proposed equalization method works well in the SIW tag design.

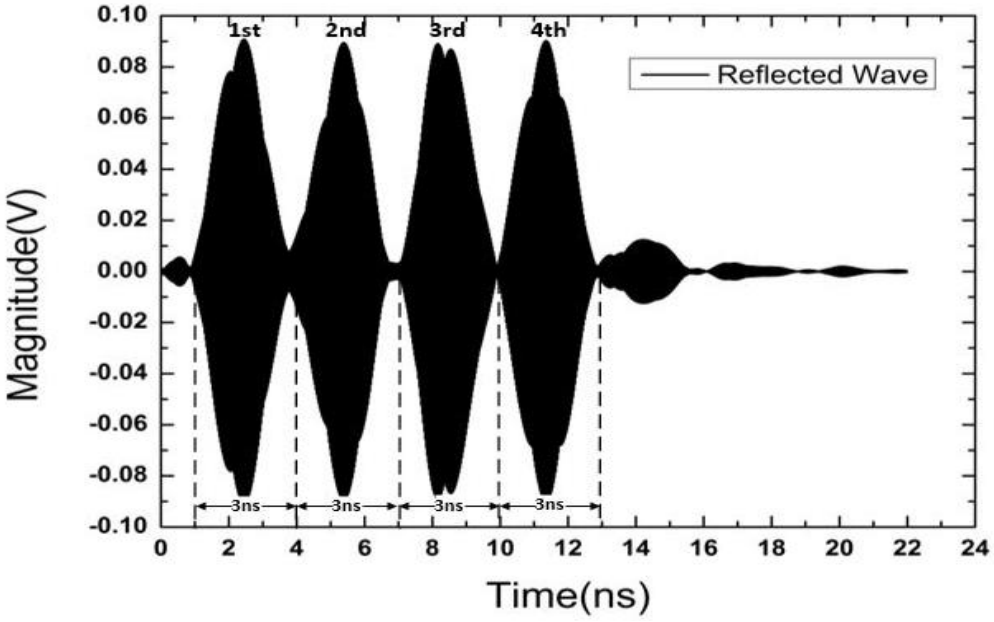

Figure 2.17 Reflected wave of SIW tag (simulation)

2.1.4.4 Measurement result

In order to read the fabricated tag, a measurement setup is constructed as shown in Figure 2.18. The pulse generator is used for generating the pulse signal of 2 ns width, which is connected to the “IF” port of the mixer, the signal generator generates the 35 GHz carrier, which is connected to the “LO” port of the mixer, the mixer will do the job of up-conversion, after the power amplifier (PA), the interrogation signal will be sent out through the horn antenna with the gain of 20 dBi, then the signal will be received by the tag antenna, after encoding the bits of information, the tag will send back the encoded signal, which will be received by another horn antenna with the same gain of 20 dBi, then another mixer will do the job of down-conversion with the signal generator. Finally, the baseband signal will be connected to the oscilloscope to decode the information stored in the tag.

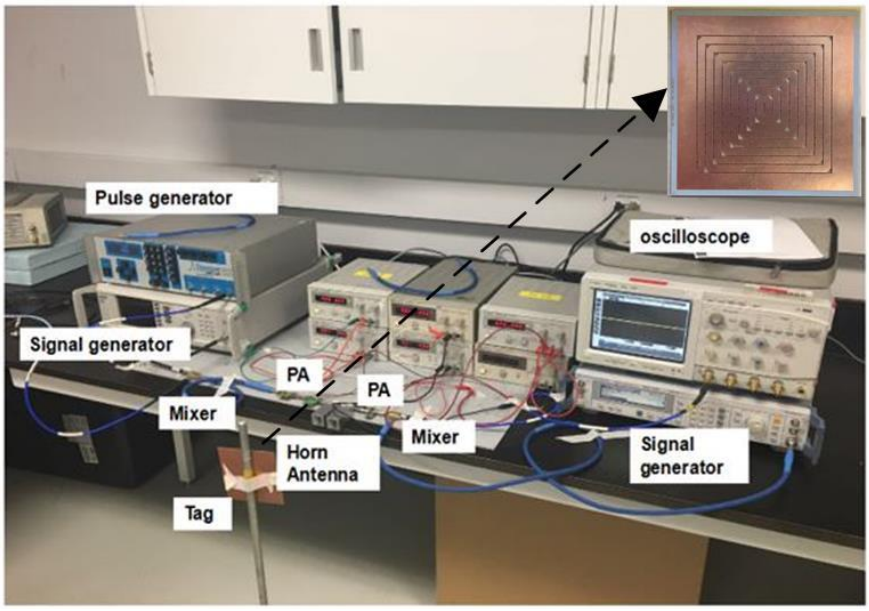

Figure 2.18 Measurement setup

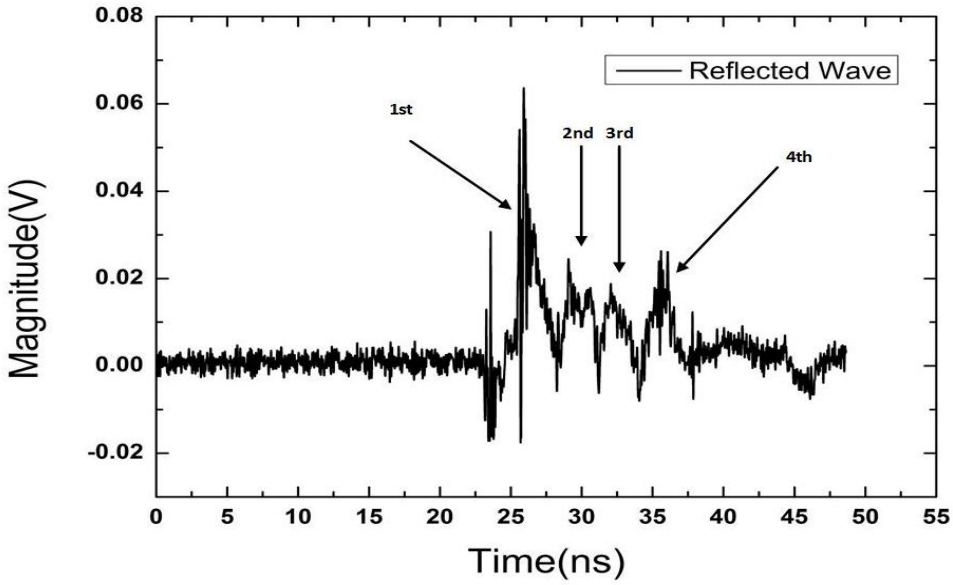

Figure 2.19 Reflected wave of SIW tag (measurement)

Figure 2.19 shows the measurement result of the SIW tag, it could be observed that the reflected wave is attenuated and delayed through the propagation in the free space and the transmission in SIW. In spite of the unexpected noise, the unique binary code "1111" could be decoded easily. The simulation result and the measurement result are in good agreement which proves that the proposed SIW tag works well at 35 GHz.

2.2 Half mode substrate integrated waveguide tag

2.2.1 Introduction

In order to reduce the size of the above-described SIW tag, half-mode substrate integrated waveguide (HMSIW) is investigated which can reduce the waveguide width by half. Figure 2.20 shows the top view of the geometry of the HMSIW, it is fed by the microstrip line with the characteristic impendence of 50 Ω, the microstrip line is well matched to the HMSIW with the taper, the upper side of the HMSIW is a series of metal slot and the bottom side is open. In the model, T_L and W represent the transmission length and width of HMSIW, respectively, L_T and W_T represent the length and the width of the taper, W_m represents the width of the microstrip line, the thickness of substrate is h and the dielectric constant of substrate is ε_r[34].

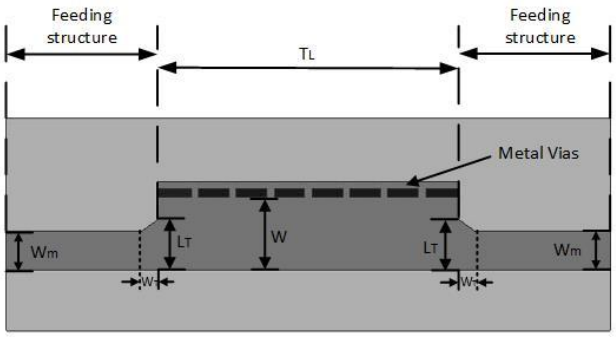

Figure 2.20 Geometry of HMSIW

Similar to SIW, the series of the metal slots could be regarded as an electrical wall, the open side could be regarded as a magnetic wall, the power is confined between the top and bottom metals and propagate along the longitudinal direction. In SIW, the dominant mode during the transmission is TE_{10} mode, in HMSIW, it can be said that the SIW is cut by half in the middle, so the dominant mode supported in the HMSIW is the quasi-$TE_{0.5,0}$ mode.

2.2.2 Extraction of propagation constant of HMSIW

2.2.2.1 Multiline method (HMSIW)

The multiline method is a common way to extract the propagation constant of a uniform transmission line [35]. In this method, first the T matrix (transfer scattering matrix) is defined as shown in Figure 2.21. In a two port network, a_1 and b_1 represent the amplitude of the incident wave

and the reflected wave in port1, respectively, a_2 and b_2 represent the amplitude of the incident wave and the reflected in port2. The network could be described by the matrix $T=\begin{bmatrix} t_{11} & t_{12} \\ t_{21} & t_{22} \end{bmatrix}$.

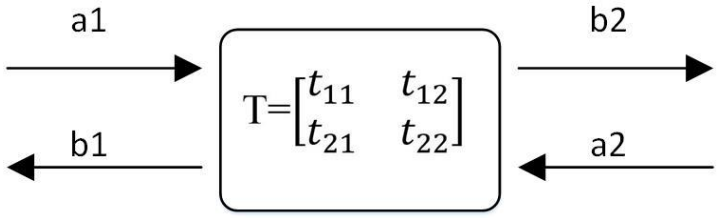

Figure 2.21 Two port network

The relationship of those parameters is shown as follows (2.11).

$$\begin{bmatrix} b_1 \\ a_1 \end{bmatrix} = \begin{bmatrix} t_{11} & t_{12} \\ t_{21} & t_{22} \end{bmatrix} \begin{bmatrix} a_2 \\ b_2 \end{bmatrix} \tag{2.11}$$

The advantage of using a T matrix is that the cascaded network could be easily described by the product of all the T matrix of each sub network. For a uniform transmission line with the length of *l*, T matrix could be regarded as the diagonal matrix, which is described in (2.12).

$$\mathrm{T} = \begin{bmatrix} \mathrm{e}^{-\gamma \mathrm{l}} & \\ & \mathrm{e}^{\gamma \mathrm{l}} \end{bmatrix} \tag{2.12}$$

where γ represents the propagation constant of the HMSIW. The relationship between the T-matrix and the S-matrix is shown in (2.13).

$$\begin{bmatrix} \mathrm{t}_{11} & \mathrm{t}_{12} \\ \mathrm{t}_{21} & \mathrm{t}_{22} \end{bmatrix} = \begin{bmatrix} -(\mathrm{s}_{11}\mathrm{s}_{22} + \mathrm{s}_{12}\mathrm{s}_{21})/\mathrm{s}_{21} & \mathrm{s}_{11}/\mathrm{s}_{21} \\ -\mathrm{s}_{22}/\mathrm{s}_{21} & 1/\mathrm{s}_{21} \end{bmatrix} \tag{2.13}$$

By adopting the multiline method in analyzing the HMSIW, the HMSIW could be divided into three parts, the left microstrip feed line with the taper, the HMSIW and the right microstrip feed line with the taper, which could be represented by the T-matrix as follows.

$$T_1 = T_{ML} * T_{HMSIW1} * T_{MR} \tag{2.14}$$

$$T_2 = T_{ML} * T_{HMSIW2} * T_{MR} \tag{2.15}$$

The middle part (HMSIW) could be regarded as the uniform transmission line, which can be represented by the equation (2.12).

$$T_{HMSIW1} = \begin{bmatrix} e^{-(\alpha+j\beta)L1} & \\ & e^{(\alpha+j\beta)L1} \end{bmatrix} \tag{2.16}$$

$$T_{HMSIW2} = \begin{bmatrix} e^{-(\alpha+j\beta)L2} & \\ & e^{(\alpha+j\beta)L2} \end{bmatrix} \tag{2.17}$$

where α and β are the attenuation constant and the phase constant of the HMSIW, respectively.

Through the simulation by HFSS, we can get the result of T_1 and T_2. Due to the same dimensions of the microstrip feed line, by subtracting T_1 and T_2, the influence of the feed line could be eliminated as follows.

$$T_{12} = T_1 - T_2 = T_{HMSIW12} \tag{2.18}$$

$$T_{HMSIW12} = \begin{bmatrix} e^{-(\alpha+j\beta)\Delta L} & \\ & e^{(\alpha+j\beta)\Delta L} \end{bmatrix} \tag{2.19}$$

where $\Delta L = L_1 - L_2$.

Finally, the attenuation constant and the phase constant of HMSIW could be calculated as follows.

$$\gamma = \frac{1}{\Delta L} * ln\left(\frac{T_1}{T_2}\right) \tag{2.20}$$

The model of multiline line method (HMSIW) is built in Figure 2.22, the HMSIW with the transmission length of 10 cm and another HMSIW with the transmission length of 30 cm are simulated in HFSS, both of them are fed by the same microstrip line, the dielectric filled in the waveguide is Rogers 6002 with the thickness of 20 mil, and the dimensions of the HMSIW are tabulated in Table 2-4.

Table 2-4 Dimensions of HMSIW

W_m	Lt	Wt	W
1.3 mm	1.66 mm	0.5 mm	2.4 mm

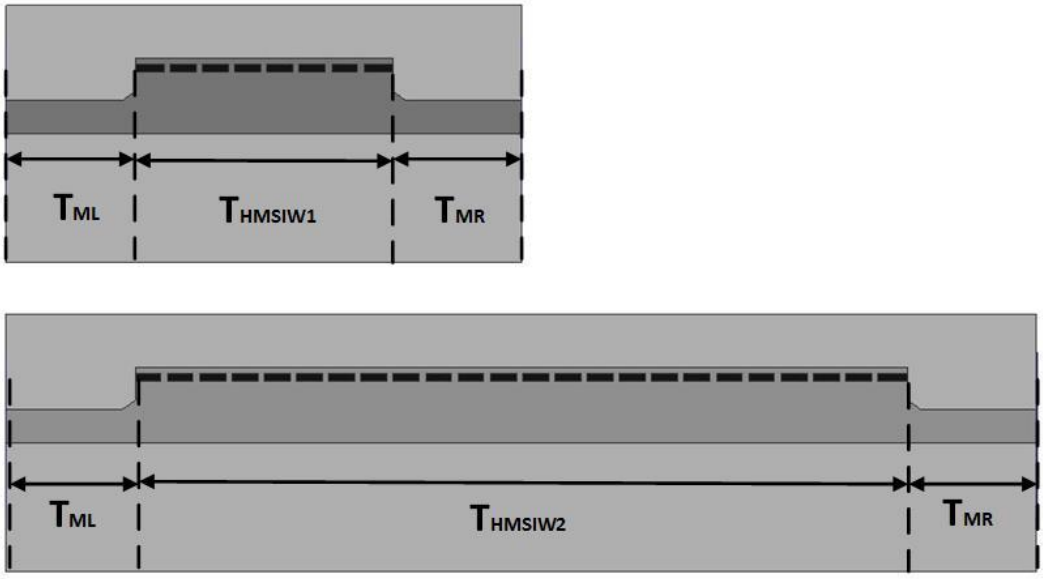

Figure 2.22 Multiline method (HMSIW)

2.2.2.2 Attenuation constant α_{hmsiw}

In HMSIW, the loss could be concluded as the total contribution of conductor loss, dielectric loss and radiation loss. The conductor loss is caused by the top and bottom metals as well as the metal slots. The dielectric loss is caused by the dielectric filled in the waveguide. The radiation loss is aroused by the leakage from the gap between the metal slots and the open part of HMSIW. Based on the multiline method, the attenuation constant α_{hmsiw} could be calculated and plotted in Figure 2.23 within the frequency range from 34 GHz to 36 GHz. As described in the figure, the attenuation constant of HMSIW is lower than that of SIW, it could be explained that for the a compact size of HMSIW, its dielectric loss and conductor loss are lower than its SIW counterpart, but the radiation loss is higher than SIW due to the open part of HMSIW. Finally, the attenuation constant of HMSIW α_{hmsiw} =1.64 neper/m at 35 GHz is considered for the equalization method proposed in chapter 1.

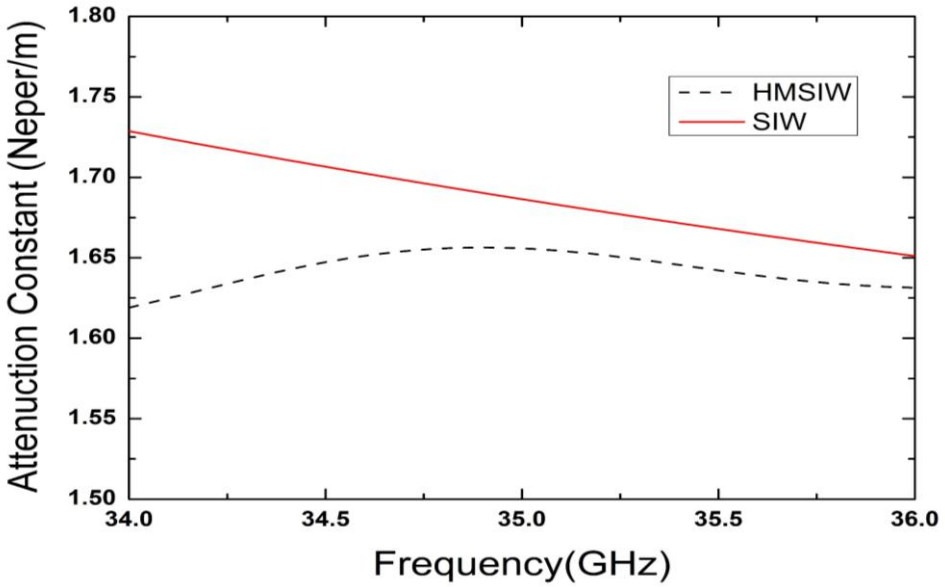

Figure 2.23 Attenuation constant of HMSIW

2.2.2.3 Phase constant *βhmsiw*

Similar to the phase constant of the SIW β_{siw}, the phase constant of HMSIW β_{hmsiw} will not only affect the group velocity but also arouse the dispersion issue.

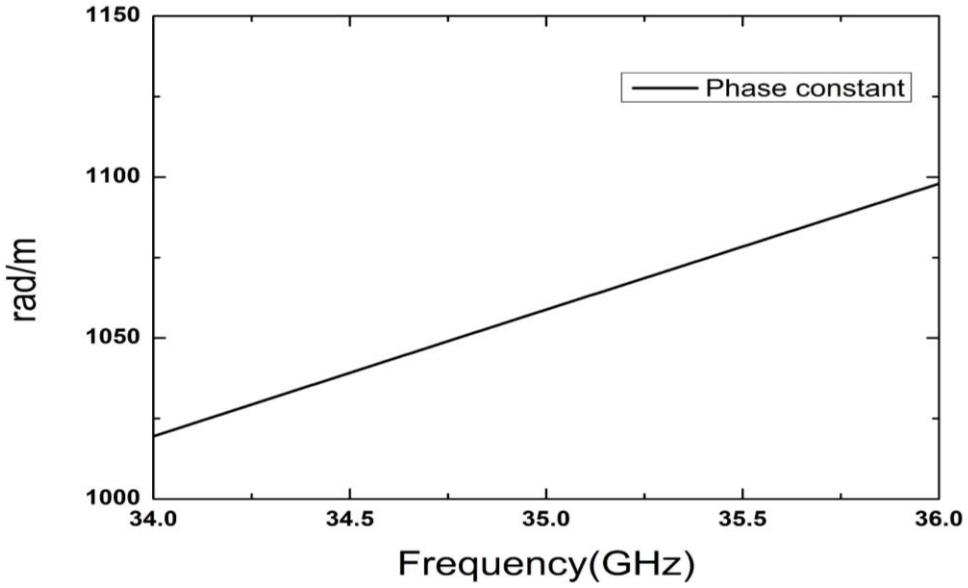

Figure 2.24 Phase constant of HMSIW

Based on the multiline method, the phase constant of HMSIW β_{hmsiw} from 34 GHz to 36 GHz is calculated in Figure 2.24. For the HMSIW tag design, the value of the phase constant β_{hmsiw} =1058 rad/m at 35 GHz is considered for the equalization method proposed in chapter 1.

2.2.3 Distortion

2.2.3.1 Group velocity of HMSIW V_{ghmsiw}

Similar to SIW, the distortion of the interrogation signal in HMSIW could be divided into two parts: dispersion and attenuation. The group delay of the HMSIW τ_{ghmsiw} can be expressed by formulation (2.7), the value of α_{hmsiw} and β_{hmsiw} over the frequency range from 34.5 GHz to 35.5 GHz is extracted, with (2.7), we can adjust the value of transmission length L to achieve the group delay of 3 ns at 35 GHz to meet the criteria set in chapter 1.

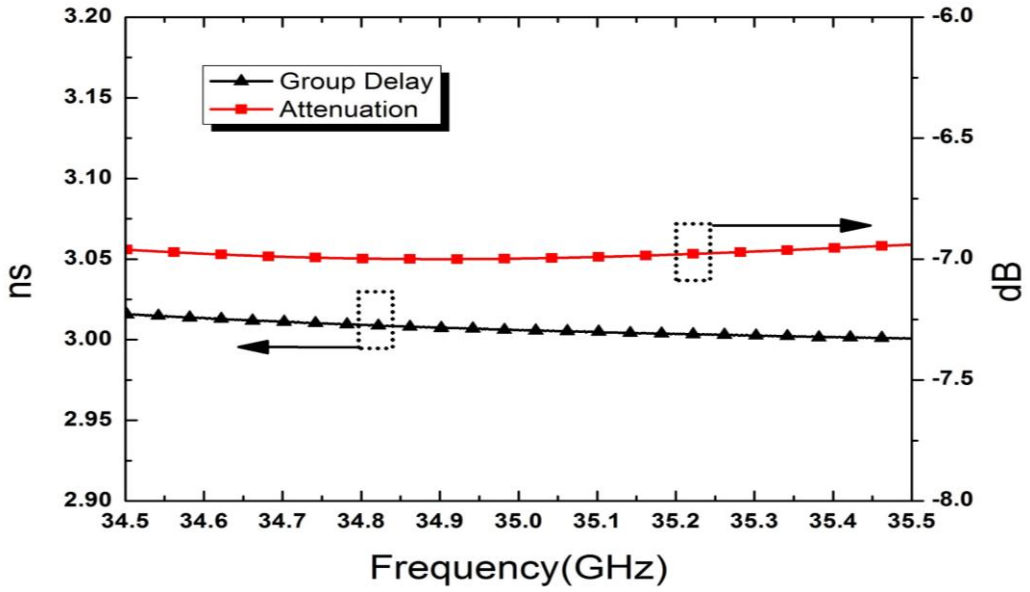

Figure 2.25 Group delay and attenuation (HMSIW)

As shown in Figure 2.25, the red curve represents the attenuation of the signal, which is almost stable at 6.8 dB, the black curve represents the group delay of the signal, which decreases with frequency. With the optimized L=48.1 cm, the group delay of 3 ns at 35 GHz is achieved and it can be observed that the interrogation signal is expanded from 3 ns to 3.01 ns. This level of distortion is acceptable for the interval of 1 ns between two neighbouring pulses.

The group velocity of signal in HMSIW V_{ghmsiw} can be calculated by the following formulation (2.21).

$$V_{ghmsiw} = \frac{L}{\tau_g} = 1.603 * 10^8\ m/s \tag{2.21}$$

2.2.3.2 Interrogation signal distortion

The spectrum of the interrogation signal after the transmission length of 48.1 cm in HMSIW could be calculated and given in Figure 2.26.

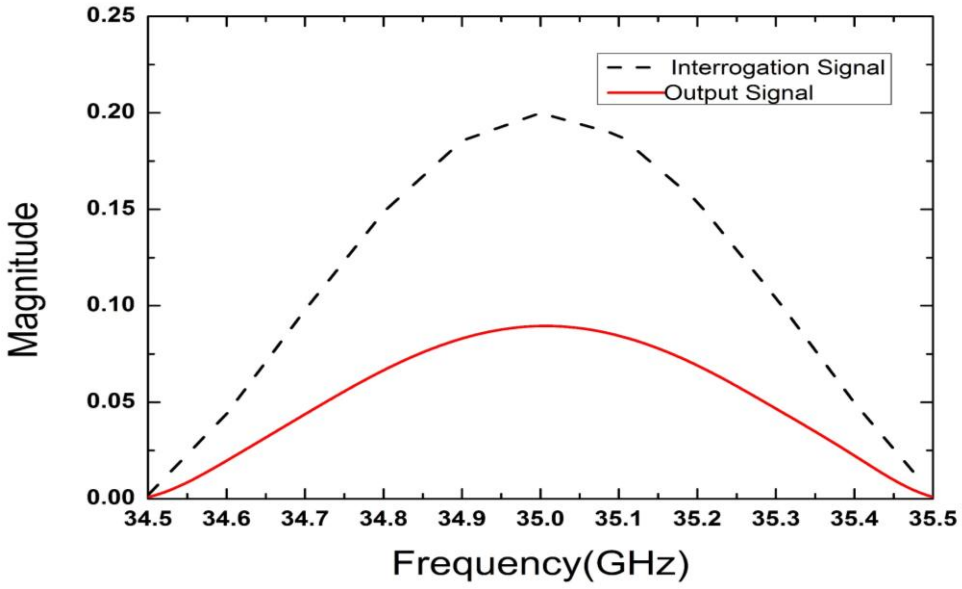

Figure 2.26 Spectrum of output signal (HMSIW)

Inverse Fourier transform is performed based on the spectrum of the output signal (HMSIW) in order to find the output signal in time domain as shown in Figure 2.27, it could be observed that the time delay of the amplitude envelop of 3 ns is obtained with the transmission length of 48.1 cm and the interrogation signal is expanded from 3 ns to 3.01 ns.

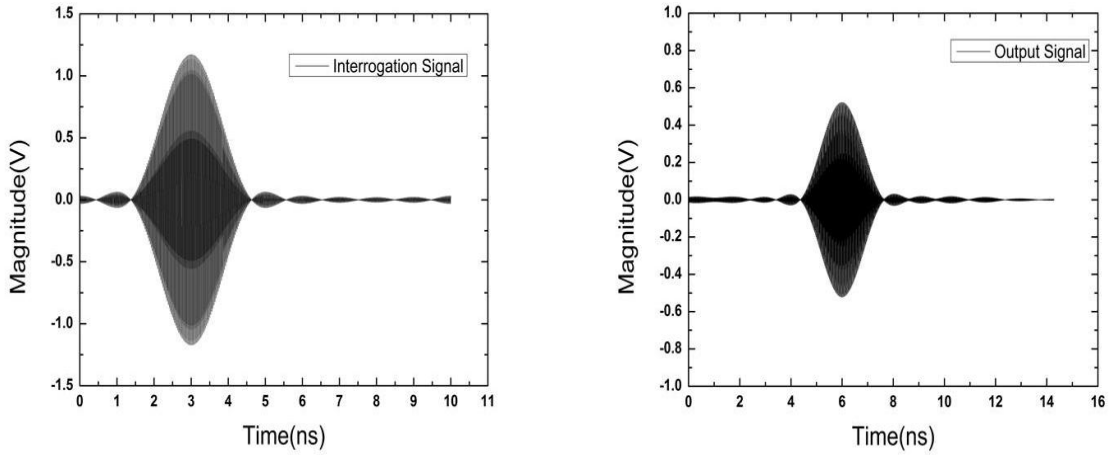

Figure 2.27 Interrogation signal and output signal (HMSIW)

2.2.4 Meander-line based HMSIW tag

2.2.4.1 Coupling between parallel HMSIW

In order to reduce the size of the HMSIW tag, a meander-line structure is used. For the SIW, since the two sides of waveguide are enclosed, the coupling between them is only coming from leakage of gaps between the metal vias, the leakage power is relatively low enough to be neglected. But in the case of HMSIW, the open side could be regarded as the magnetic wall, so it will arouse a higher coupling between the neighbouring HMSIW structures.

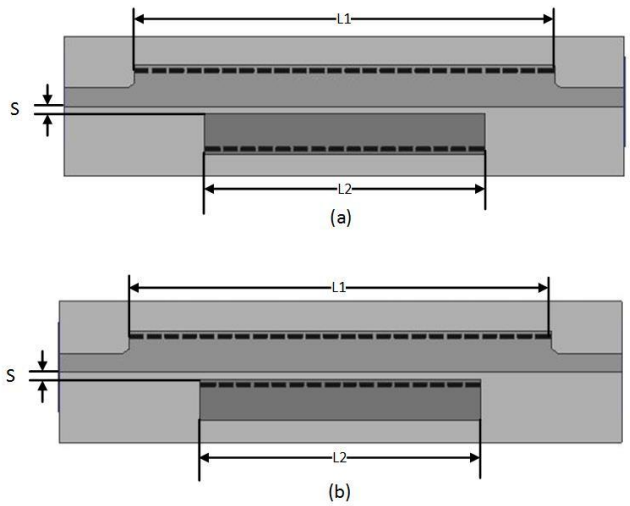

Figure 2.28 Position (HMSIW) (a) open side to open side (b) open side to enclosed side

In the meander-line HMSIW design, there are two ways to arrange the position. The first way is related to the open side to the open side as shown in Figure 2.28 (a), the upper side is the HMSIW with transmission length L_1=30 mm fed by a microstrip line, the bottom side is the HMSIW with transmission length L_2=20 mm without any feeding line, the dielectric filled in both are the Rogers 6002 with the thickness of 20 mil, S represents the space between the two HMSIW lines. The other way is the open side to the enclosed side as shown in Figure 2.28 (b), all the dimensions are equal to the model in Figure 2.28 (a) except the direction of the HMSIW at the bottom side. In order to characterize the coupling between the two HMSIW, a full wave simulation is carried out by HFSS over the frequency range from 30 GHz to 40 GHz as a function of different value of S.

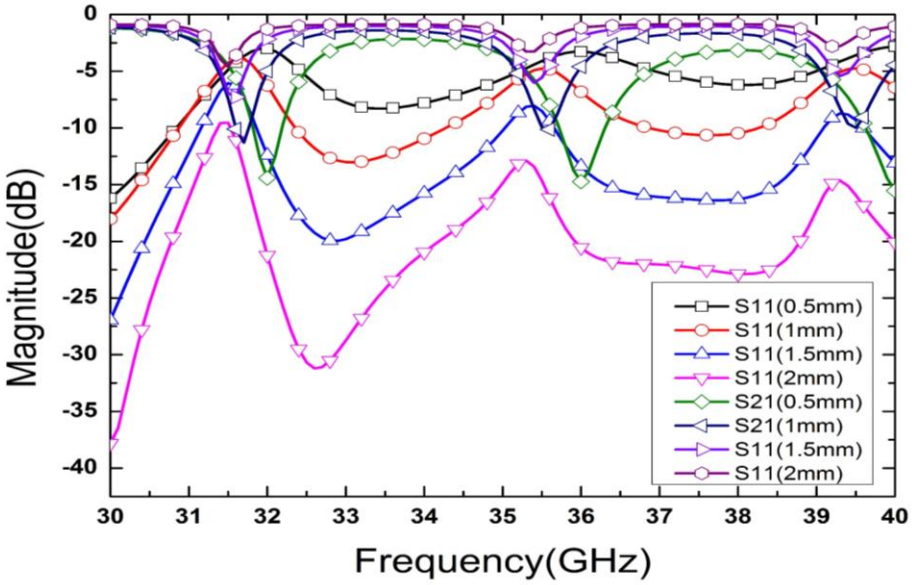

Figure 2.29 Coupling between HMSIW (open side to open side)

Figure 2.29 shows S parameter results of the "open side to open side" HMSIWs, within the frequency range from 34.5 GHz to 35.5 GHz, with spacing S=0.5 mm, 1 mm, 1.5 mm, 2 mm, all the S_{11} results are over -20 dB, which means that the bottom HMSIW will affect the transmission of the upper HMSIW due to the coupling issue. So this type of position is not considered to build the proposed meander-line HMSIW tag.

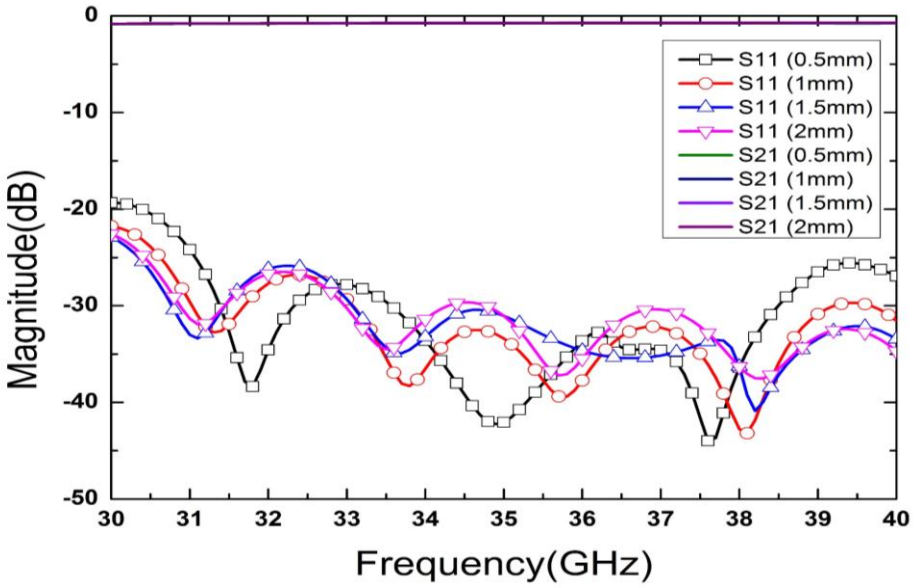

Figure 2.30 Coupling between HMSIW (open side to enclosed side)

Figure 2.30 shows S parameter results of the "enclosed side to open side" HMSIWs, within the frequency range from 34.5 GHz to 35.5GHz, with spacing S=0.5 mm, 1 mm, 1.5 mm, 2 mm, all the S_{11} results are below -20 dB, which means that the coupling between the two HMSIW is low enough to be neglected. Basically, for the tag design, the closer the spacing is, the smaller the tag becomes. Therefore, S=0.5 mm is considered for the meander-line HMSIW design.

2.2.4.2 Discontinuities

With the extracted α_{hmsiw}=1.64 neper/m, β_{hmsiw}=1058 rad/m, and V_{ghmsiw}=1.603*10^8 m/s, by applying the equalization method proposed in chapter 1, the reflection coefficient of every discontinuity could be calculated and plotted in Figure 2.31, the maximum amplitude of the reflected wave for the binary code "1101" is 0.081 when the amplitude of the interrogation signal is normalized to 1.

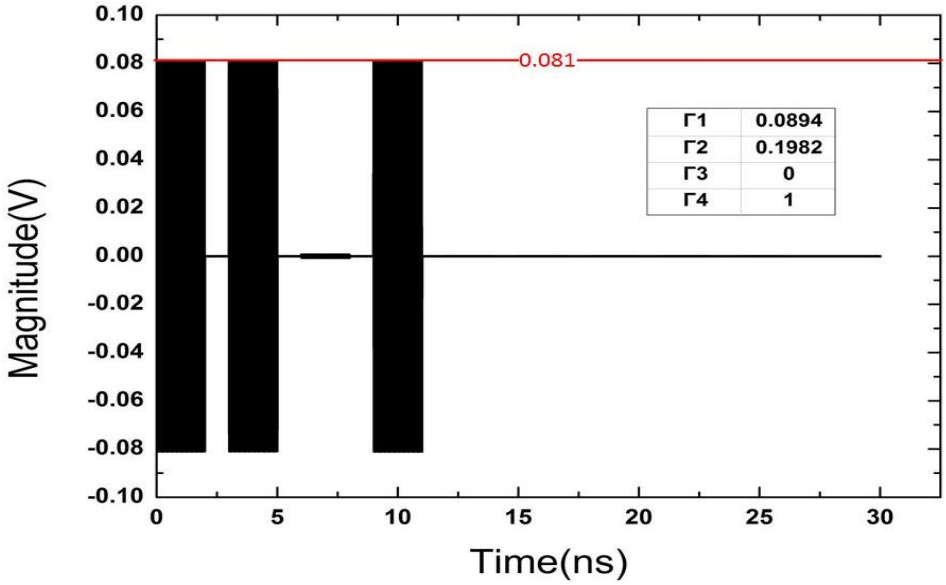

Figure 2.31 Reflected wave in HMSIW (matlab)

For the HMSIW tag design, a single iris in H-plane is considered for encoding the bits of information as shown in Figure 2.32. By adjusting the width of the iris, the reflection coefficient of this kind of discontinuity can cover the range from 0 to 1 as shown in Figure 2.33.

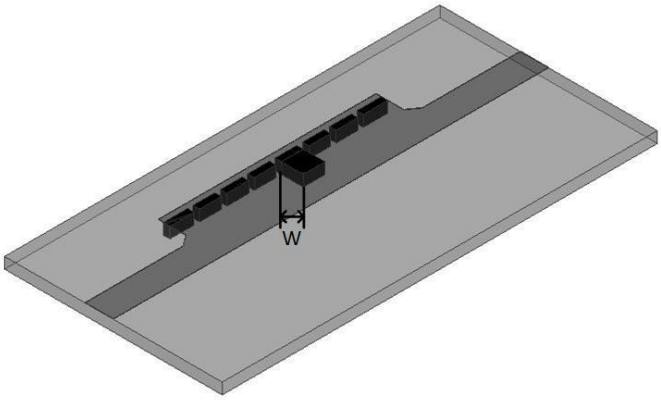

Figure 2.32 Single iris in H-plane (HMSIW)

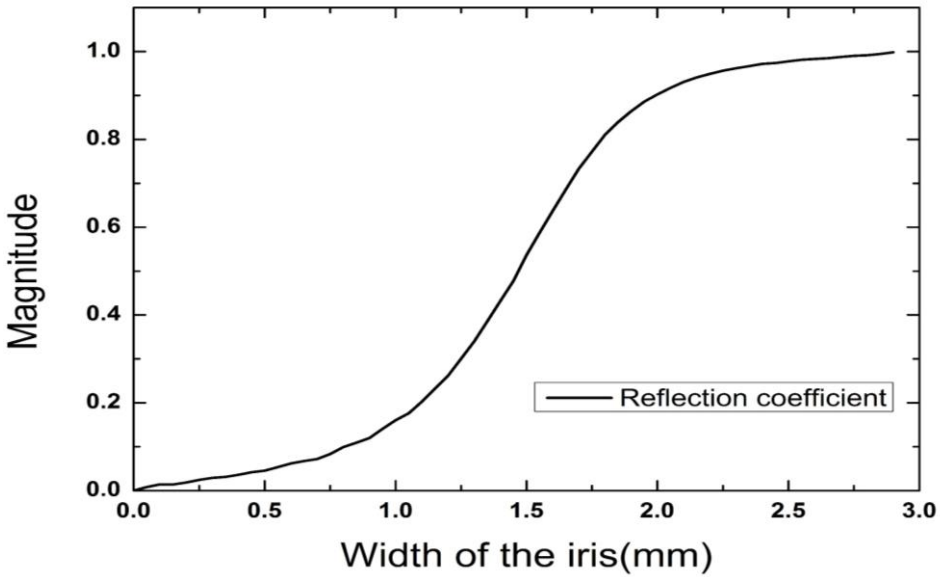

Figure 2.33 Reflection coefficient of single iris in H-plane (HMSIW)

With the value of four calculated Γi in Figure 2.31, the dimensions of each iris could be calculated based on the curve in Figure 2.33, which are tabulated in Table 2-5.

Table 2-5 Dimensions of discontinuities (HMSIW)

	$\boldsymbol{\Gamma_1}$	$\boldsymbol{\Gamma_2}$	$\boldsymbol{\Gamma_3}$	$\boldsymbol{\Gamma_4}$
Magnitude	0.0894	0.1982	0	1
Width (mm)	0.77	1.09	0	2.9

2.2.4.3 Antenna of HMSIW tag

In the HMSIW tag design, the slot antenna is considered for its integration with the MMID tag. As shown in Figure 2.34, this antenna is designed on Rogers 6002 with the thickness of 20 mil, in order to make the slot resonating at 35 GHz, a barrier is added in the HMSIW to improve the matching, L_b and W_b represent the length and width of the barrier, respectively, L_s and W_s represent the length and width of the slot, W_{hmsiw} represents the width of the HMSIW, P_L represents the distance between the slots and the metal vias and the antenna is fed by a microstrip line with impedance of 50 Ω.

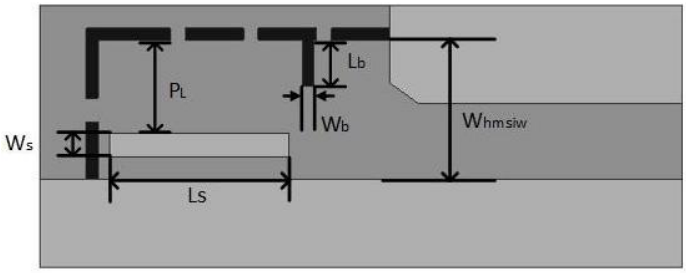

Figure 2.34 Topology of HMSIW slot antenna

The antenna is simulated in HFSS with the dimensions tabulated in Table 2-6 over the frequency range from 30 GHz to 40 GHz.

Table 2-6 Dimensions of HMSIW slot antenna

W_b	L_b	W_S	L_S	W_{hmsiw}	P_L
0.2 mm	0.8 mm	0.4 mm	3.08 mm	2.4 mm	1.6 mm

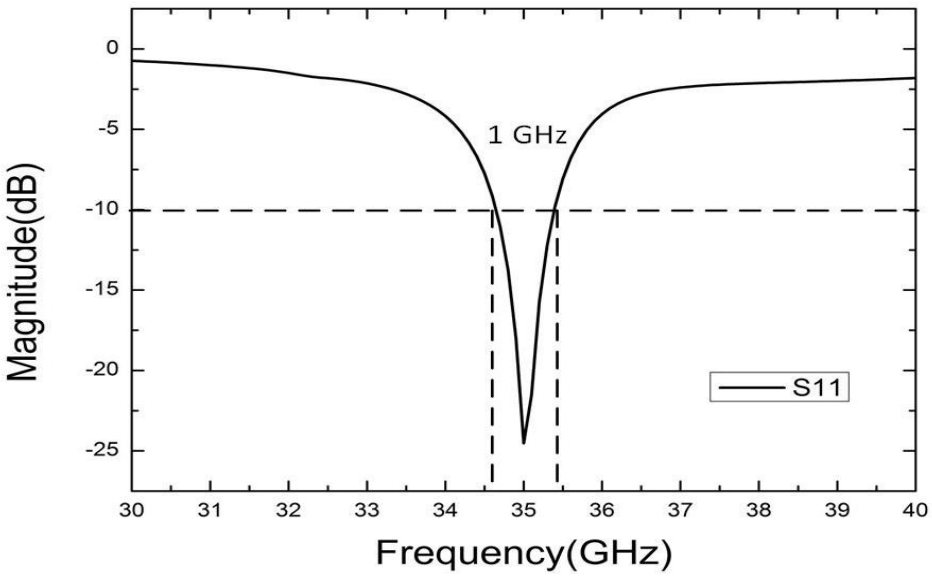

Figure 2.35 Return loss of HMSIW slot antenna

Figure 2.35 shows the return loss of HMSIW slot antenna, the antenna is operating at the centre frequency of 35 GHz with the bandwidth of 1 GHz, which meets the goal we set in chapter 1 and the gain of the antenna is 4.14 dBi.

2.2.4.4 Simulation result

The 4-bits HMSIW tag is proposed to achieve the millimeter-wave identification as well as to verify the equalization method.

The total transmission length of HMSIW tag L_{hmsiw} is calculated in the following (2.22)

$$L_{hmsiw} = \frac{(3 * (t_s + t_i) + t_0)v_{ghmsiw}}{2} = 80\ cm \tag{2.22}$$

Similar to SIW tag, the terminal of the HMSIW tag is a short circuit and an extra length of 5 cm between the last bit and the terminal of the tag is reserved for the reader to distinguish the terminal. So the total length of the HMSIW tag L_{hmsiw} is 85 cm.

By connecting the HMSIW slot antenna, the topology of the HMSIW tag is shown in Figure 2.36.

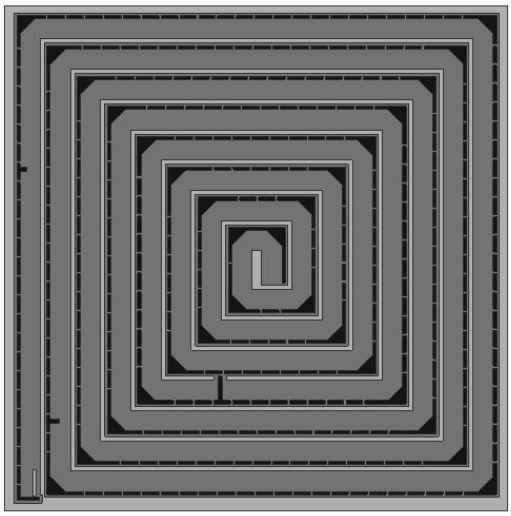

Figure 2.36 Topology of HMSIW tag

The size of the tag is 6.5 cm×6.5 cm with the total transmission length of 85 cm, three single irises in H-plane are added into the structure to encode the bits of information. Time domain simulation is carried out by CST, the tag is excited at the bottom-left corner without the antenna. The simulation result is shown in Figure 2.37, the three peaks are easy to be found which represents the binary code “1101”, the magnitude of each is nearly equal, which can demonstrate the validity of the proposed equalization method.

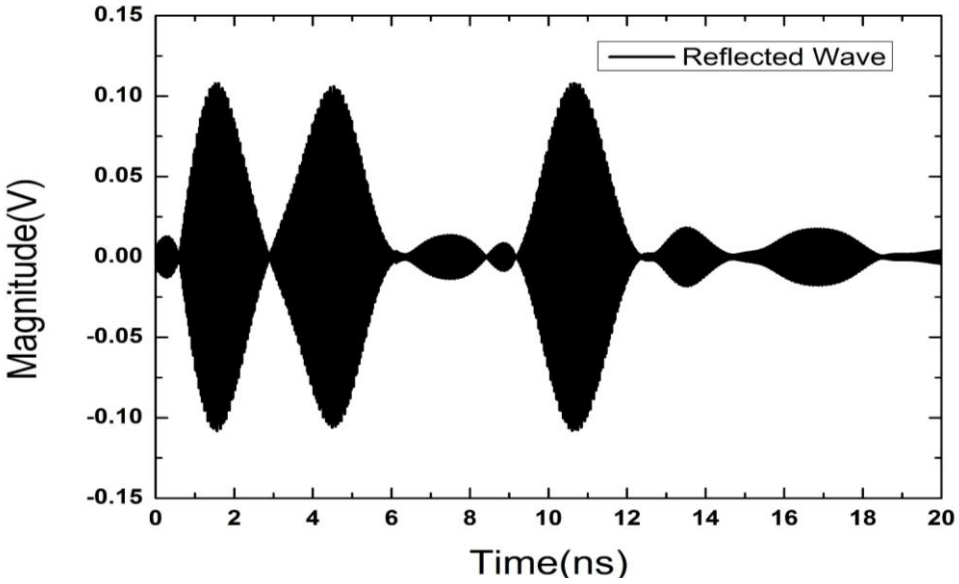

Figure 2.37 Reflected wave of HMSIW tag (simulation)

2.2.4.5 Measurement Results

The same setup is constructed as SIW to read the fabricated HMSIW tag.

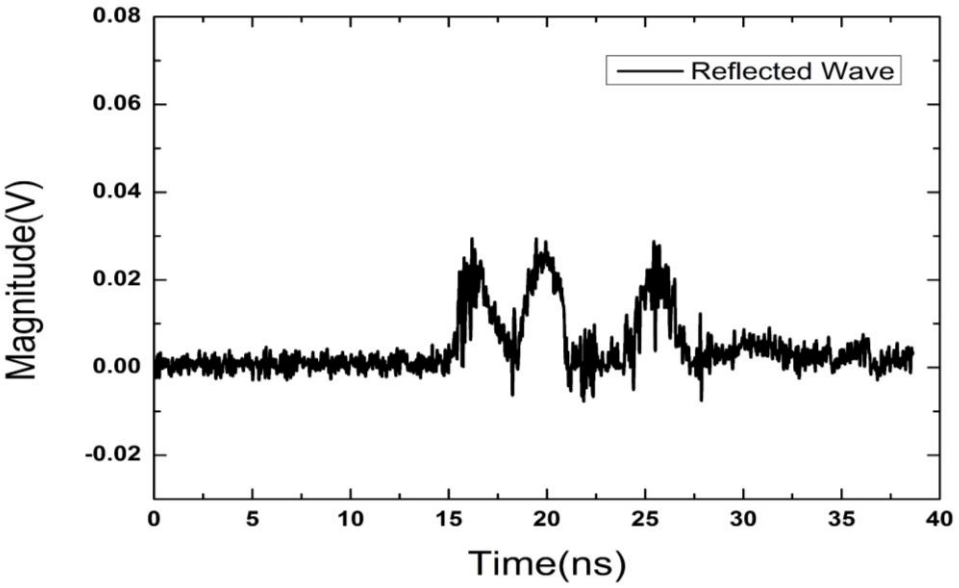

Figure 2.38 Reflected wave of HMSIW tag (measurement)

Figure 2.38 shows the measurement result of the HMSIW tag, it can be seen that the reflected wave is attenuated and delayed through the propagation in the free space and the transmission in HMSIW. In spite of the unexpected noise, the unique binary code “1101” could be decoded easily.

The simulation result and the measurement result are in good agreement which can prove that the proposed HMSIW tag again works well at 35 GHz.

2.3 Slow wave substrate integrated waveguide tag

2.3.1 Introduction

A slow wave substrate integrated waveguide (SW-SIW) is investigated in order to reduce the group velocity of SIW. In [36, 37], the blind vias array is studied to achieve a slow wave effect.

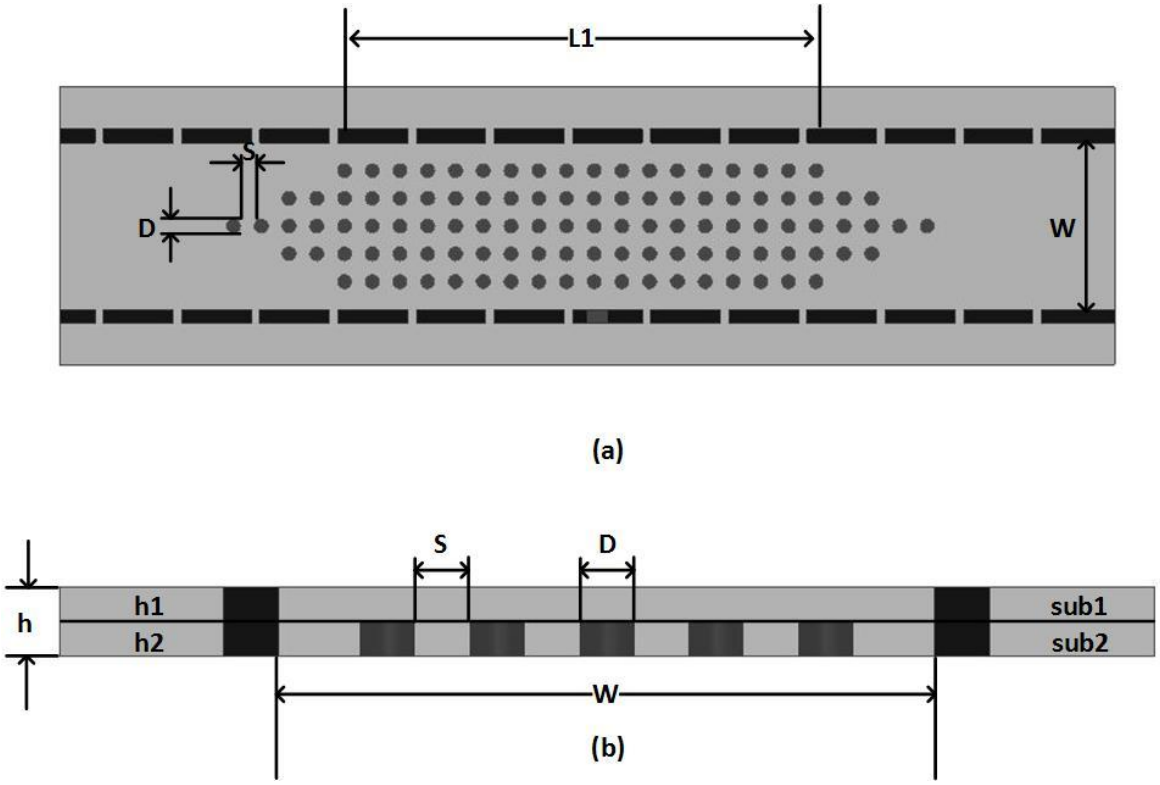

Figure 2.39 SW-SIW (a) top view (b) side view

Figure 2.39 (a) and Figure 2.39 (b) show the top view and side view of the SW-SIW, an array of metallic blind vias is added into the conventional SIW, a taper is added in order to reduce the return loss from the fast wave to the slow wave structure. In the figure, *D* represents the diameter of the blind via, *S* represents the space between the blind vias, *W* represents the width of SIW, *h* represents the thickness of substrate, *h1* represents the thickness of *sub1*, *h2* represents the

thickness of *sub2* and *L1* represents the length of the SW-SIW, the SW-SIW is designed on the Rogers 6002 with the thickness of 20 mil.

When the interrogation signal transmits through the blind vias array, the electric field of the wave will be concentrated on the upper *sub1*, which increases the effective dielectric permittivity in the center of the waveguide. Figure 2.40 shows the magnitude of electric field in the SW-SIW, the wavelength is obviously reduced, the electric field and the magnetic field are separated while travelling through the blind vias array, which is the typical phenomenon for the slow wave transmission line.

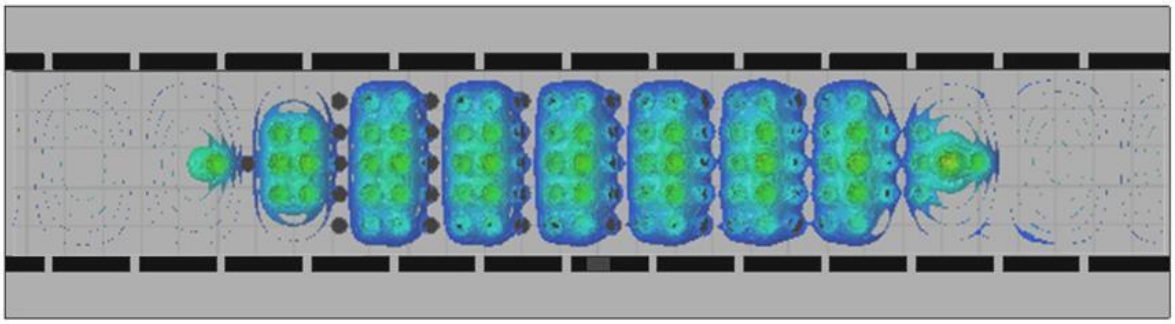

Figure 2.40 Magnitude of the electric field in SW-SIW

The return loss S_{11} of SW-SIW is calculated with the dimensions tabulated in Table 2-7 based on different value of *h2* in Figure 2.41. Generally, the higher the blind vias array is, the slower the wave becomes, but the worse the S_{11} is. Considering the loss issue and the noise during the transmission, *h2*=10 mil is considered to build the SW-SIW tag.

Table 2-7 Dimensions of SW-SIW

W	***D***	***S***	***h***	***L1***
4.8 mm	0.4 mm	0.4 mm	20 mil	12.8 cm

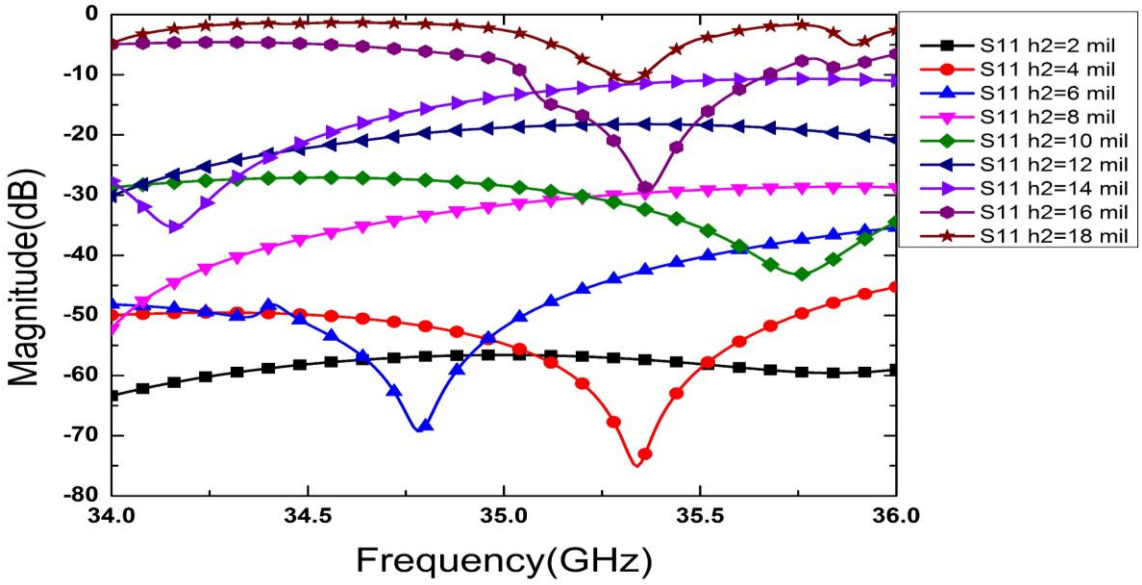

Figure 2.41 S_{11} of SW-SIW

2.3.2 Extraction of the propagation constant of SW-SIW

2.3.2.1 Multiline method (SW-SIW)

The multiline method is adopted to extract the propagation constant of SW-SIW, the model is built in HFSS as shown in Figure 2.42, a section of SW-SIW with the transmission length of 12.8 cm and another section of SW-SIW with the transmission length of 23.2 cm are simulated over the frequency range from 34 GHz to 36 GHz in HFSS.

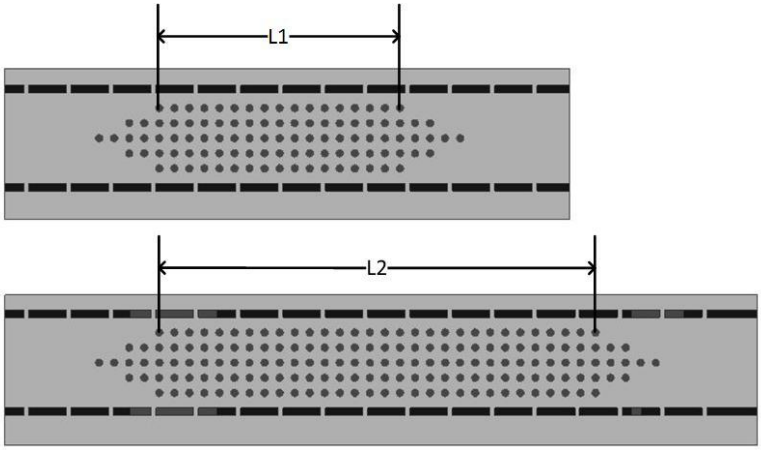

Figure 2.42 Multiline method (SW-SIW)

2.3.2.2 Attenuation constant $\alpha_{sw\text{-}siw}$

In the SW-SIW, the conductor loss is caused by the metal slots, top and bottom copper as well as the blind vias array, the dielectric loss is caused by the dielectric filled in the waveguide and the radiation loss is caused by the leakage power through the gap of the metal slots. Based on the model in Figure 2.42, the attenuation constant of SW-SIW $\alpha_{sw\text{-}siw}$ over the frequency range from 34 GHz to 36 GHz could be extracted in Figure 2.43. The attenuation constant of SW-SIW $\alpha_{sw\text{-}siw}$ =2.73 neper/m at 35 GHz is considered for the equalization method proposed in chapter 1.

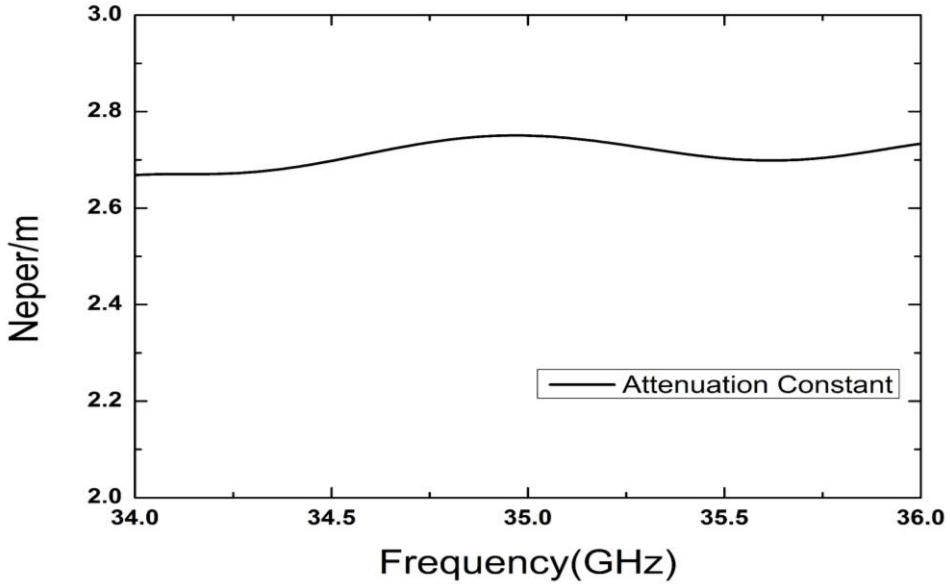

Figure 2.43 Attenuation constant of SW-SIW

2.3.2.3 Phase constant $\beta_{sw\text{-}siw}$

Similar to the phase constant of the SIW, the value of $\beta_{sw\text{-}siw}$ will not only affect the group velocity but also arouse the dispersion issue.

Based on the multiline method model in Figure 2.42, the value of $\beta_{sw\text{-}siw}$ from 34 GHz to 36 GHz is calculated in Figure 2.44. For the SW-SIW tag design, the value of phase constant $\beta_{sw\text{-}siw}$ =1230 rad/m at 35 GHz is considered for the equalization method proposed in chapter 1.

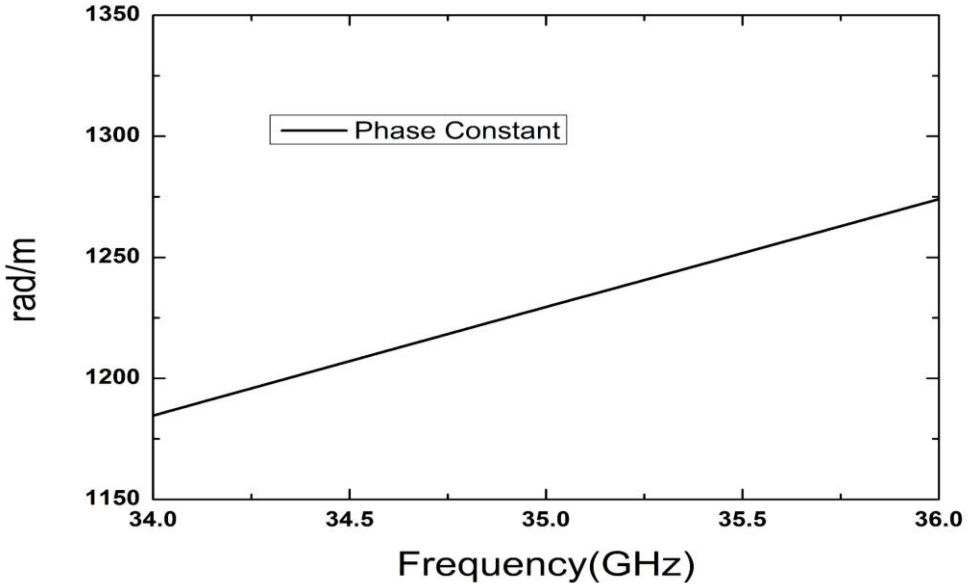

Figure 2.44 Phase constant of SW-SIW

2.3.3 Distortion

2.3.3.1 Group delay of SW-SIW $V_{gsw\text{-}siw}$

Similar to SIW, the distortion of an interrogation signal in SW-SIW could be divided into two parts: dispersion and attenuation. The group delay of the SW-SIW $\tau_{gsw-siw}$ could be expressed by the formulation (2.7), the value of α_{sw-siw} and β_{sw-siw} over the frequency range from 34.5 GHz to 35.5 GHz is extracted, with (2.7), we can adjust the value of transmission length L to achieve the group delay of 3 ns at 35 GHz to meet the criteria set in chapter 1.

As shown in Figure 2.45, the red curve represents the attenuation of SW-SIW, the black curve represents the group delay of signal in SW-SIW. With the optimized L=38.6 cm, the group delay of 3 ns at 35 GHz is achieved and it could be observed that the interrogation signal is expanded from 3 ns to 3.03 ns. This level of distortion is acceptable for the interval of 1 ns between two neighbouring pulses.

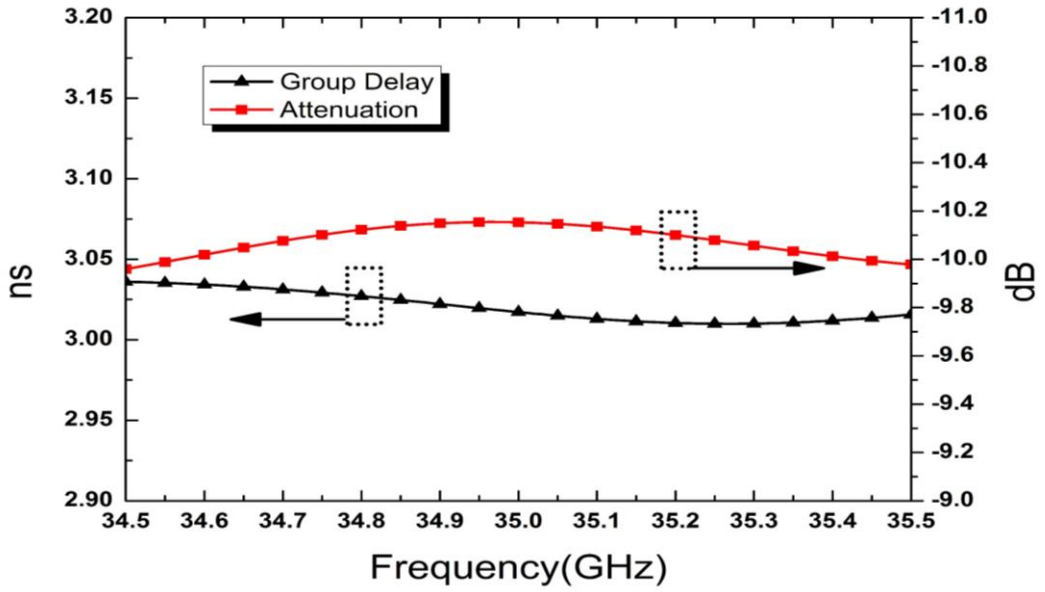

Figure 2.45 Group delay and attenuation (SW-SIW)

The group velocity of SW-SIW could be calculated by the following (2.23).

$$V_{gsw-siw} = \frac{L}{\tau_g} = 1.287 * 10^8\ m/s \tag{2.23}$$

The slowing factor is defined as the ratio of the group velocity in the slow wave structure to the group velocity in the normal structure, which is used for describing the degree of slowing. The slowing factor of SW-SIW could be calculated by the following (2.24).

$$K = \frac{V_{g(SW-SIW)}}{V_{g(SIW)}} = 90.6\% \tag{2.24}$$

2.3.3.2 Interrogation signal distortion

The spectrum of the interrogation signal after the transmission length of 38.6 cm in SW-SIW could be calculated in Figure 2.46.

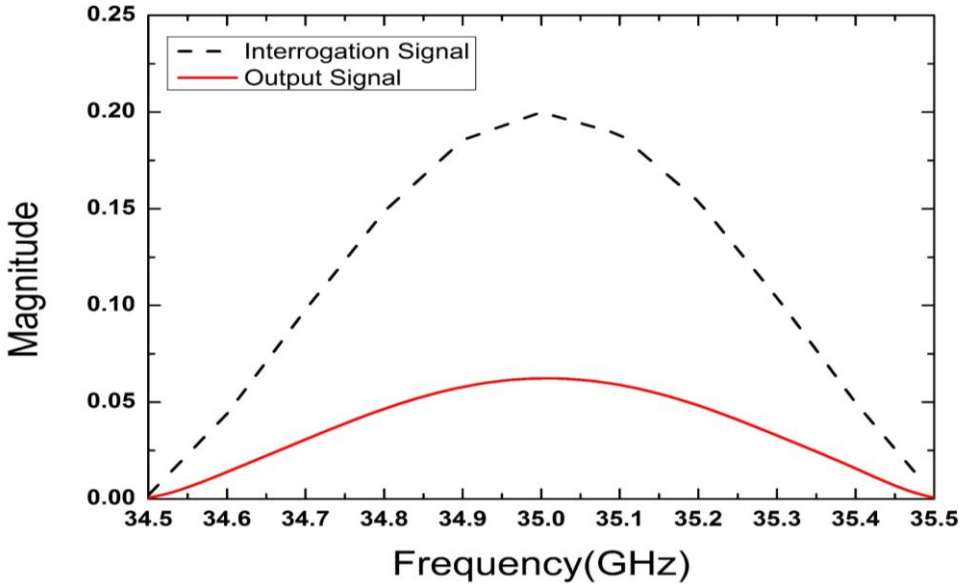

Figure 2.46 Spectrum of output signal (SW-SIW)

Inverse Fourier transform is performed based on the spectrum of the output signal (SW-SIW) in order to find the output signal in time domain as shown in Figure 2.47, it can be seen that the time delay of the amplitude envelop of 3 ns is achieved with the transmission length of 38.6 cm and the interrogation signal is expanded from 3 ns to 3.03 ns.

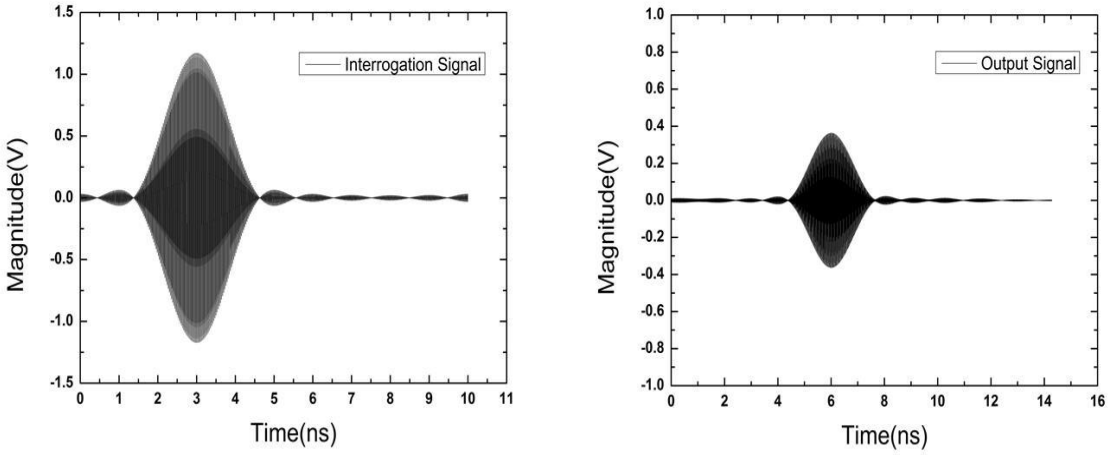

Figure 2.47 Interrogation signal and output signal (SW-SIW)

2.3.4 Meander-line based SW-SIW tag

2.3.4.1 Discontinuities

With the extracted $\alpha_{sw\text{-}siw}$=2.73 neper/m, $\beta_{sw\text{-}siw}$=1230 rad/m, and $V_{gsw\text{-}siw}$=1.287*10^8 m/s, by applying the equalization method proposed in chapter 1, the reflection coefficient of every discontinuity could be calculated and plotted in Figure 2.48, the maximum amplitude of the reflected wave for the binary code "1001" is 0.044 when the amplitude of the interrogation signal

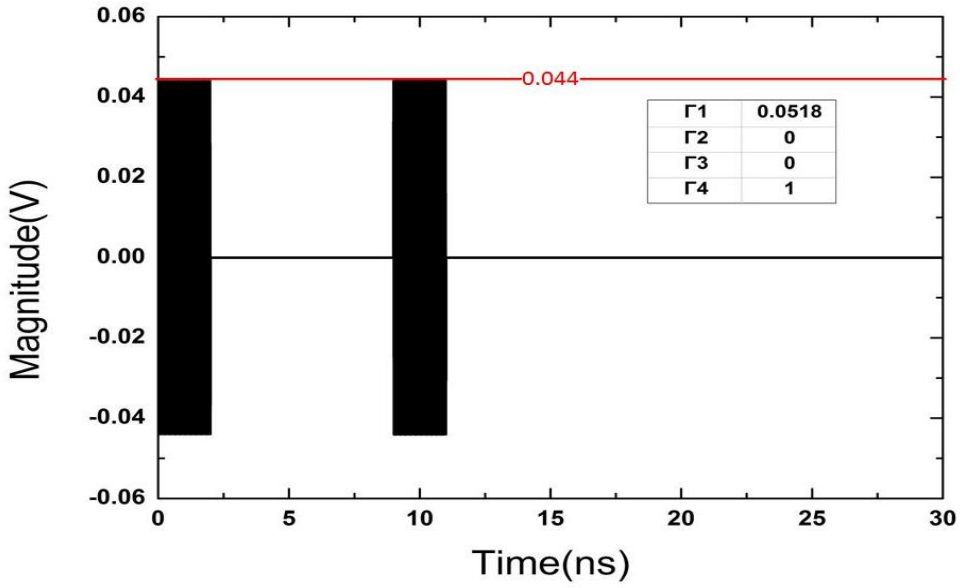

Figure 2.48 Reflected wave in SW-SIW (Matlab)

is normalized to 1.

For the SW-SIW tag design, the discontinuity is realized by changing the height of the selected row of the blind vias as shown in Figure 2.49, the reflection coefficient of this kind of discontinuity could cover the range from 0 to 1 as shown in Figure 2.50.

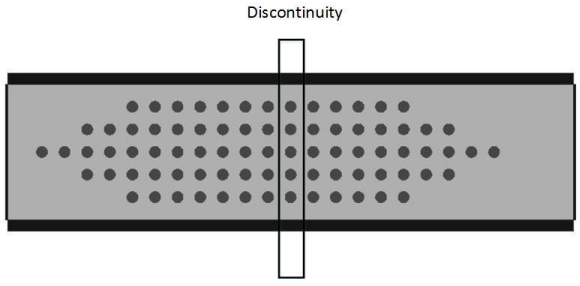

Figure 2.49 Discontinuity in SW-SIW

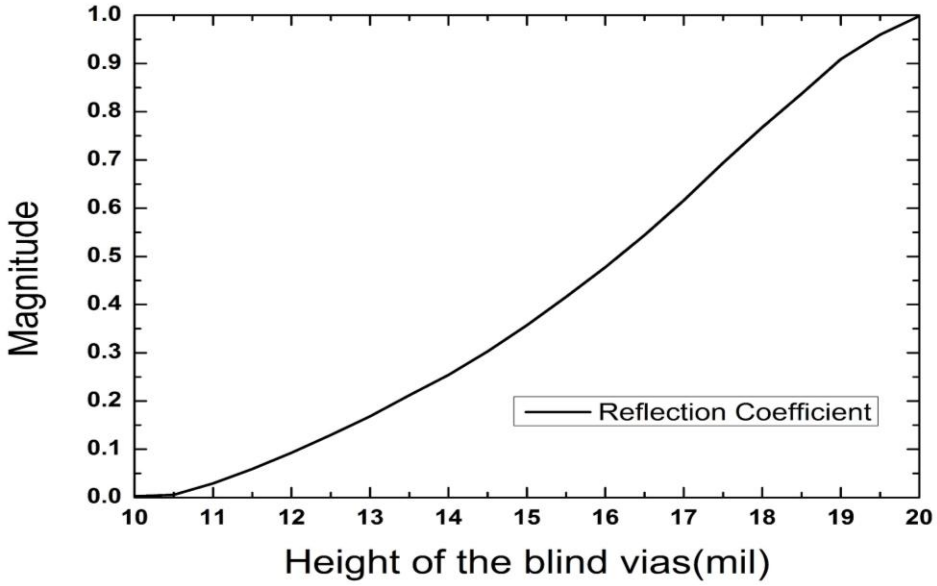

Figure 2.50 Reflection coefficient of discontinuity in SW-SIW

With the value of four calculated Γi in Figure 2.48, the dimensions of the selected row of blind vias could be calculated based on the curve in Figure 2.50, which are tabulated in Table 2-8.

Table 2-8 Dimensions of discontinuities (SW-SIW)

	$\boldsymbol{\Gamma_1}$	$\boldsymbol{\Gamma_2}$	$\boldsymbol{\Gamma_3}$	$\boldsymbol{\Gamma_4}$
Magnitude	0.058	0	0	1
Height (mil)	11	0	0	20

2.3.4.2 Simulation results

The 4-bits SW-SIW tag is proposed to achieve the millimeter-wave identification as well as to verify the equalization method.

The total transmission length of SW-SIW tag $L_{sw\text{-}siw}$ is calculated as follows (2.25)

$$L_{sw-siw} = \frac{(3 * (t_s + t_i) + t_0)v_{gsw-siw}}{2} = 63\ cm \tag{2.25}$$

Similar to the SIW tag, the terminal of the SW-SIW tag is a short circuit and an extra length of 5 cm between the last bit and the terminal of the tag is reserved for the reader to distinguish the terminal. So the total length of the SW-SIW tag $L_{sw\text{-}siw}$ is 68 cm, by connecting the SIW slot antenna, the topology of the SW-SIW tag is shown in Figure 2.51, the size of the tag is 6.6 cm×6.6 cm. Time domain simulation of the tag is executed by CST, the tag is excited at the bottom-left corner without the antenna.

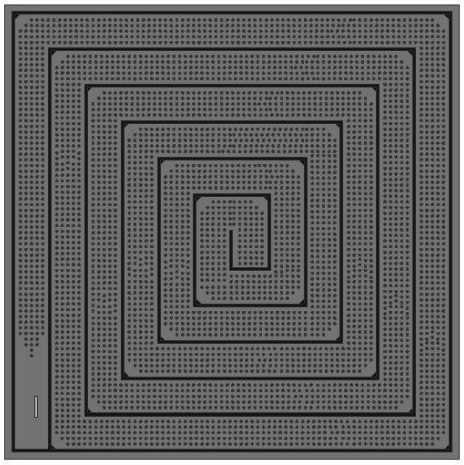

Figure 2.51 Topology of SW-SIW tag

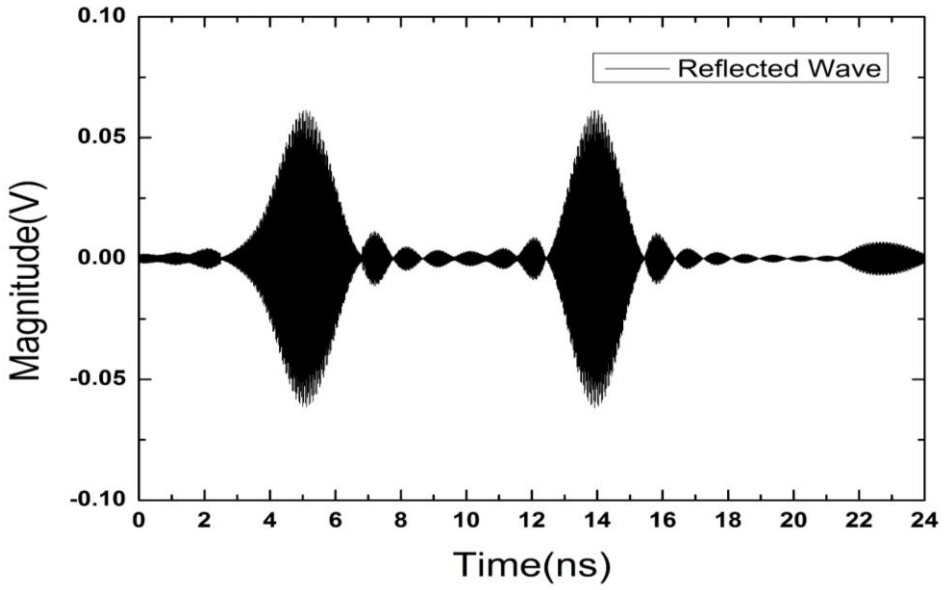

Figure 2.52 Reflected wave of SW-SIW tag (simulation)

Figure 2.52 shows the reflected wave of the SW-SIW tag, the noise in the SW-SIW tag is larger than that in the SIW tag and HMSIW tag. In spite of the noise, the binary code "1001" could be decoded, which could be concluded that the proposed SW-SIW tag works well at 35 GHz.

2.4 Slow-wave half-mode substrate integrated waveguide tag

2.4.1 Introduction

In order to reduce the waveguide width as well as to reduce the group velocity of SIW, a slow wave half mode substrate integrated waveguide (SW-HMSIW) is proposed.

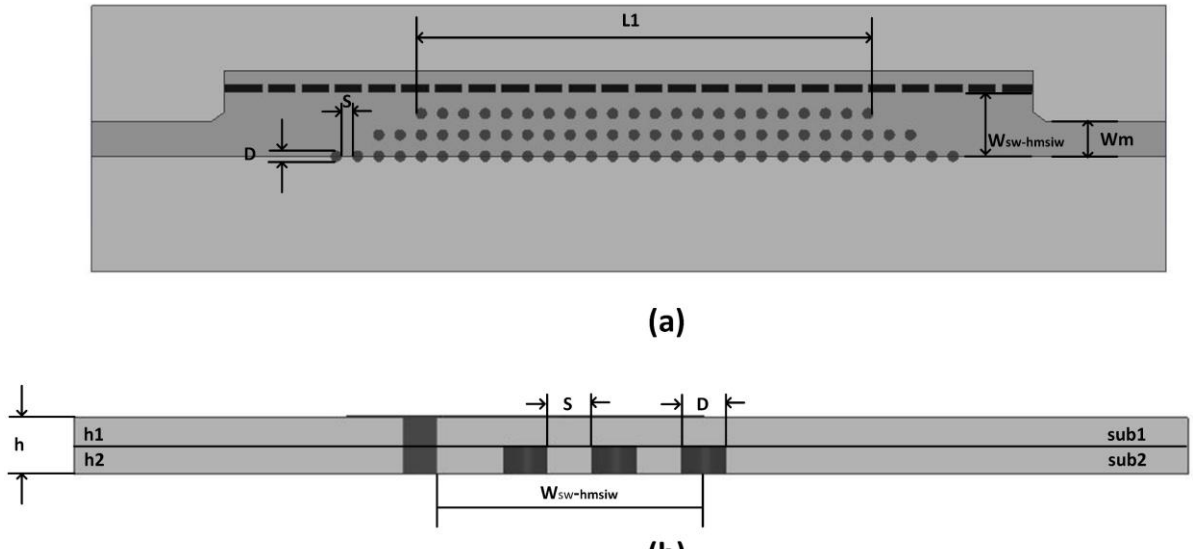

Figure 2.53 SW-HMSIW (a) top view (b) side view

Figure 2.53 (a) and Figure 2.53 (b) show the top view and the side view of the SW-HMSIW, an array of metallic blind vias is added into the conventional HMSIW, a taper is designed in order reduce the mismatch from HMSIW to SW-HMSIW, the SW-HMSIW is fed by the microstrip line. In the model, *D* represents the diameter of the blind via, *S* represents the space between two blind vias, $W_{sw\text{-}hmsiw}$ represents the width of the SW-HMSIW, W_m represents the width of the microstrip line, *h* represents the height of substrate, *h2* represents the height of blind vias, *L1* represents the transmission length of the SW-HMSIW and the SW-HMSIW is designed on Rogers 6002 with the thickness of 20 mil.

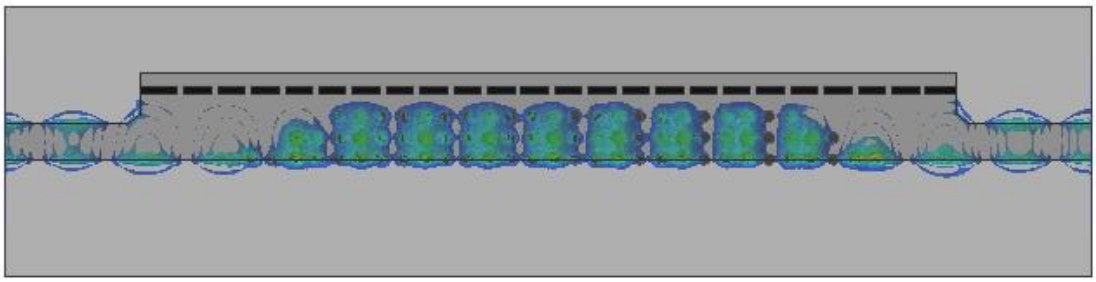

Figure 2.54 Magnitude of electric field in SW-HMSIW

Similar to SW-SIW, when the signal transmits through the blind vias array, the electric field of the wave will be concentrated on the upper *sub1*, which increases the related effective dielectric permittivity in the center of the waveguide. Figure 2.54 shows the magnitude of the electric field in SW-HMSIW, the wavelength is obviously reduced, the electric field and the magnetic field are separated in space while travelling through the blind vias array.

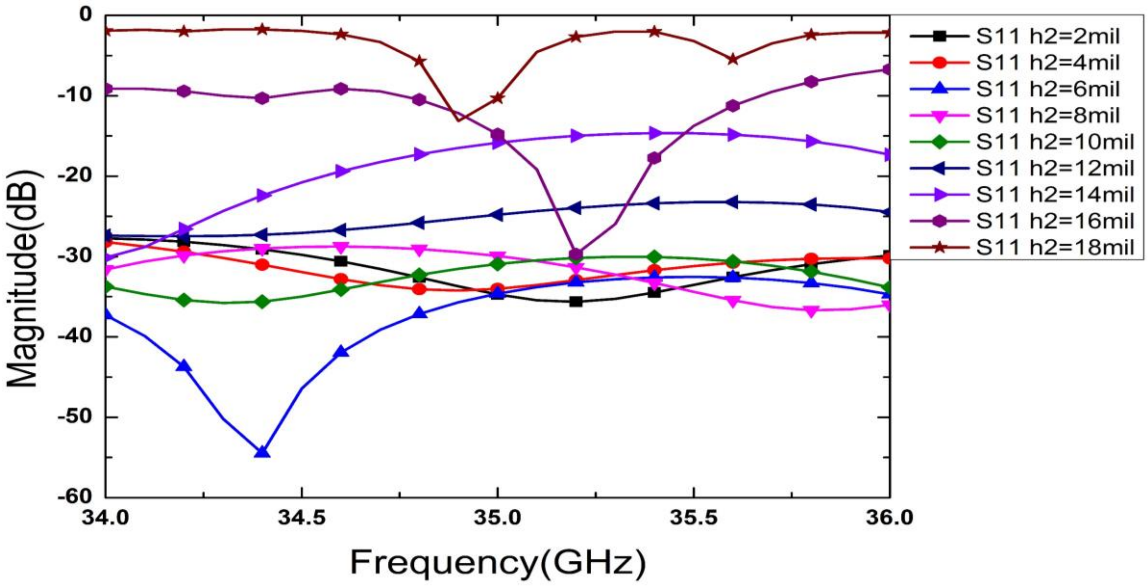

Figure 2.55 S_{11} of SW-HMSIW

The return loss S_{11} of SW-HMSIW is calculated with the dimensions tabulated in Table 2-9 based on different height of *h2* in Figure 2.55. Generally, the higher the blind vias array is, the slower the wave becomes, but the worse the S_{11} is. Considering the loss issue and the noise during the transmission, *h2*=12 mil is considered to build the SW-HMSIW tag.

Table 2-9 Dimensions of SW-HMSIW

W_{hmsiw}	W_m	S	D	$L1$
3.8 mm	1.3 mm	0.4 mm	0.4 mm	12.8 cm

2.4.2 Extraction of the propagation constant of SW-HMSIW

2.4.2.1 Multiline method (SW-HMSIW)

The multiline method is again adopted to extract the propagation constant of SW-HMSIW, the model is built in HFSS as shown in Figure 2.56, a section of SW-HMSIW with the transmission length of 12.8 cm and the other section of SW-HMSIW with the transmission length of 23.2 cm are simulated over the frequency range from 34 GHz to 36 GHz in HFSS.

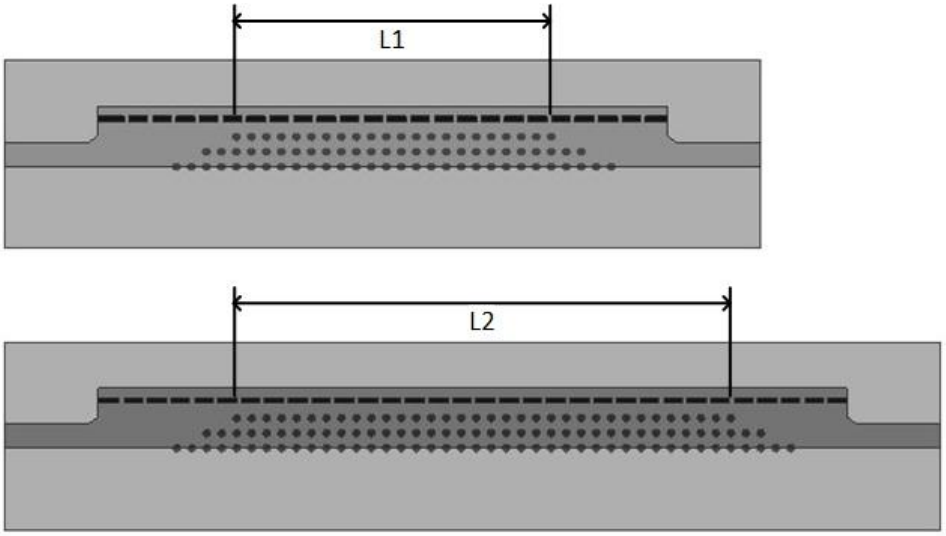

Figure 2.56 Multiline method (SW-HMSIW)

2.4.2.2 Attenuation constant $\alpha_{sw\text{-}hmsiw}$

In the SW-HMSIW, the conductor loss is caused by the top and bottom copper as well as the metal vias and the blind vias array. The dielectric loss is caused by the dielectric filled in the waveguide. The radiation loss is caused by the leakage through the gap between the metallic vias and the radiation from the open part. Based on the model in Figure 2.56, the attenuation constant

of SW-HMSIW $\alpha_{sw\text{-}hmsiw}$ over the frequency range from 34 GHz to 36 GHz could be extracted and given in Figure 2.57, the comparison with SW-SIW is also illustrated in Figure 2.57.

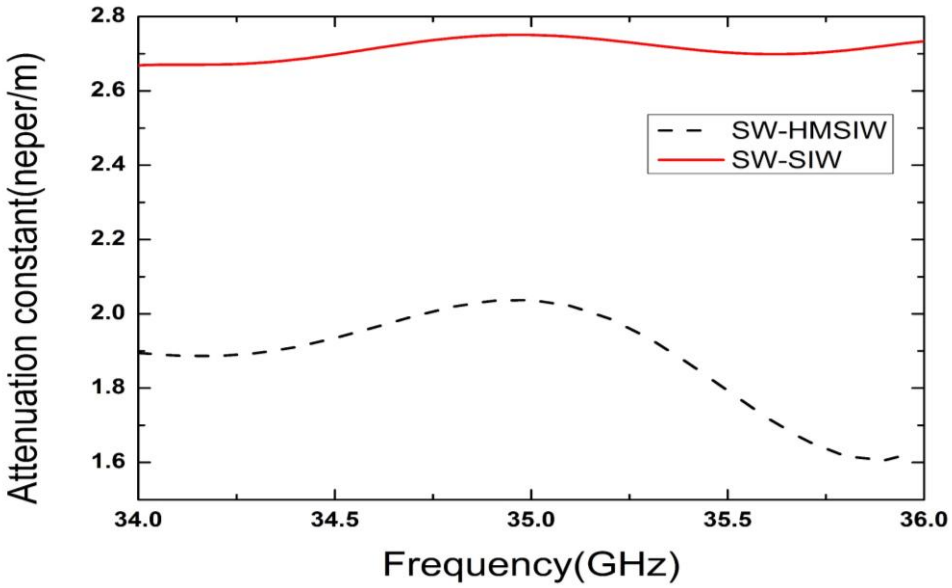

Figure 2.57 Attenuation constant of SW-HMSIW

As shown in the figure, the value of $\alpha_{sw\text{-}hmsiw}$ is lower than α_{hmsiw} within the frequency range from 34 GHz to 36 GHz, the reason is that even the SW-HMSIW suffers from the radiation loss issue, but the size is reduced by half as compared with the SW-SIW, which in turn reduces the conductor loss and the dielectric loss. The attenuation constant of SW-HMSIW $\alpha_{sw\text{-}hmsiw}$=2.02 neper/m at 35 GHz is considered for the equalization method proposed in chapter 1.

2.4.2.3 Phase constant $\beta_{sw\text{-}hmsiw}$

Similar to the phase constant of the SIW, the value of $\beta_{sw\text{-}hmsiw}$ will not only affect the group velocity but also arouse the dispersion issue.

Based on the model in Figure 2.56, the phase constant of SW-HMSIW $\beta_{sw\text{-}hmsiw}$ from 34 GHz to 36 GHz is calculated in Figure 2.58. For the SW-HMSIW tag design, the value of the phase constant $\beta_{sw\text{-}hmsiw}$ =1337 rad/m at 35 GHz is considered for the equalization method proposed in chapter 1.

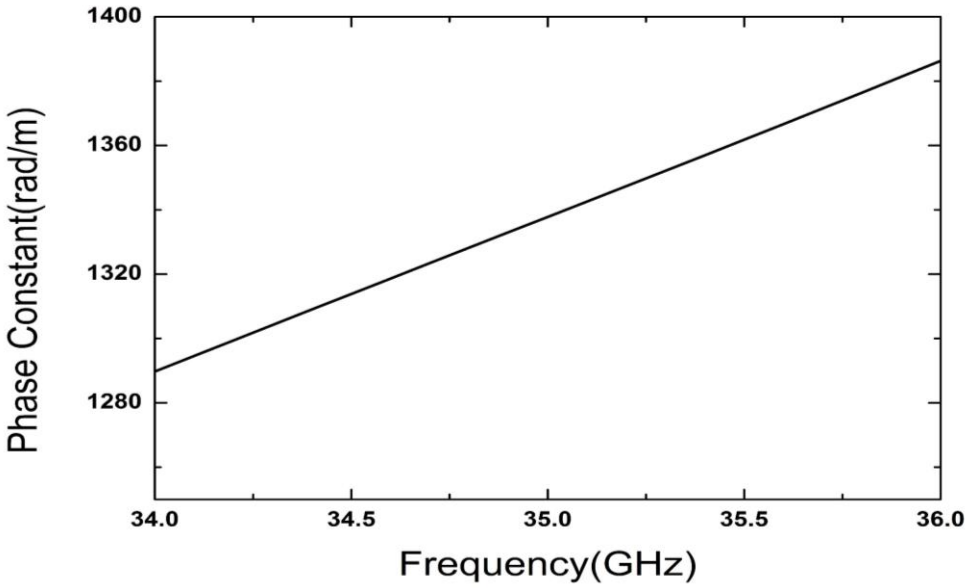

Figure 2.58 Phase constant of SW-HMSIW

2.4.3 Distortion

2.4.3.1 Group delay of SW-HMSIW $V_{gsw\text{-}siw}$

Similar to SIW, the distortion of an interrogation signal in the SW-HMSIW could be divided into two parts: dispersion and attenuation. The group delay of the SW-HMSIW $\tau_{gsw-hmsiw}$ could be expressed by the formulation (2.7), the value of $\alpha_{sw-hmsiw}$ and $\beta_{sw-hmsiw}$ over the frequency range from 34.5 GHz to 35.5 GHz is extracted, with (2.7), we can adjust the value of transmission length *L* to achieve the group delay of 3 ns at 35 GHz.

As shown in Figure 2.59, the red curve represents the attenuation of SW-HMSIW, the black curve represents the group delay of signal in SW-HMSIW. With the optimized *L*=37 cm, the group delay of 3 ns at 35 GHz is achieved and it can be seen that the interrogation signal is expanded from 3 ns to 3.05 ns. This level of distortion is acceptable for the interval of 1 ns between two neighbouring pulses.

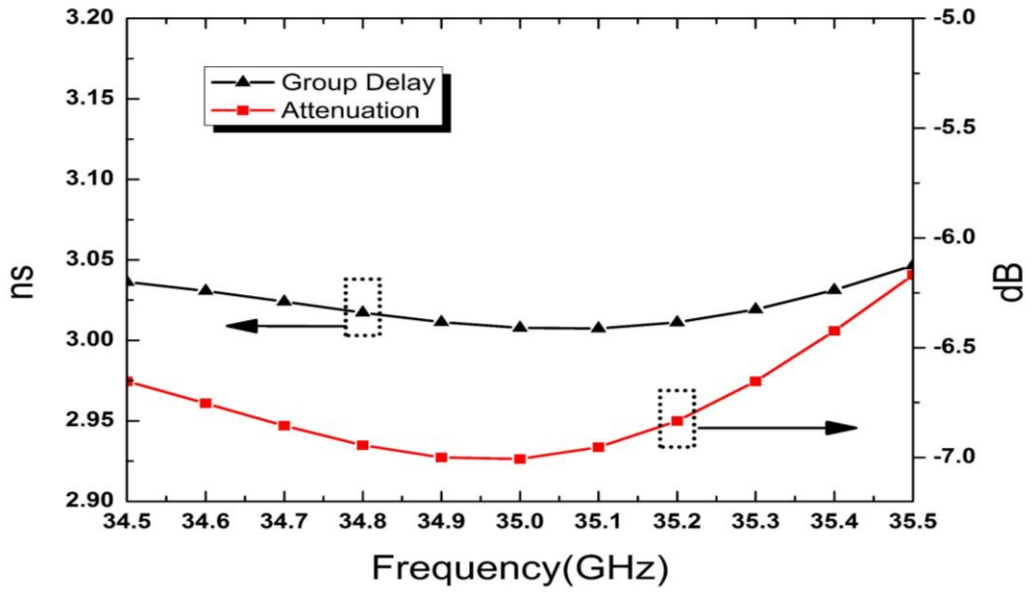

Figure 2.59 Group delay and attenuation (SW-HMSIW)

The group velocity of SW-HMSIW could be calculated as follows (2.26).

$$V_{gsw-hmsiw} = \frac{L}{\tau_g} = 1.233 * 10^8\ m/s \tag{2.26}$$

The slowing factor of SW-HMSIW *K* could be calculated by (2.27).

$$K = \frac{V_{g(SW-HMSIW)}}{V_{g(HMSIW)}} = 77.1\% \tag{2.27}$$

2.4.3.2 Interrogation signal distortion

The spectrum of an interrogation signal through a transmission length of 37 cm in the SW-HMSIW could be calculated and then plotted in Figure 2.60.

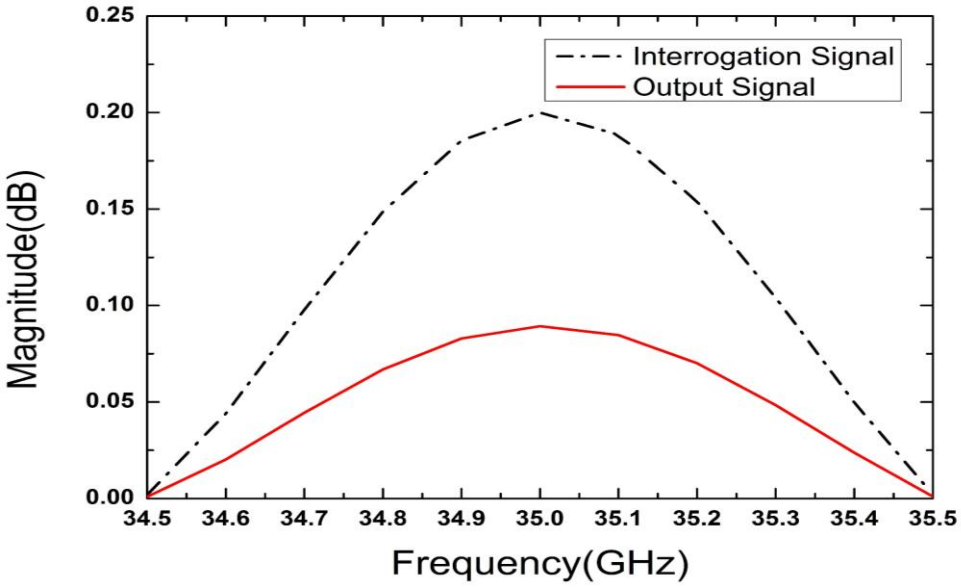

Figure 2.60 Spectrum of output signal (SW-HMSIW)

Inverse Fourier transform is performed based on the spectrum of the output signal (SW-HMSIW) in order to find the output signal in time domain as shown in Figure 2.61, it could be observed that the time delay of the amplitude envelop of 3 ns is achieved with the transmission length of 37 cm and the interrogation signal is expanded from 3 ns to 3.05 ns.

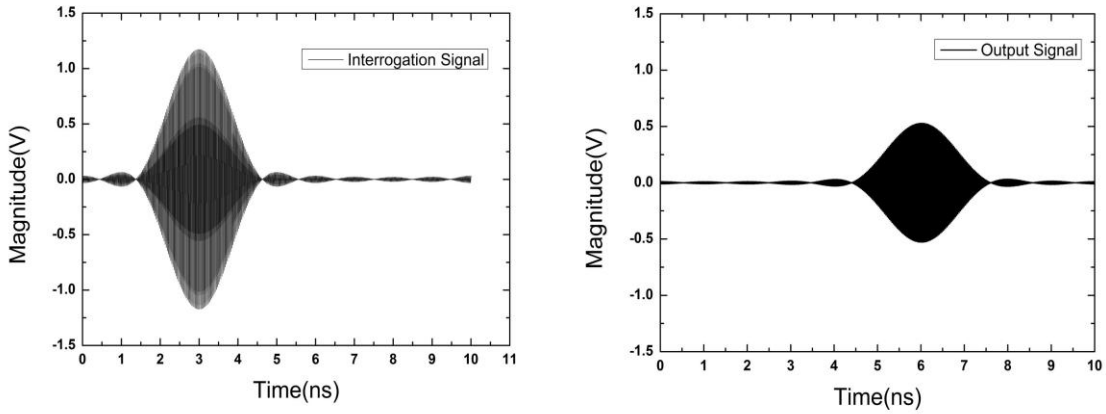

Figure 2.61 Interrogation signal and output signal (SW-HMSIW)

2.4.4 Meander-line based SW-HMSIW tag

2.4.4.1 Coupling between the parallel SW-HMSIW

In order to reduce the size of SW-HMSIW tag, the meander-line structure is considered. Because one side of SW-HMSIW is open which could be regarded as a magnetic wall, it will lead to higher coupling between the neighbouring SW-HMSIW.

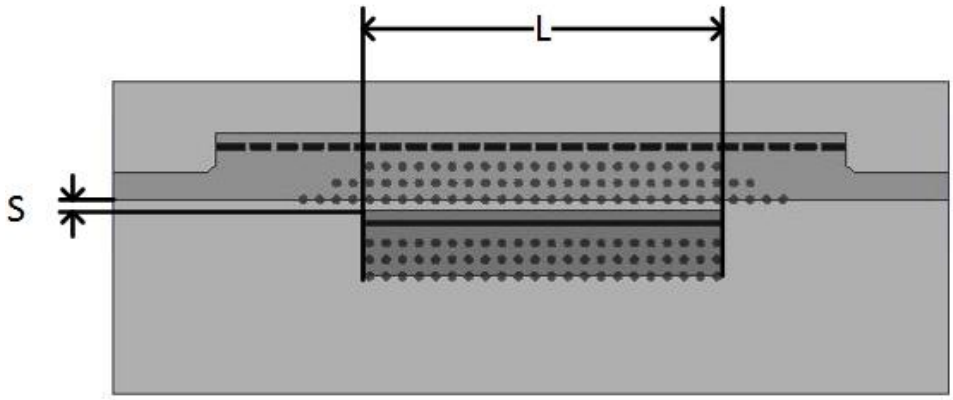

Figure 2.62 SW-HMSIW (open side to close side)

Similar to the case of HMSIW, "open side to enclose side" structure is considered to build the meander-line SW-HMSIW tag. The model is simulated in HFSS as shown in Figure 2.62, the upper part is the SW-HMSIW with a transmission length L=20 mm, which is fed by a microstrip line, the bottom part is the SW-HMSIW with the same transmission length L= 20 mm with no feeding line, the dielectric filled in both cases is Rogers 6002 with the thickness of 20 mil, S represents the spacing between the two structures. A full -ave simulation is carried out by HFSS over the frequency range from 30 GHz to 40 GHz based on different values of S.

Figure 2.63 shows S parameter results of the presented model, S_{11} is below -20 dB when S=0.5 mm and 1 mm and S_{11} is over -20 dB with spacing S=0.2 mm. For the SW-HMSIW tag design, the closer the spacing is, the smaller the tag becomes. Therefore, S=0.5 mm is considered for the design of meander-line SW-HMSIW tag.

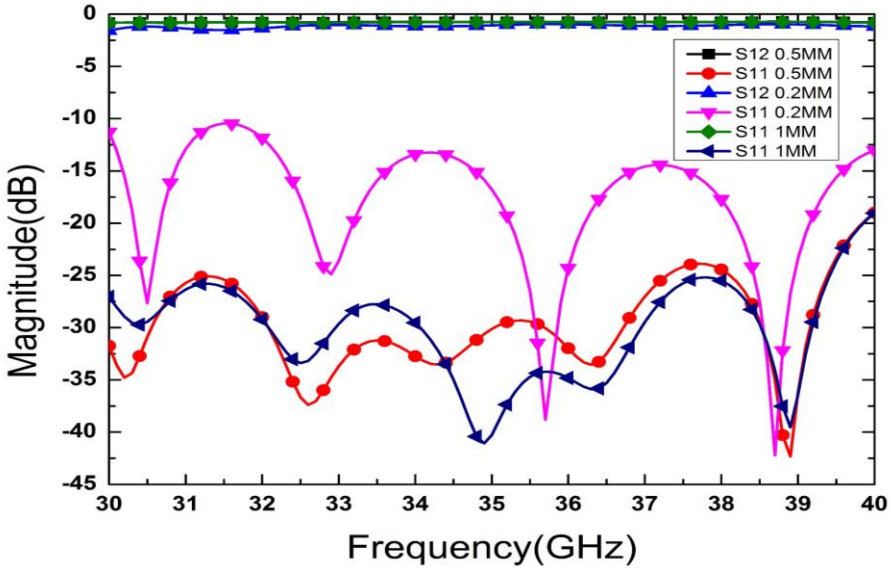

Figure 2.63 Coupling between SW-HMSIW (open side to enclosed side)

2.4.4.2 Discontinuities

With the extracted $\alpha_{sw\text{-}hmsiw}$=2.02 neper/m, $\beta_{sw\text{-}hmsiw}$=1230 rad/m and $V_{gsw\text{-}hmsiw}$=1.233*10^8 m/s, by applying the equalization method proposed in chapter 1, the reflection coefficient of every discontinuity could be calculated as shown in Figure 2.64, the maximum amplitude of the reflected wave for the binary code "1101" is 0.09 when the amplitude of the interrogation signal is

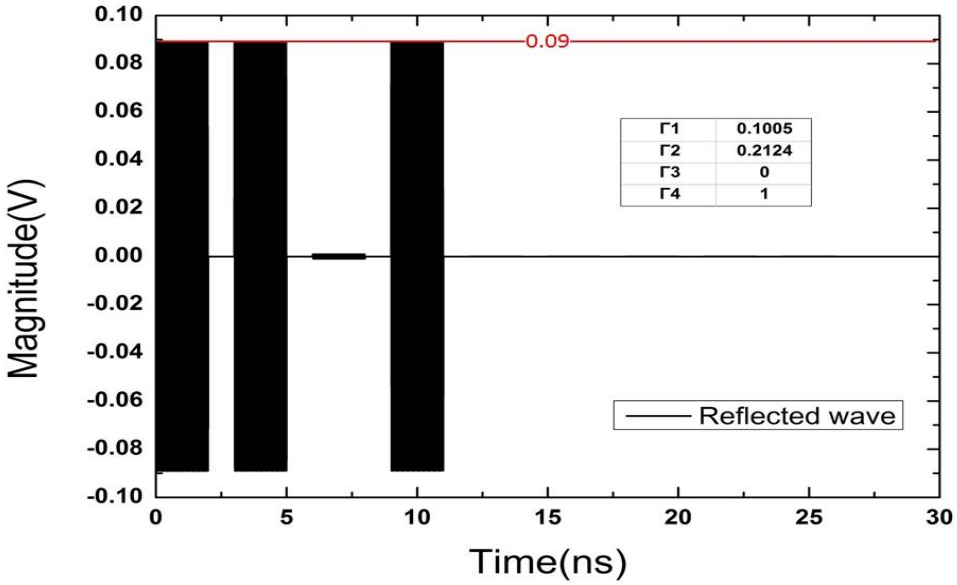

Figure 2.64 Reflected wave in SW-HMSIW (matlab)

normalized to 1.

For the SW-HMSIW tag design, the discontinuity is realized by changing the height of a selected row of the blind vias as shown in Figure 2.65, the reflection coefficient of this kind of discontinuity could cover the range from 0 to 1 as shown in Figure 2.66.

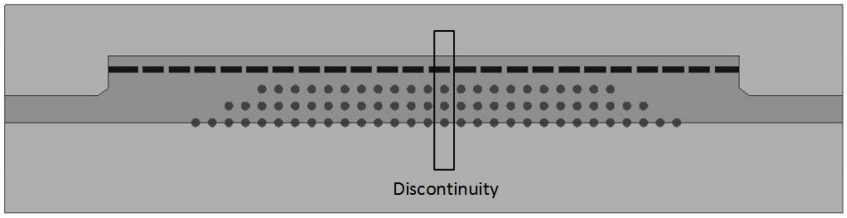

Figure 2.65 Discontinuity in SW-HMSIW

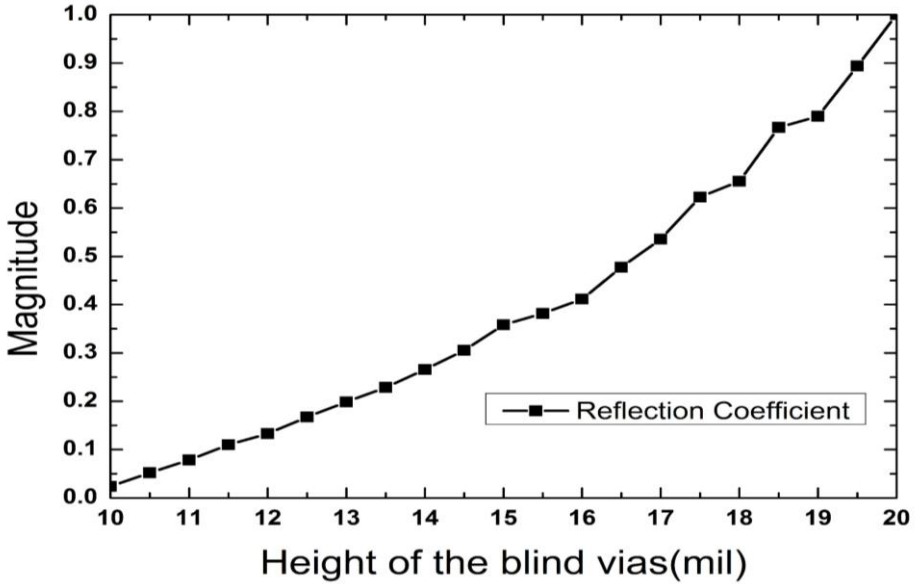

Figure 2.66 Reflection coefficient of discontinuity in SW-HMSIW

With the value of four calculated Γi in Figure 2.64, the dimensions of the selected row of blind vias could be calculated based on the curve in Figure 2.66, which are tabulated in Table 2-10.

Table 2-10 Dimensions of discontinuities (SW-HMSIW)

	Γ_1	Γ_2	Γ_3	Γ_4
Magnitude	0.1005	0.2124	0	1
Height (mil)	11	13	0	20

2.4.4.3 Simulation result

The 4-bits SW-HMSIW tag is proposed to achieve the millimeter-wave identification as well as to verify the equalization method presented in this work.

The total transmission length of SW-HMSIW tag $L_{sw\text{-}hmsiw}$ is calculated as follows (2.28)

$$L_{sw-hmsiw} = \frac{(3 * (t_s + t_i) + t_0)v_{gsw-hmsiw}}{2} = 62\ cm \tag{2.28}$$

Similar to the SIW tag, the terminal of the SW-HMSIW tag is a short circuit and an extra length of 5 cm between the last bit and the terminal of the tag is reserved for the reader to distinguish the terminal. So the total length of the SW-HMSIW tag $L_{sw\text{-}hmsiw}$ is 67 cm, by connecting the HMSIW slot antenna, the topology of the SW-HMSIW tag could be shown in Figure 2.67, the size of the tag is 5 cm×5 cm. Time domain simulation of the tag is carried out by the use of CST, the tag is excited at the bottom-left corner without antenna.

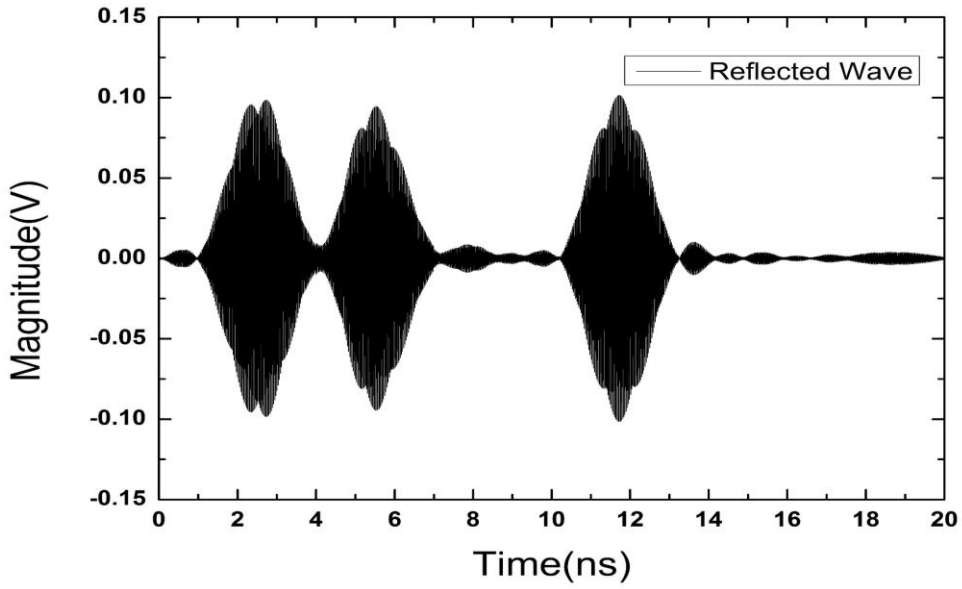

Figure 2.67 Reflected wave of SW-HMSIW tag (simulation)

Figure 2.67 shows the reflected wave of SW-HMSIW tag. In spite of the noise, the binary code "1101" could be decoded, which can be concluded that the proposed SW-HMSIW tag also works well at 35 GHz.

2.5 Comparison

The comparison of these four TDR MMID tags based on different kinds of transmission line is conducted to show the difference as described in Table 2-11.

Table 2-11 Comparison of TDR MMID tags

	SIW tag	**HMSIW tag**	**SW-SIW tag**	**SW-HMSIW tag**
Attenuation constant(neper/m)	1.68	1.64	2.73	2.02
Phase constant (rad/m)	1008	1058	1230	1337
Group velocity (m/s)	$1.41*10^8$	$1.603*10^8$	$1.287*10^8$	$1.233*10^8$
Size (cm)	7.5×7.5	6.5×6.5	6.6×6.6	5×5
Maximum amplitude	0.089	0.076	0.04	0.085
Noise	Low	Low	High	Medium

Through the comparison, it can be concluded that the SW-HMSIW tag has the smallest size, the SIW tag has the best performance with reference to the amplitude and noise aspects. The fabrication process of the SW-SIW tag and the SW-HMSIW tag is more complicated than the SIW tag and HMSIW tag.

CHAPTER 3 CHIPLESS MMID TAG BASED ON PHASE MODULATION

3.1 Introduction

A RFID system based on phase modulation (PM) encodes the binary code by varying the phase of an interrogation signal [38-40], the operating principle of the system is shown in Figure 3.1.

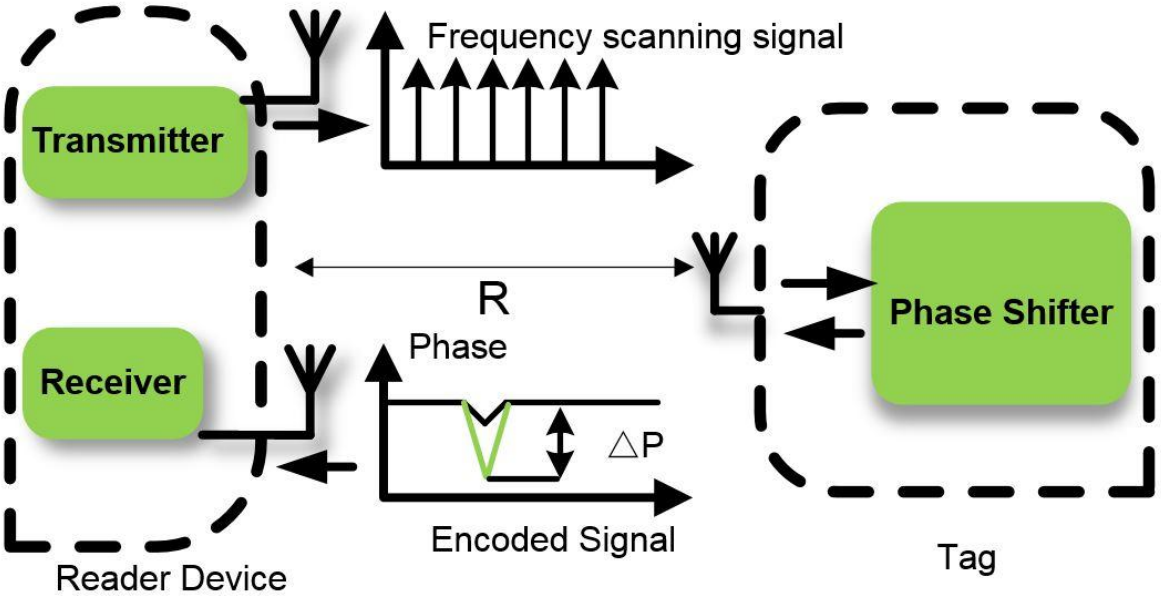

Figure 3.1 Chipless RFID system based on phase modulation

The operating principle of PM RFID system is similar to the frequency modulation (FM) RFID system. In both cases, the reader will send the frequency scanning signal during the operation, the signal will be received by the tag and the tag will send back the encoded signal. The difference is that in the FM RFID system, the tag will encode the information by modifying the spectrum of the reflected signal, but for the PM RFID system, the tag will encode the information by varying the instantaneous phase of the signal while keeping the spectrum of the interrogation signal unaltered.

3.2 SIW phase shifter

Substrate integrated waveguide (SIW) technique is again considered in this work to build the phase shifter due to its low loss (high Q), self-consistent shielding characteristic and the outstanding performance in millimeter-wave applications.

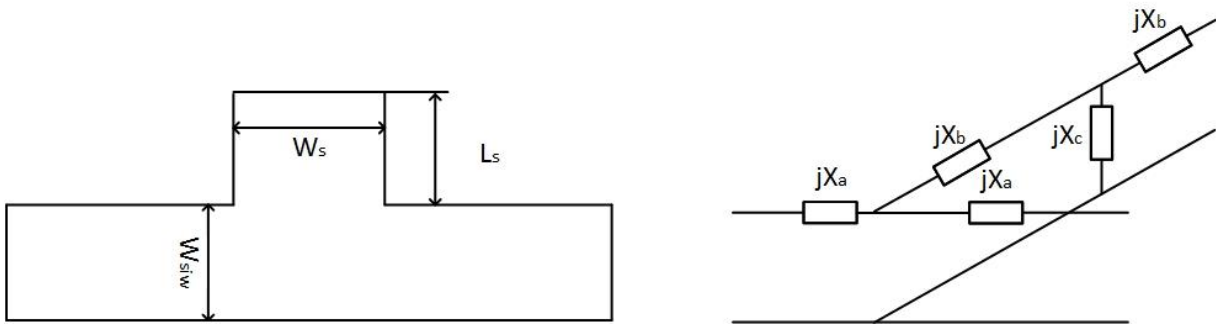

Figure 3.2 H-plane stub and equivalent circuit

The geometry of SIW phase shifter and its equivalent circuit are shown in Figure 3.2, where W_{siw} represents the width of SIW, W_s represents the width of the stub, L_s represents the length of the stub. The reason of phase shift by adding H-plane stub in SIW could be explained by assuming the SIW is long enough, the stub could be regarded as a pure shunt junction. During the transmission, due to the effect of magnetic field, coupling will occur from the longitudinal magnetic field in the main SIW to the transverse magnetic field in the stub line, which will cause a change of the phase of the interrogation signal [30].

In order to characterize the performance of the proposed SIW phase shifter, the model is developed in HFSS as shown in Figure 3.3, the upper side is the SIW phase shifter and the bottom side is the reference line with the same transmission length, the phase shifter is designed on Rogers 6002 with thickness of 10 mil, dielectric permittivity is 2.94. A full-wave simulation is carried out over the frequency range from 33 GHz to 37 GHz with the dimensions tabulate in Table 3-1.

Table 3-1 Dimensions of SIW phase shifter

W_{siw}	L_{siw}	L_s	W_s
3.8 mm	40 mm	4.1 mm	4.8 mm

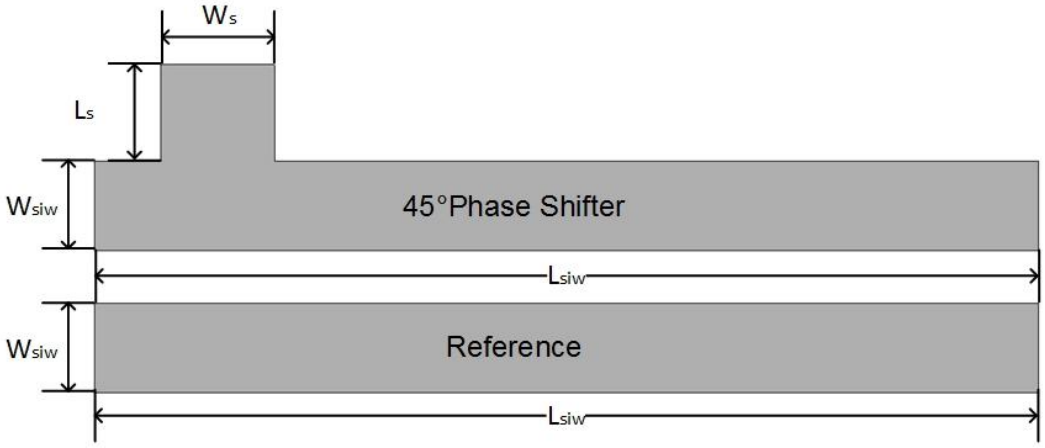

Figure 3.3 Topology of SIW phase shifter (1 stub)

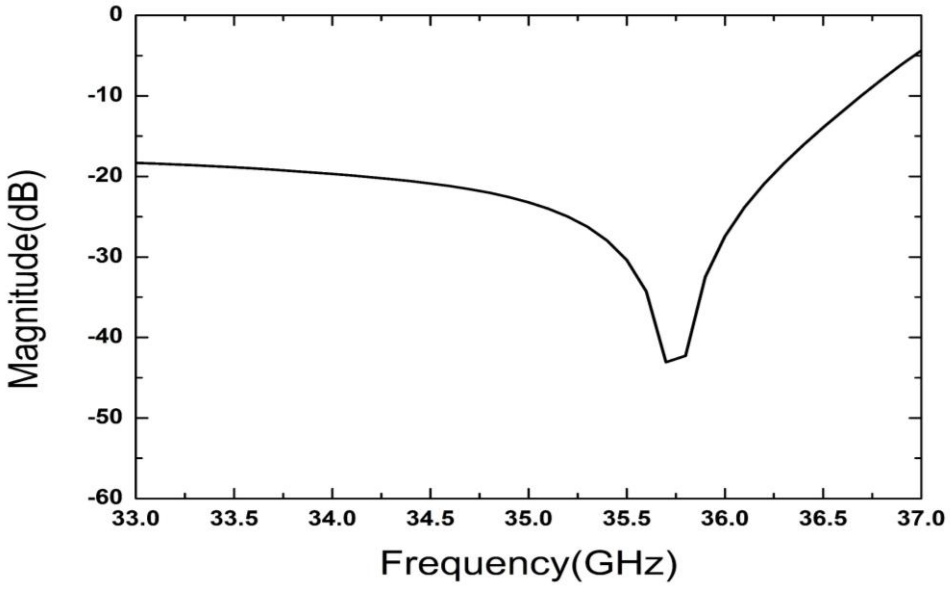

Figure 3.4 S_{11} of SIW phase shifter (1 stub)

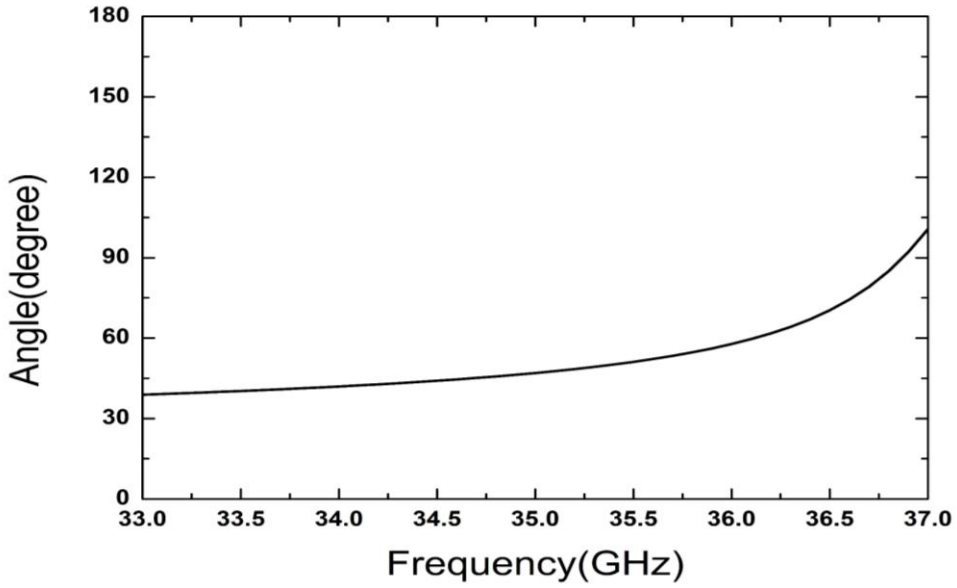

Figure 3.5 Simulated phase shift (1 stub)

As shown in Figure 3.4, the return loss S_{11} is below -20 dB from 34.5 GHz to 35.5 GHz, which means that the H-plane stub could be used for building a two port SIW phase shifter. Through Figure 3.5, it could be observed that the maximum phase shift of 45° at 35 GHz is achieved by adding one stub in H-plane. Within the bandwidth from 34.5 GHz to 35.5 GHz, the PS could cover the phase shift range from 40° to 50°.

In the PM MMID system, we can suppose that the total phase range for encoding the bits of information is from 0° to 180°, if the reader is accurate enough to detect the signal with the resolution of 1 degree, then 180 bits of information could be encoded into the tag. In this work, in order to just verify the proposed concept, the resolution of 45° is considered for building the tag, so the phase shifters of 90°, 135°, and 180° are designed in Figure 3.6, where two stubs, three stubs and four stubs are added into the SIW to achieve the phase shift of 90°, 135° and 180°.

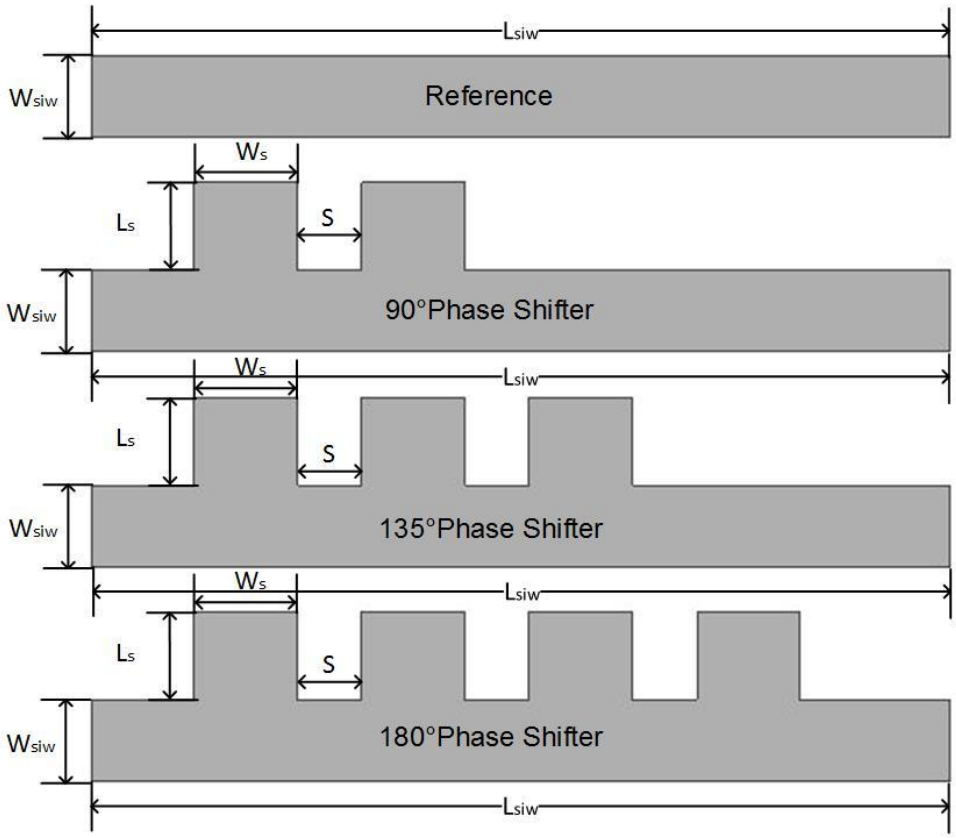

Figure 3.6 Topology of SIW phase shifter (2, 3, 4 stubs)

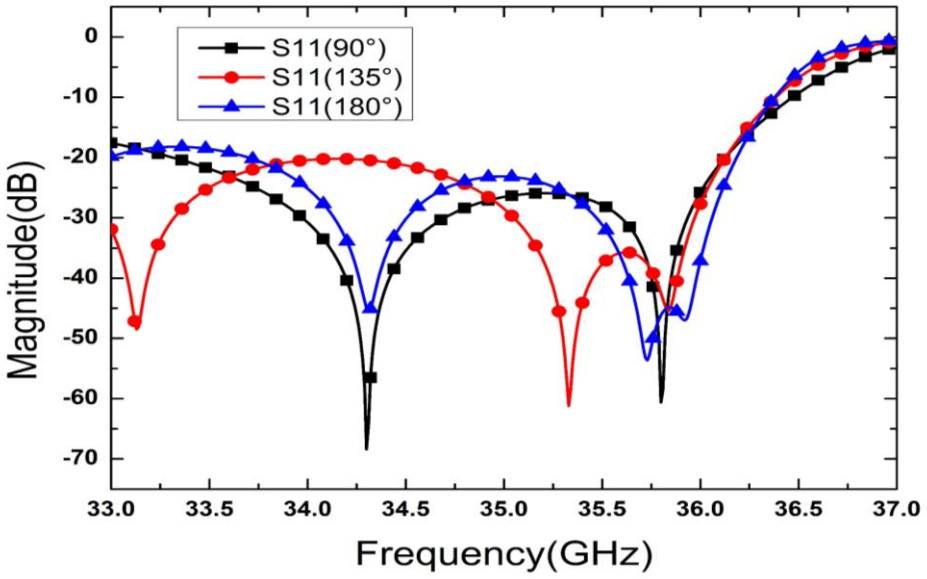

Figure 3.7 S_{11} of SIW phase shifter (2, 3, 4 stubs)

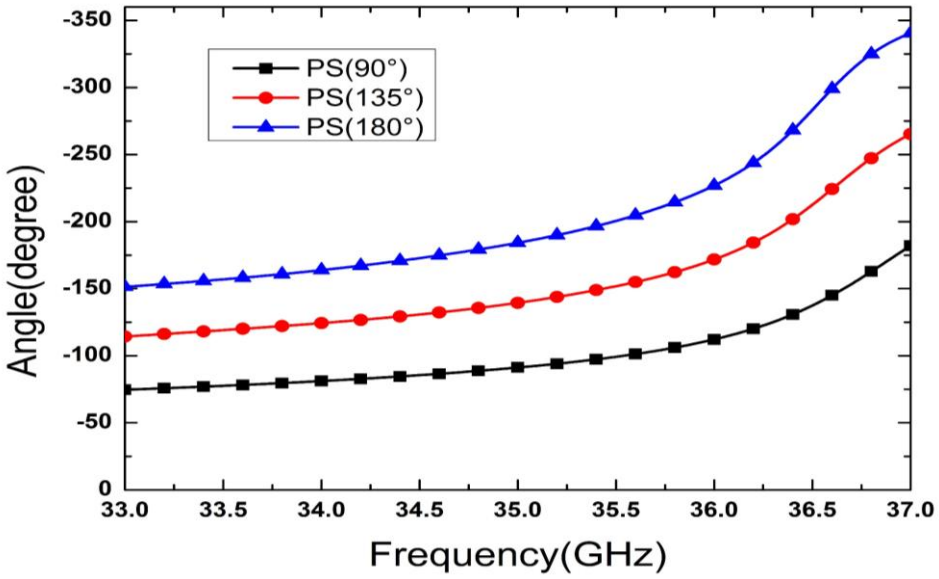

Figure 3.8 Simulated phase shift (2, 3, 4 stubs)

As shown in Figure 3.7, with the optimized spacing *S*=3 mm between the neighbouring stubs, the return losses are below -20 dB within the frequency range from 34.5 GHz to 35.5 GHz. According to Figure 3.8, the phase shift of 90°, 135°, and 180° can be achieved at the centre frequency of 35 GHz.

3.3 MMID tag

Because the proposed SIW phase shifter is a two-port device, two antennas should be integrated to realize the function of receiving the interrogation signal and sending back the encoded signal. In order to avoid the interaction between them, a method of adding two cross-polarized slot-antennas is proposed to communicate with the reader device, then the MMID tag is designed with the dimensions tabulated in Table 3-2, which are shown in Figure 3.9.

Table 3-2 Dimensions of MMID tag

L1	***L2***	***S***	***Ls***	***Ps***	***Ws***
40 mm	17 mm	3.4 mm	3.4 mm	1.7 mm	0.35 mm

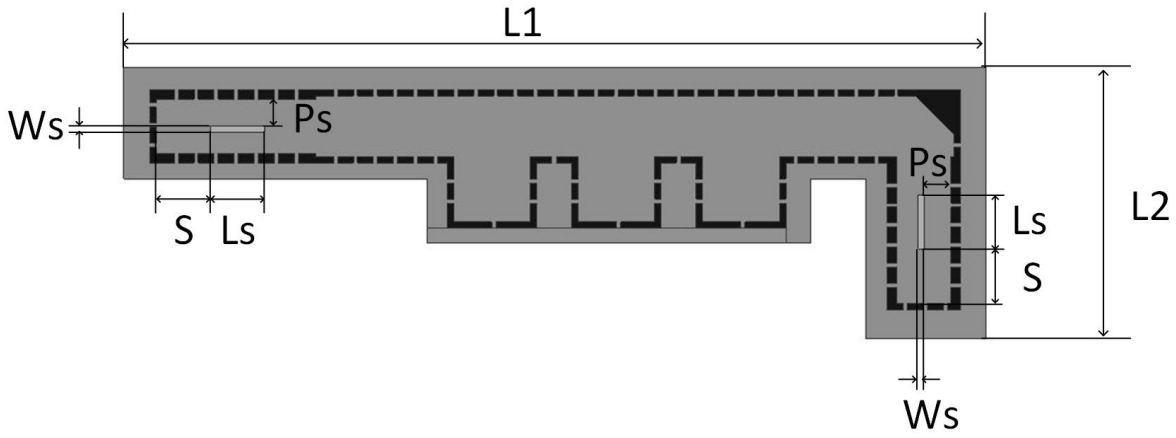

Figure 3.9 Topology of PM MMID tag

In Figure 3.9, W_s represents the width of the slot antenna, L_s represents the length of the slot antenna, P_s represents the distance between the antenna and the metal vias, *L1* represents the length of the MMID tag and *L2* represents the width of the MMID tag.

3.4 Simulation result

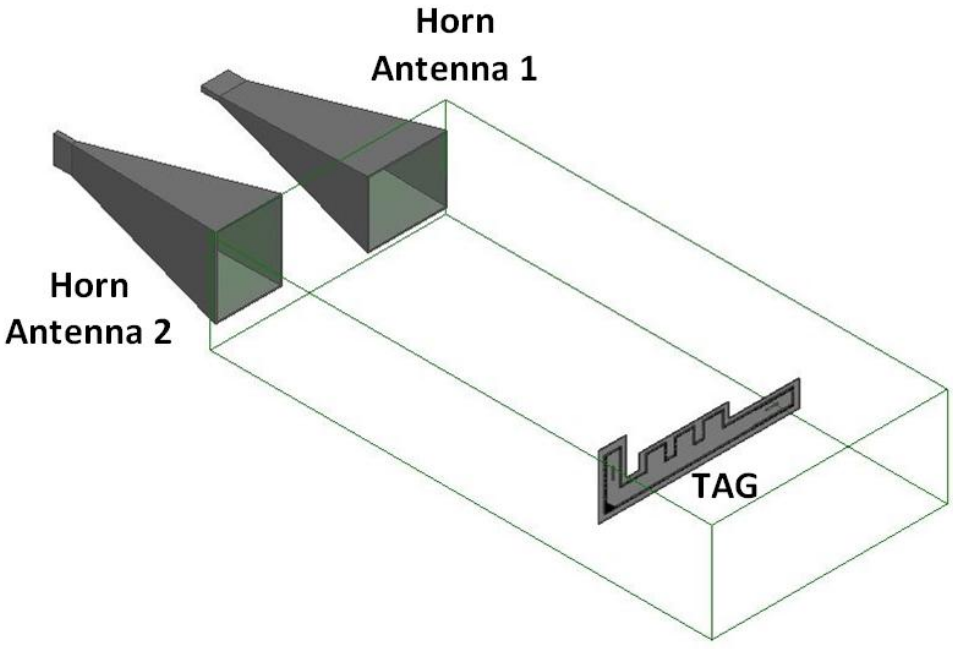

Figure 3.10 Measurement setup (simulation)

The modeling of measurement setup is carried out by the use of HFSS as shown in Figure 3.10, a horn antenna is considered to send the swept-frequency signal covering the range from 34 GHz to 36 GHz, the other horn antenna which is rotated by 90 degrees is used for receiving the signal, the MMID tag is fixed with a distance of 10 cm away from the horn antennas.

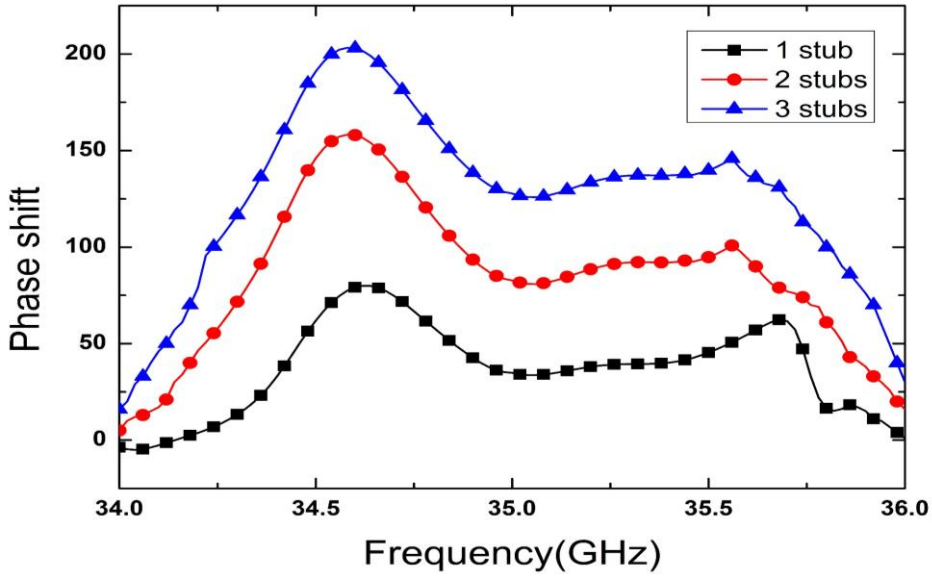

Figure 3.11 Phase shift of PM MMID tag (simulation)

Figure 3.11 shows the phase shift of PM MMID tag with one stub, two stubs, and three stubs normalized to the reference line, it could be observed that a phase shift of 43°, 85°, and 125° is achieved at the centre frequency of 35 GHz.

3.5 Measurement result

The measurement setup is constructed to validate the proposed encoding technique as shown in Figure 3.12. In this case, a vector network analyzer (VNA) is used to generate the swept-frequency signal covering the frequency from 34 GHz to 36 GHz through a horn antenna with the gain of 20 dBi, the phase response of the tag encoded in the backscattered signal is detected by the other horn antenna with the same gain of 20 dBi.

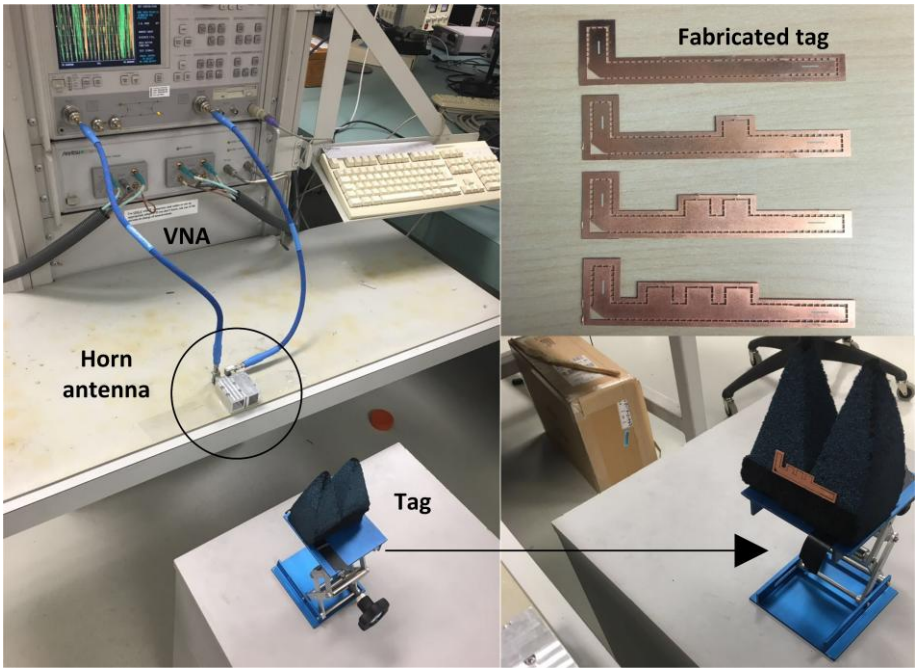

Figure 3.12 Measurement setup

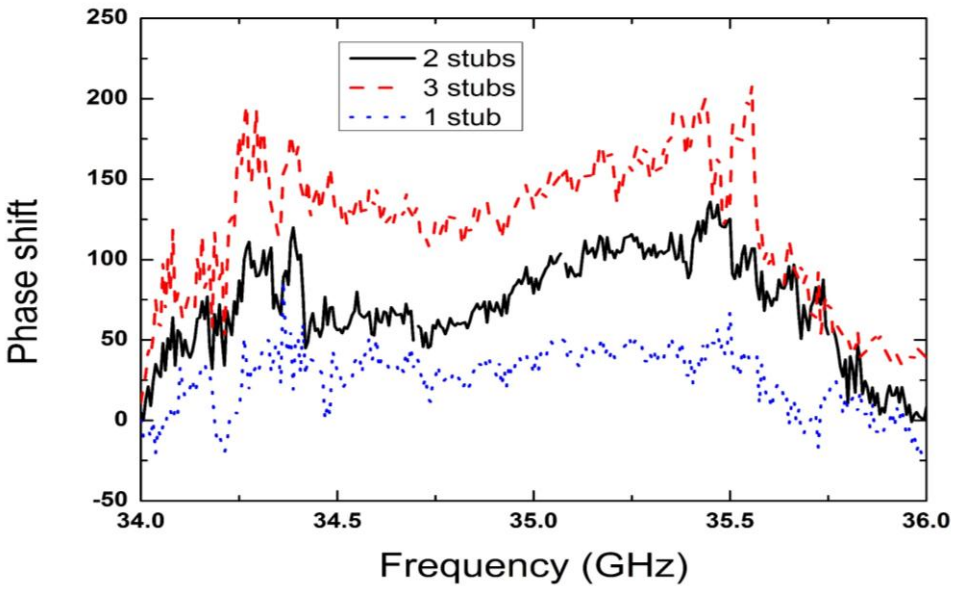

Figure 3.13 Phase shift of PM MMID tag (measurement)

Figure 3.13 shows the phase of S_{21} of the MMID tag with one stub, two stubs and three stubs normalized to the reference tag, at the resonance frequency of 35 GHz, the phase deviation of 41°, 87° and 126° have been found which can demonstrate the proposed technique.

CONCLUSION AND FUTURE WORK

Conclusion

The scope of this dissertation focuses on the TDR MMID system, the TDR MMID tag and the PM MMID tag. The major contributions of this work can be summarized as follows:

- A generalized theoretical modelling considering the multireflection issue during the TDR RFID tag design is developed which is applicable to the analysis of any kind of RFID tag based on the TDR technique.
- The link budget of the TDR MMID system is studied and an equalization method is proposed and presented to maximize the encodable bits in the tag design.
- A novel transmission line named “SW-HMSIW” is presented which can be used for the design of passive components.
- The TDR MMID tags based on SIW, HM-SIW, SW-SIW and SW-HMSIW technologies are presented, and these tags are studied theoretically and experimentally, which shows the feasibility of the TDR MMID system.
- The PM MMID tag based on SIW technology is presented, which shows the feasibility of a PM MMID system.

Future work

Following the theoretical and experimental studies as described in this dissertation, some of the issues should be further investigated and improved as follows.

- Active components in the reader part of the TDR MMID system should be studied to generate much narrower pulse signals, the expected narrower pulse signals will decrease transmission time in the TDR MMID tag, which will help to encode more bits of information in the MMID tag design with the same physical size.
- Multiple modulation types (time, frequency, phase and polarization) should be integrated into the same design platform of MMID tag to enhance its bit density, and we expect that in the future, more than 1000 bits of information could be integrated in the such hybrid MMID tags with the size of a normal ID card.

BIBLIOGRAPHY

[1] K. Finkenzeller, *RFID Handbook: Radio-frequency identification fundamentals and applications*: Wiley, 1999.

[2] J. Landt, "The history of RFID," *IEEE potentials,* vol. 24, pp. 8-11, 2005.

[3] B. Nath, F. Reynolds, and R. Want, "RFID technology and applications," *IEEE Pervasive Computing,* vol. 5, pp. 22-24, 2006.

[4] K. Domdouzis, B. Kumar, and C. Anumba, "Radio-Frequency Identification (RFID) applications: A brief introduction," *Advanced Engineering Informatics,* vol. 21, pp. 350-355, 2007.

[5] R. Want, "An introduction to RFID technology," *IEEE Pervasive Computing,* vol. 5, pp. 25-33, 2006.

[6] M. A. Khan, M. Sharma, and H. Prabhu, "A survey of RFID tags," 2009.

[7] S. Preradovic and N. C. Karmakar, *Multiresonator-based Chipless RFID: Barcode of the Future*: Springer Science & Business Media, 2012.

[8] S. Preradovic and N. C. Karmakar, "Chipless RFID: bar code of the future," *IEEE Microwave Magazine,* vol. 7, pp. 87-97, 2010.

[9] K. Wu, P. Burasa, T. Djerafi, and N. Constantin, "Millimeter-wave identification for future sensing, tracking, positioning and communicating systems," in *2016 Global Symposium on Millimeter Waves (GSMM) & ESA Workshop on Millimetre-Wave Technology and Applications*, 2016, pp. 1-4.

[10] A. Chamarti and K. Varahramyan, "Transmission delay line based ID generation circuit for RFID applications," *IEEE microwave and wireless components letters,* vol. 16, pp. 588-590, 2006.

[11] V. P. Plessky and L. M. Reindl, "Review on SAW RFID tags," *IEEE transactions on ultrasonics, ferroelectrics, and frequency control,* vol. 57, pp. 654-668, 2010.

[12] S. Preradovic and N. Karmakar, "Chipless millimeter wave identification (MMID) tag at 30 GHz," in *Microwave Conference (EuMC), 2011 41st European*, 2011, pp. 123-126.

[13] N. C. Karmakar and C. K. Pern, "Mm-wave chipless RFID tag for low-cost item tagging," in *Asia-Pacific Microwave Conference 2011*, 2011, pp. 1462-1465.

[14] T. Djerafi, K. Wu, A. Marque, and A. Ghiotto, "Chipless substrate integrated waveguide tag for millimeter wave identification," in *Millimeter Waves (GSMM), 2015 Global Symposium On*, 2015, pp. 1-3.

[15] D. M. Pozar, *Microwave engineering*: John Wiley & Sons, 2009.

[16] W. Williams and A. Chakrabarti, "Reflection at a Discontinuity in a Transmission Line," *IMA Journal of Applied Mathematics,* vol. 28, pp. 185-195, 1982.

[17] R. Lall, T. J. Donohue, S. Marino, and J. C. Mitchell, "Optimizing ethanol production selectivity," *Mathematical and Computer Modelling,* vol. 53, pp. 1363-1373, 2011.

[18] M. U. s. Guide, "The mathworks," *Inc., Natick, MA,* vol. 5, p. 333, 1998.

[19] J. D. Griffin and G. D. Durgin, "Complete link budgets for backscatter-radio and RFID systems," *IEEE Antennas and Propagation Magazine,* vol. 51, pp. 11-25, 2009.

[20] J. D. Griffin, G. D. Durgin, A. Haldi, and B. Kippelen, "RF tag antenna performance on various materials using radio link budgets," *IEEE Antennas and Wireless Propagation Letters,* vol. 5, pp. 247-250, 2006.

[21] A. Lazaro, D. Girbau, and D. Salinas, "Radio link budgets for UHF RFID on multipath environments," *IEEE Transactions on Antennas and Propagation,* vol. 57, pp. 1241-1251, 2009.

[22] H. Yoon and B.-J. Jang, "LINK BUDGET CALCULATION FOR UHF RFID SYSTEMS," *Microwave Journal,* vol. 51, 2008.

[23] S. Kai, H. Yigang, L. Bing, H. Zhouguo, and Z. Yanqing, "Passive UHF RFID link budget analysis," *Chinese Journal of Scientific Instrument,* vol. 5, p. 005, 2010.

[24] P. V. Nikitin, K. Rao, and S. Lazar, "An overview of near field UHF RFID," in *IEEE international Conference on RFID*, 2007.

[25] M. Bozzi, A. Georgiadis, and K. Wu, "Review of substrate-integrated waveguide circuits and antennas," *IET Microwaves, Antennas & Propagation,* vol. 5, pp. 909-920, 2011.

[26] L. Wu, "Substrate Integrated Waveguide Antenna Applications," University of Kent, 2015.

[27] L. Yan, W. Hong, K. Wu, and T. Cui, "Investigations on the propagation characteristics of the substrate integrated waveguide based on the method of lines," *IEE Proceedings-Microwaves, Antennas and Propagation,* vol. 152, pp. 35-42, 2005.

[28] X. Feng and W. Ke, "Guided-wave and leakage characteristics of substrate integrated waveguide," *IEEE Transactions on Microwave Theory and Techniques,* vol. 53, pp. 66-73, 2005.

[29] M. Bozzi, M. Pasian, and L. Perregrini, "Modeling of losses in substrate integrated waveguide components," in *Numerical Electromagnetic Modeling and Optimization for RF, Microwave, and Terahertz Applications (NEMO), 2014 International Conference on*, 2014, pp. 1-4.

[30] N. Marcuvitz, *Waveguide handbook*: Iet, 1951.

[31] L. Yan, W. Hong, G. Hua, J. Chen, K. Wu, and T. J. Cui, "Simulation and experiment on SIW slot array antennas," *IEEE Microwave and Wireless Components Letters,* vol. 14, pp. 446-448, 2004.

[32] K. Lemberg, O. Nazarov, V. Panko, and Y. Salomatov, "X-band substrate integrated waveguide (SIW) slot antenna array," in *2013 International Siberian Conference on Control and Communications (SIBCON)*, 2013.

[33] S. Moitra, A. K. Mukhopadhyay, and A. K. Bhattacharjee, "Ku-Band substrate integrated waveguide (SIW) slot array antenna for next generation networks," *Global Journal of Computer Science and Technology,* vol. 13, 2013.

[34] W. Hong, B. Liu, Y. Wang, Q. Lai, H. Tang, X. X. Yin, *et al.*, "Half mode substrate integrated waveguide: A new guided wave structure for microwave and millimeter wave

application," in *2006 Joint 31st International Conference on Infrared Millimeter Waves and 14th International Conference on Teraherz Electronics*, 2006, pp. 219-219.

[35] Q. Lai, C. Fumeaux, W. Hong, and R. Vahldieck, "Characterization of the propagation properties of the half-mode substrate integrated waveguide," *IEEE Transactions on Microwave Theory and Techniques,* vol. 57, pp. 1996-2004, 2009.

[36] A. Niembro-Martín, V. Nasserddine, E. Pistono, H. Issa, A.-L. Franc, T.-P. Vuong, *et al.*, "Slow-wave substrate integrated waveguide," *IEEE Transactions on microwave theory and techniques,* vol. 62, pp. 1625-1633, 2014.

[37] T. Djerafi, K. Wu, and S. Tatu, "Substrate-integrated waveguide phase shifter with rod-loaded artificial dielectric slab," *Electronics Letters,* vol. 51, pp. 707-709, 2015.

[38] I. Balbin and N. C. Karmakar, "Phase-encoded chipless RFID transponder for large-scale low-cost applications," *IEEE microwave and wireless components letters,* vol. 19, pp. 509-511, 2009.

[39] S. Harma, W. G. Arthur, C. S. Hartmann, R. G. Maev, and V. P. Plessky, "Inline SAW RFID tag using time position and phase encoding," *IEEE transactions on ultrasonics, ferroelectrics, and frequency control,* vol. 55, pp. 1840-1846, 2008.

[40] A. Vena, E. Perret, and S. Tedjini, "Chipless RFID tag using hybrid coding technique," *IEEE Transactions on Microwave Theory and Techniques,* vol. 59, pp. 3356-3364, 2011.